Atlantic Centre for Atomistic Modelling (ACAM)

Quantum Mechanics of Photosynthesis

David Coker

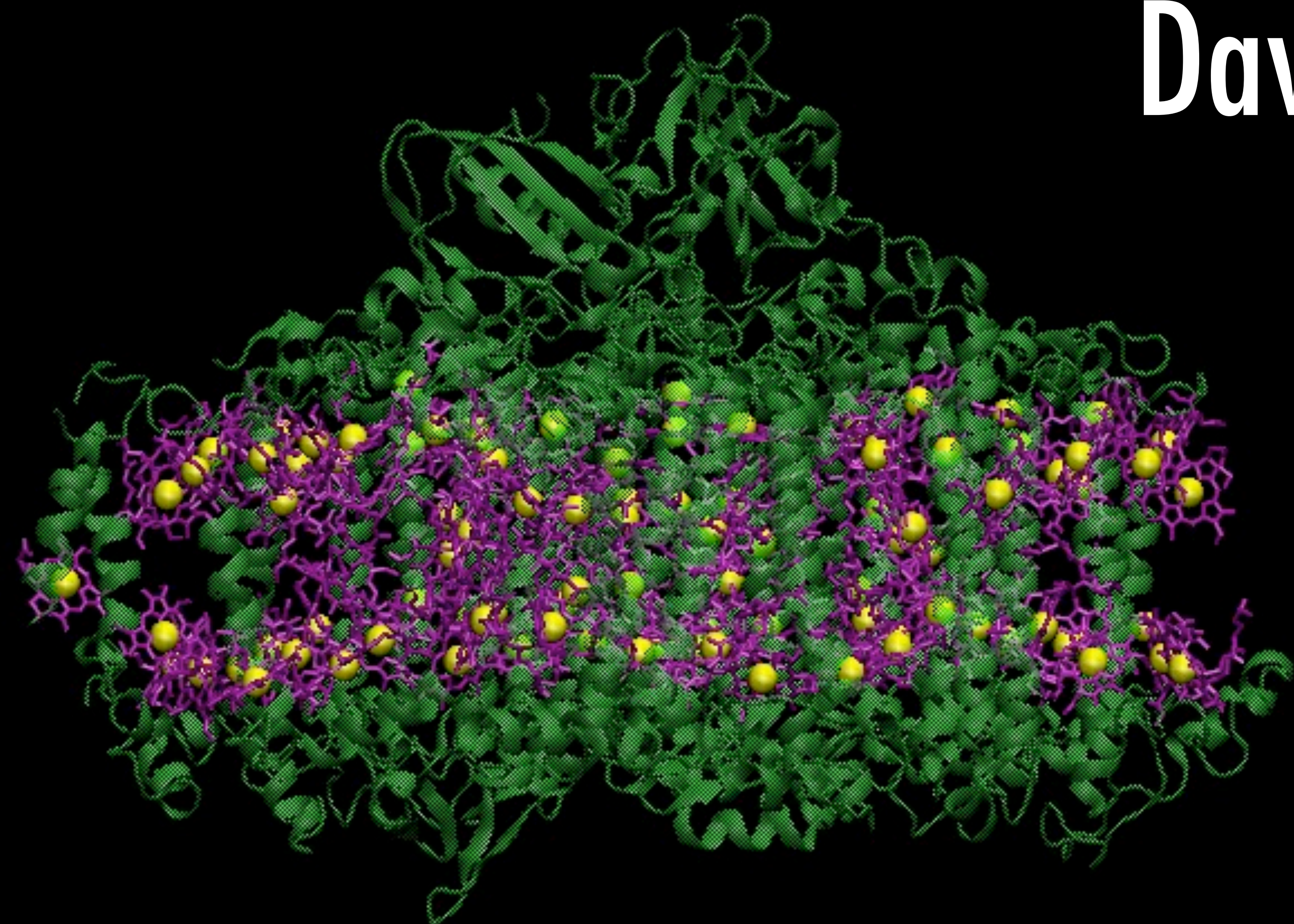

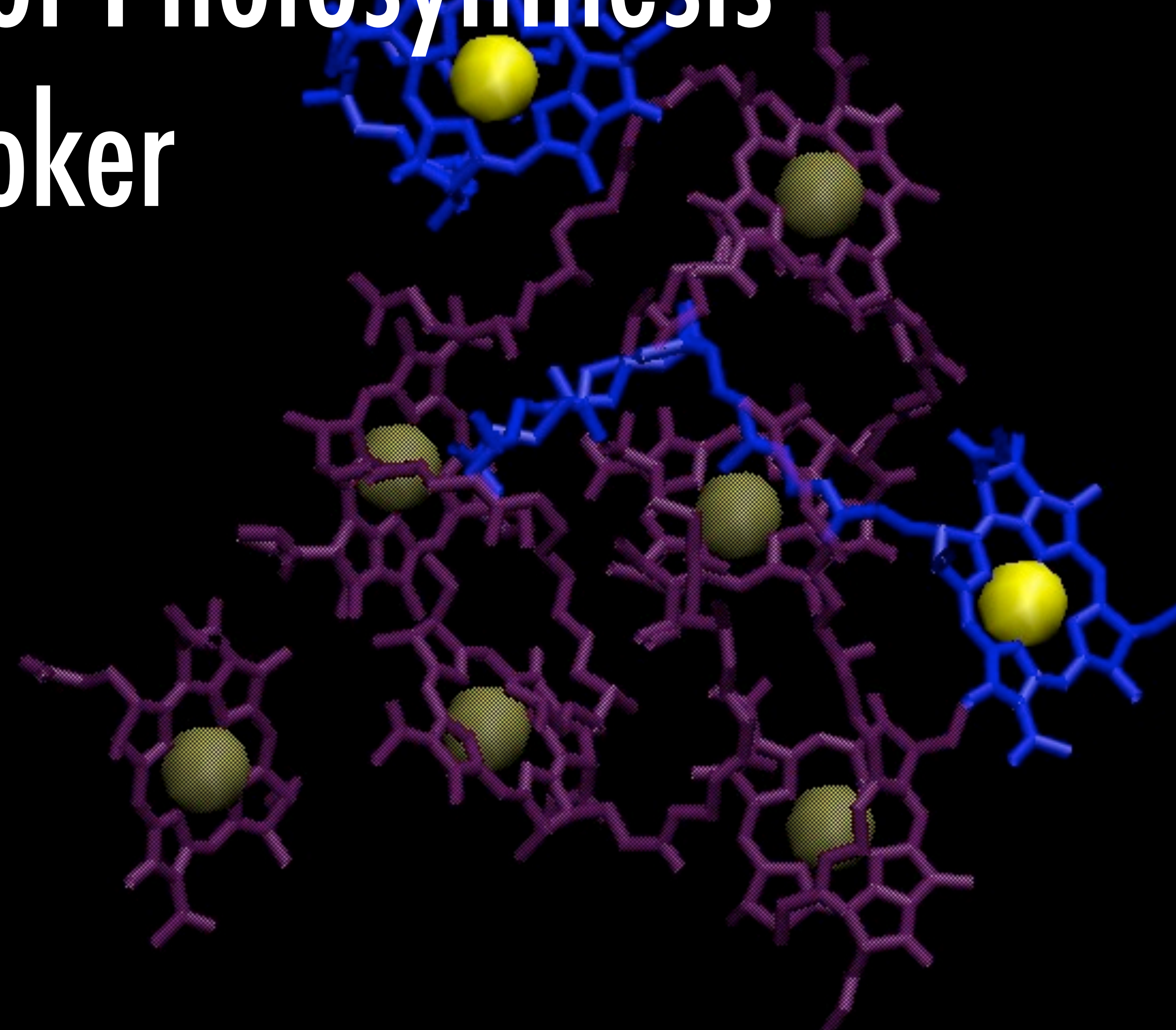

UCD DUBLIN

sfi
science foundation ireland
fondúireacht eolaíochta éireann

cecam
Centre Européen de Calcul Atomique et Moléculaire

ACAM
Atlantic Centre for Atomistic Modelling

Coherent Excitation Energy Transfer in Photosynthetic Light Harvesting Systems

David F. Coker
Department of Chemisty, Boston University
Department of Physics, University College Dublin
New CECAM node: ACAM (acam.ie)

Thanks to: Sara Bonella, Emily Dunkel, Pengfei (Frank) Huo
Tina Rivera

Funding: NSF, SFI, UCD

"Decoherence in Quantum Dynamical Systems", ECT* Workshop, Trento, Italy, April 26-30, 2010

Outline:

(1) Motivation: Collective long-range environmental response apparently responsible for long-lived quantum coherent dynamics in photosynthetic antenna arrays

(2) Iterative linearized density matrix propagation provides a successively correctible trajectory based mixed quantum-classical dynamics method that can represent environmental decoherence and non-adiabatic effects, beyond perturbative limts.

(3) Iterating "short" time linearized propagators for long time density matrix dynamics, Monte Carlo density matrix element sampling & taming the exponential growth of trajectories.

(4) Explore applications to large scale models of excitation energy transfer, high efficiency of light harvesting, long range correlated motions, coherence?

Quantum Mechanics (4): Entangled states & interaction with environment (relationship to measurement)

(initially separable)

$$\Psi(0) = \underline{(\psi_1(r) + \psi_2(r))}\chi(R) \;= \psi_1(r)\chi(R) + \psi_2(r)\chi(R)$$

subsystem (r) in superposition state

State of environment

$$i\hbar\frac{\partial}{\partial t}\Psi = \hat{H}\Psi$$

$$\Psi(t) = \psi_1\,(\mathbf{r})\,\chi_1(R,t) + \psi_2\,(\mathbf{r})\,\chi_2(R,t)$$

Non-separable ENTANGLED state

"Schroedinger's Cat"

Quantum Mechanics (5): Quantum DECOHERENCE, environment interactions collapse the wave function!

Only study the system (sum over all realizations of the environment)

$$
\begin{aligned}
P_{red}(r,t) &= \int dR |\Psi(t)|^2 \\
&= |\psi_1(\mathbf{r})|^2 \int dR |\chi_1(R,t)|^2 \\
&\quad + |\psi_2(\mathbf{r})|^2 \int dR |\chi_2(R,t)|^2 \\
&\quad + 2\psi_1(\mathbf{r})\,\psi_2(\mathbf{r}) \int dR\, \chi_1(R,t)\chi_2(R,t)
\end{aligned}
$$

Overlap of environment wavefunctions

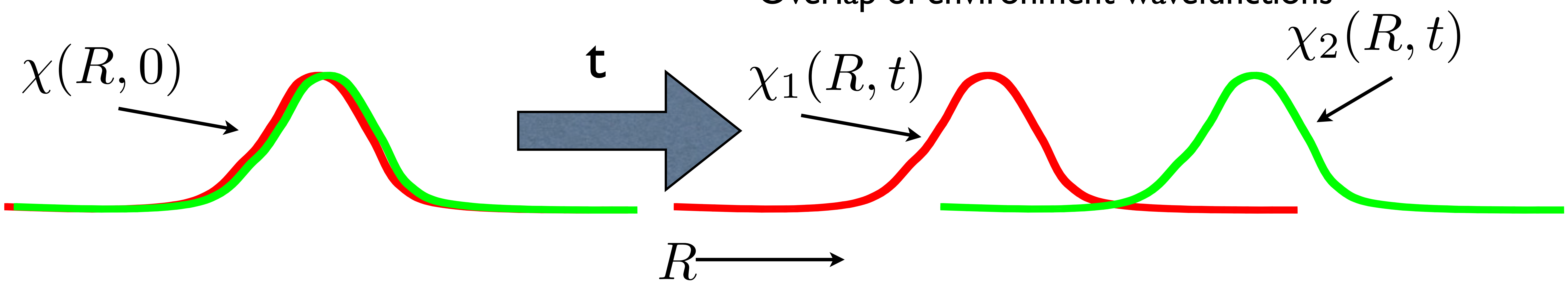

FMO complex from green sulfur bacteria

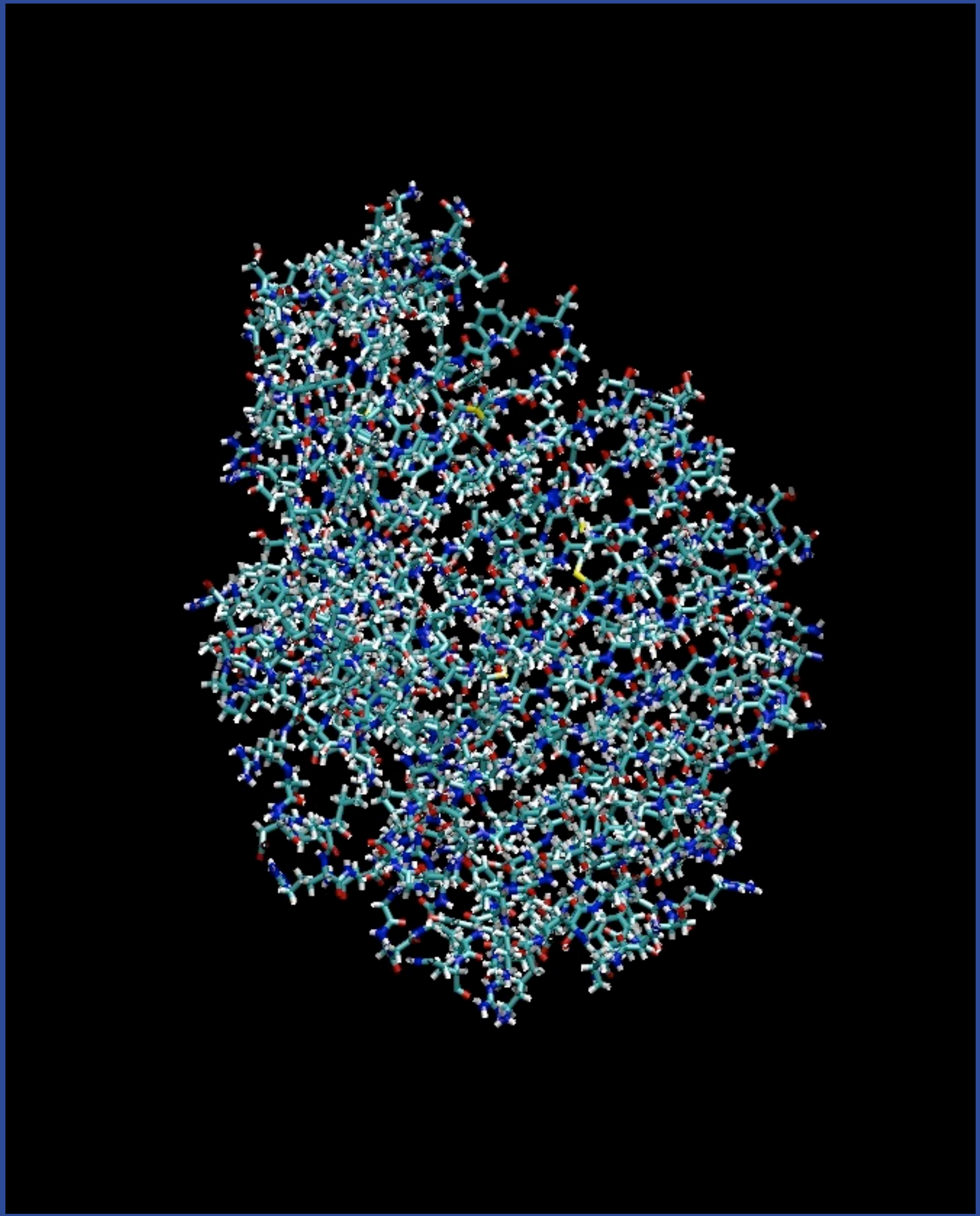

ACAM
Atlantic Centre for Atomistic Modelling

FMO complex from green sulfur bacteria

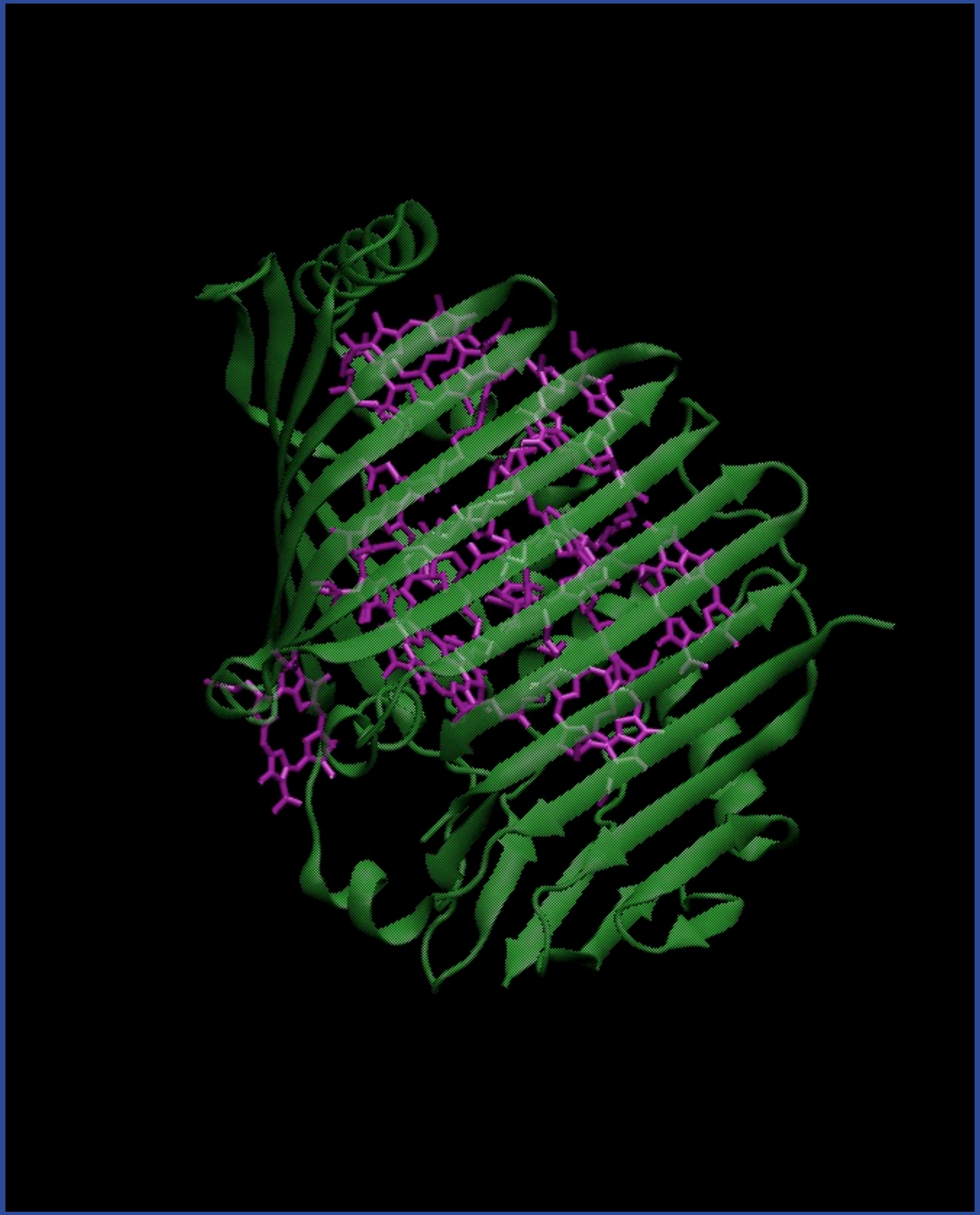

Atlantic Centre for Atomistic Modelling

FMO complex from green sulfur bacteria

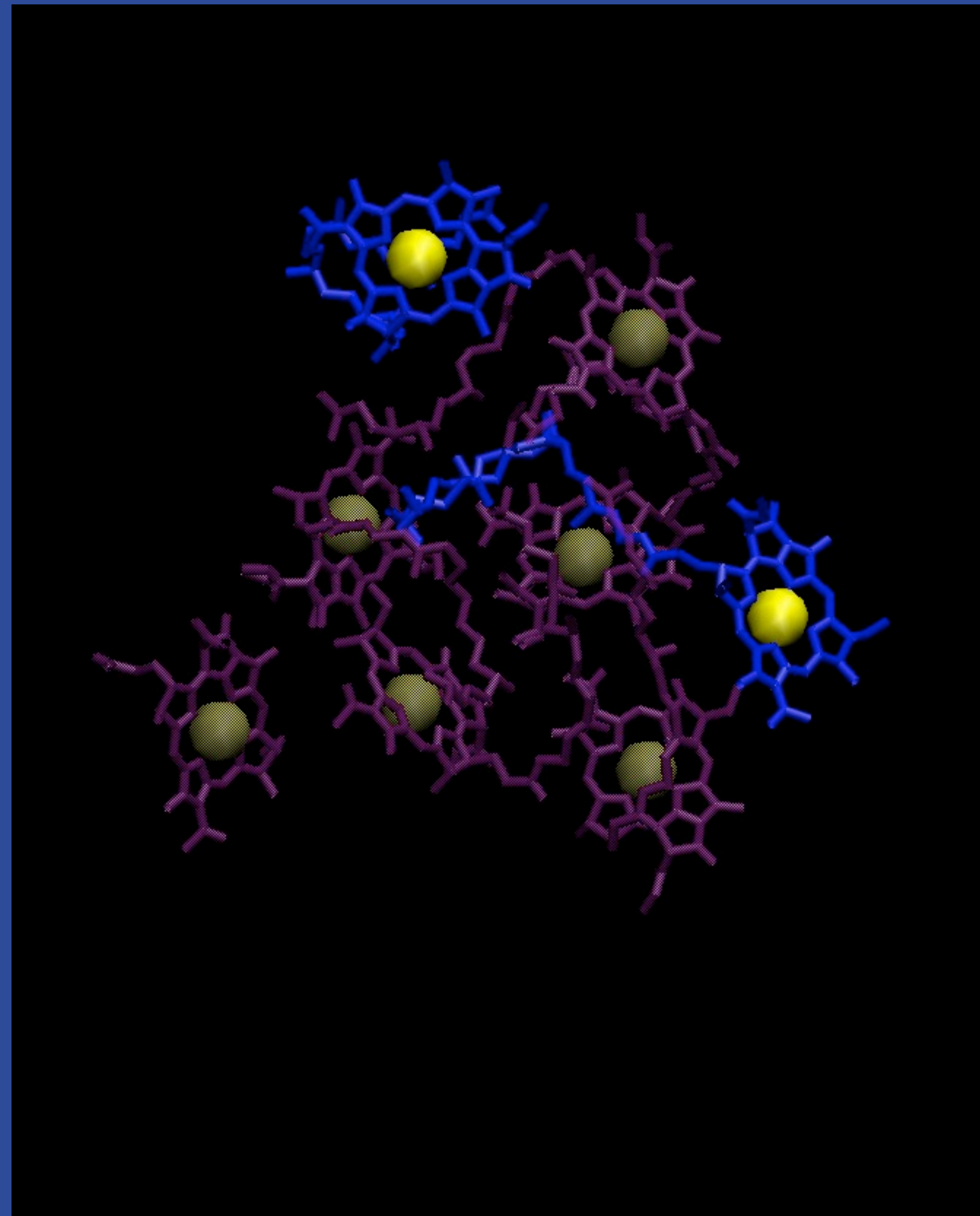

ACAM
Atlantic Centre for Atomistic Modelling

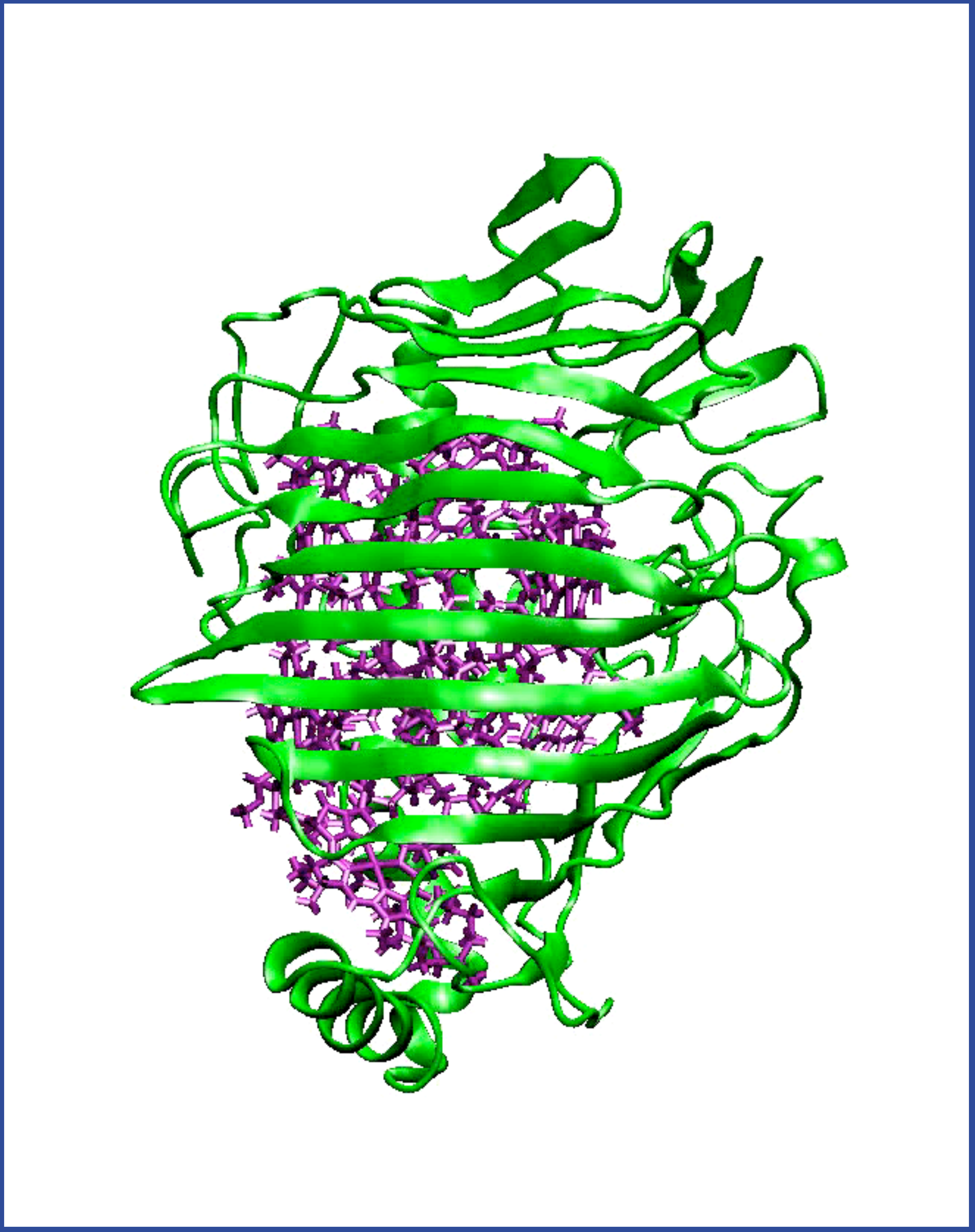

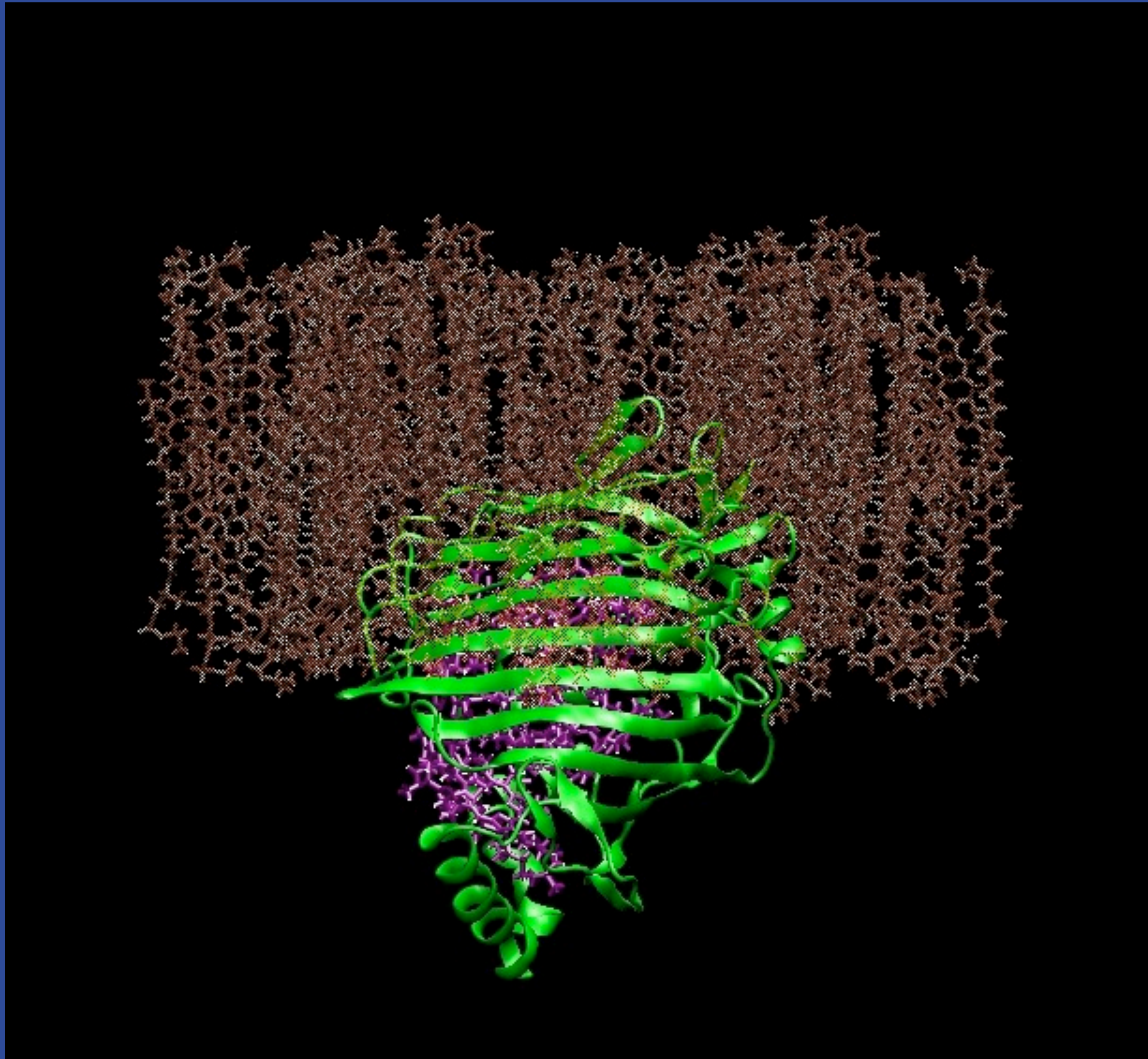

Evidence for wavelike energy transfer through quantum coherence in photosynthetic systems

Gregory S. Engel[1,2], Tessa R. Calhoun[1,2], Elizabeth L. Read[1,2], Tae-Kyu Ahn[1,2], Tomáš Mančal[1,2]†, Yuan-Chung Cheng[1,2], Robert E. Blankenship[3,4] & Graham R. Fleming[1,2]

Nature, 446, 782 (2007)

FMO

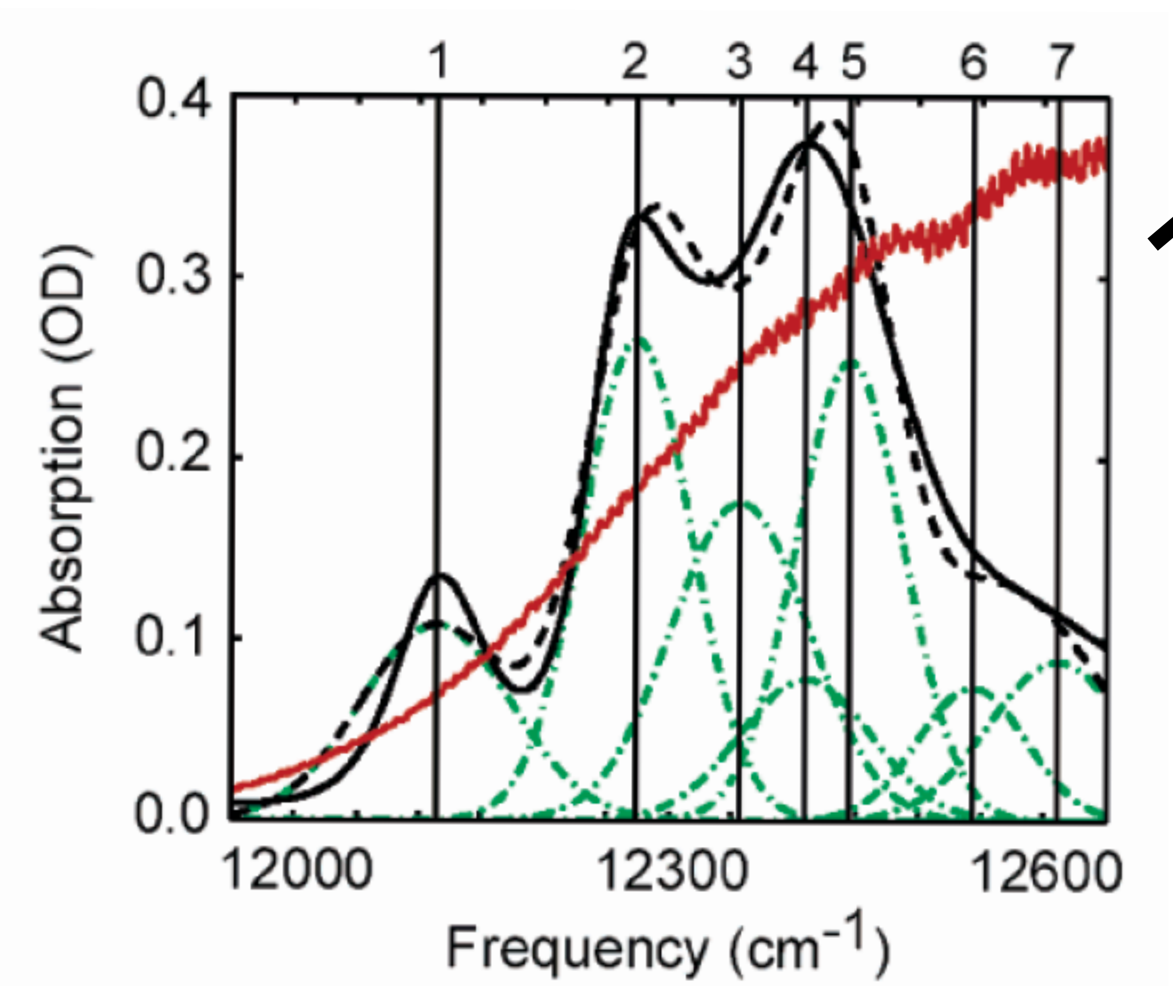

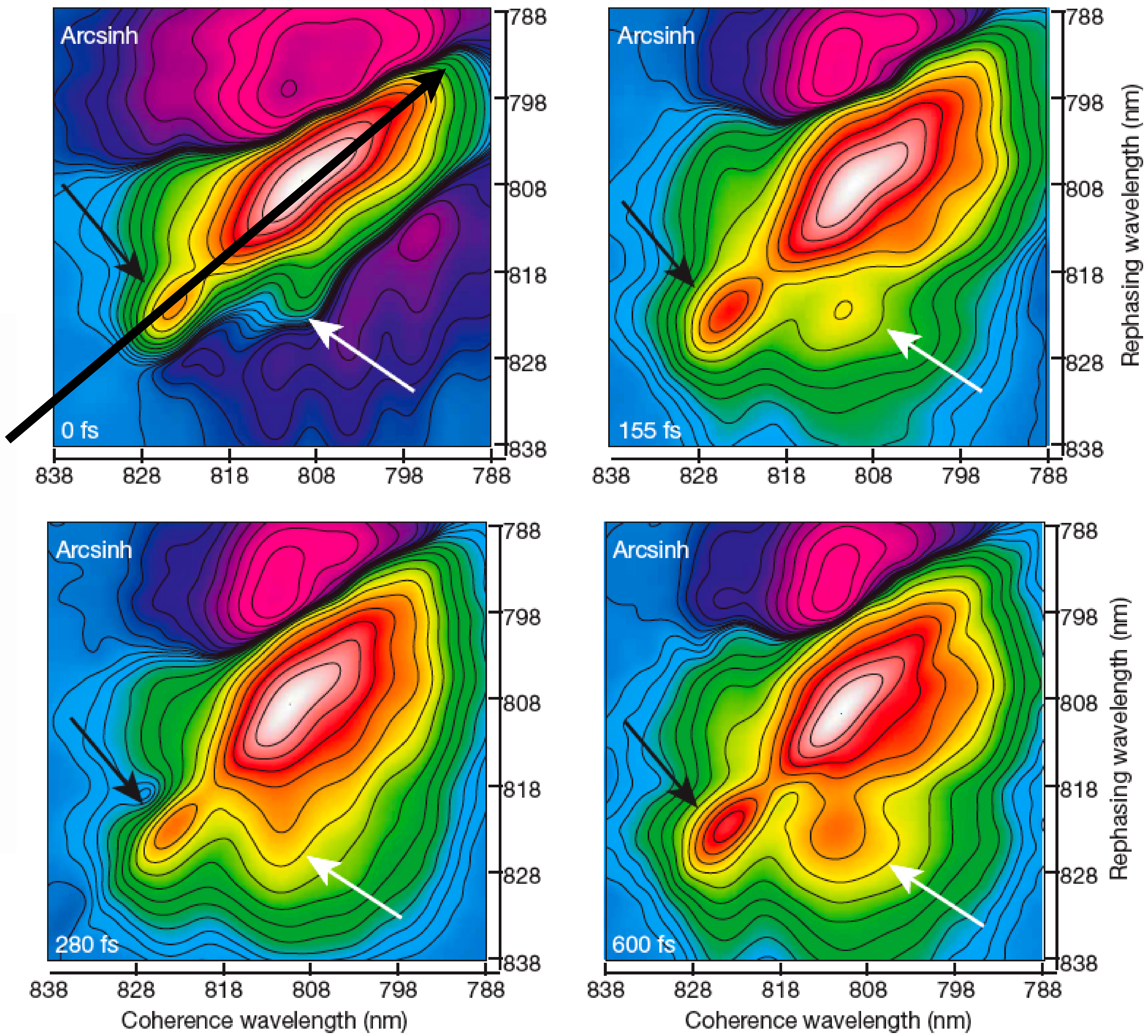

Figure 1 | Two-dimensional electronic spectra of FMO. Selected two-dimensional electronic spectra of FMO are shown at population times from $T = 0$ to 600 fs demonstrating the emergence of the exciton 1–3 cross-peak (white arrows), amplitude oscillation of the exciton 1 diagonal peak (black arrows), the change in lowest-energy exciton peak shape and the oscillation of the 1–3 cross-peak amplitude. The data are shown with an arcsinh coloration to highlight smaller features: amplitude increases from blue to white (for a three-dimensional representation of the coloration see Fig. 3a).

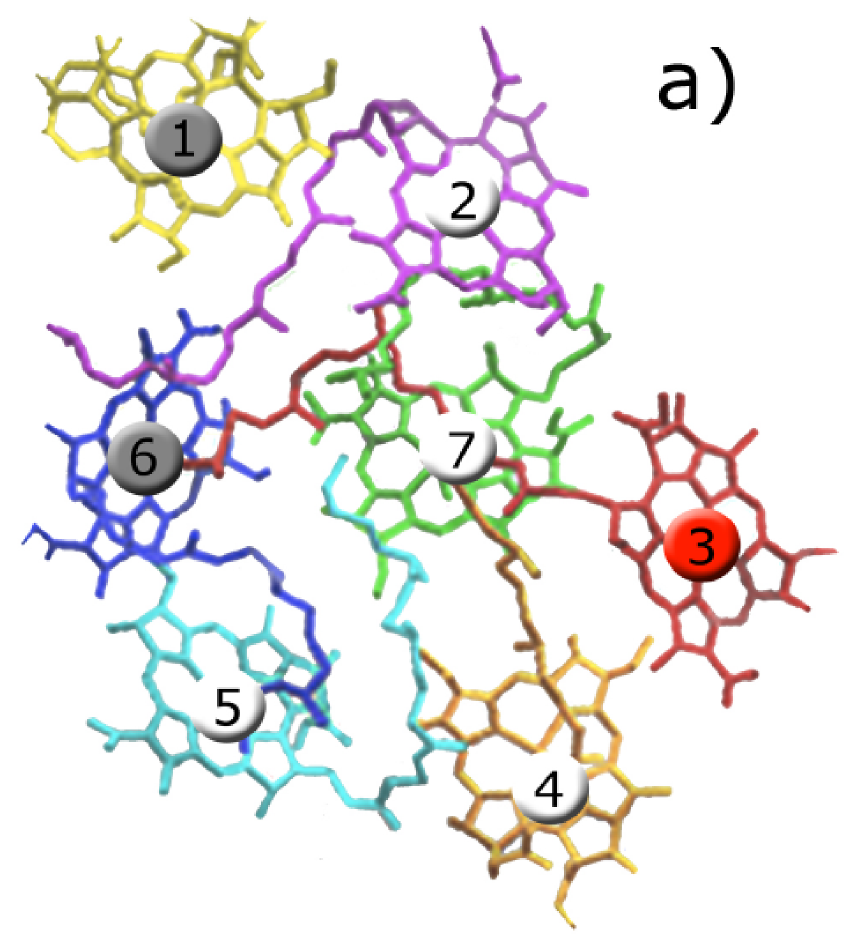

LHC2 B800-B850

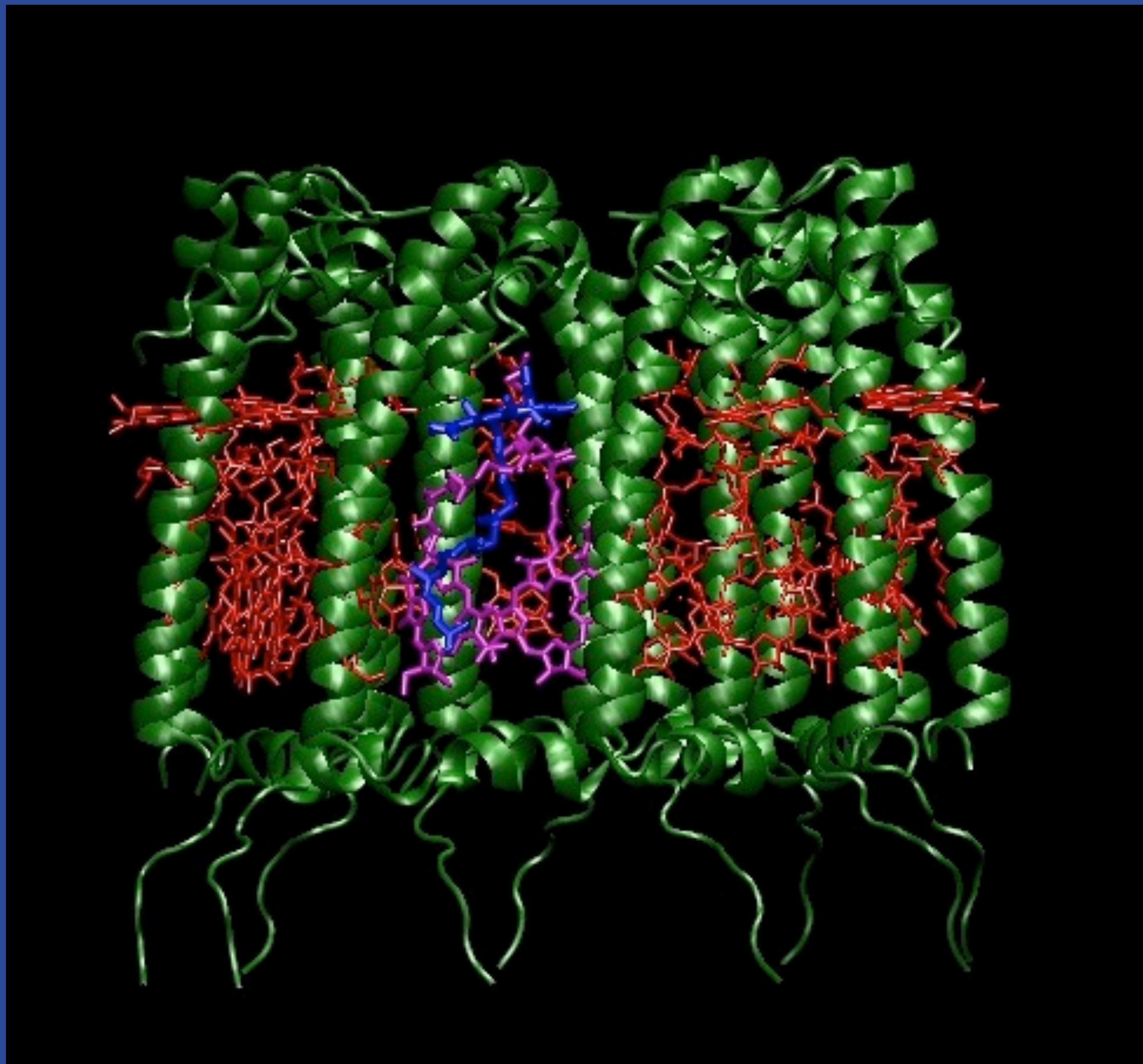

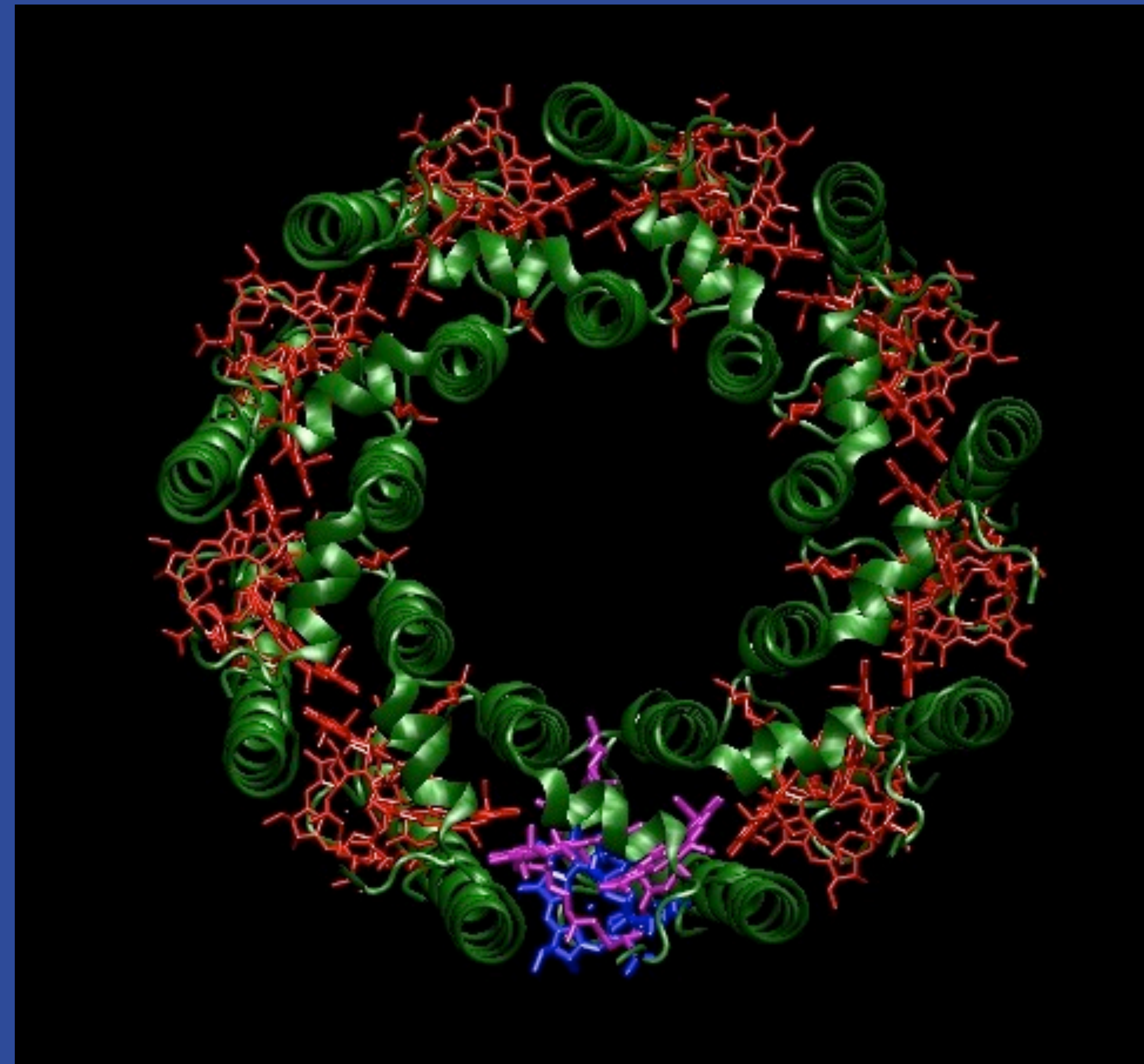

Purple bacteria photosynthetic membrane vesicle structure: Sener, Olsen, Hunter, Schulten; PNAS, 104, 15723 (2007)

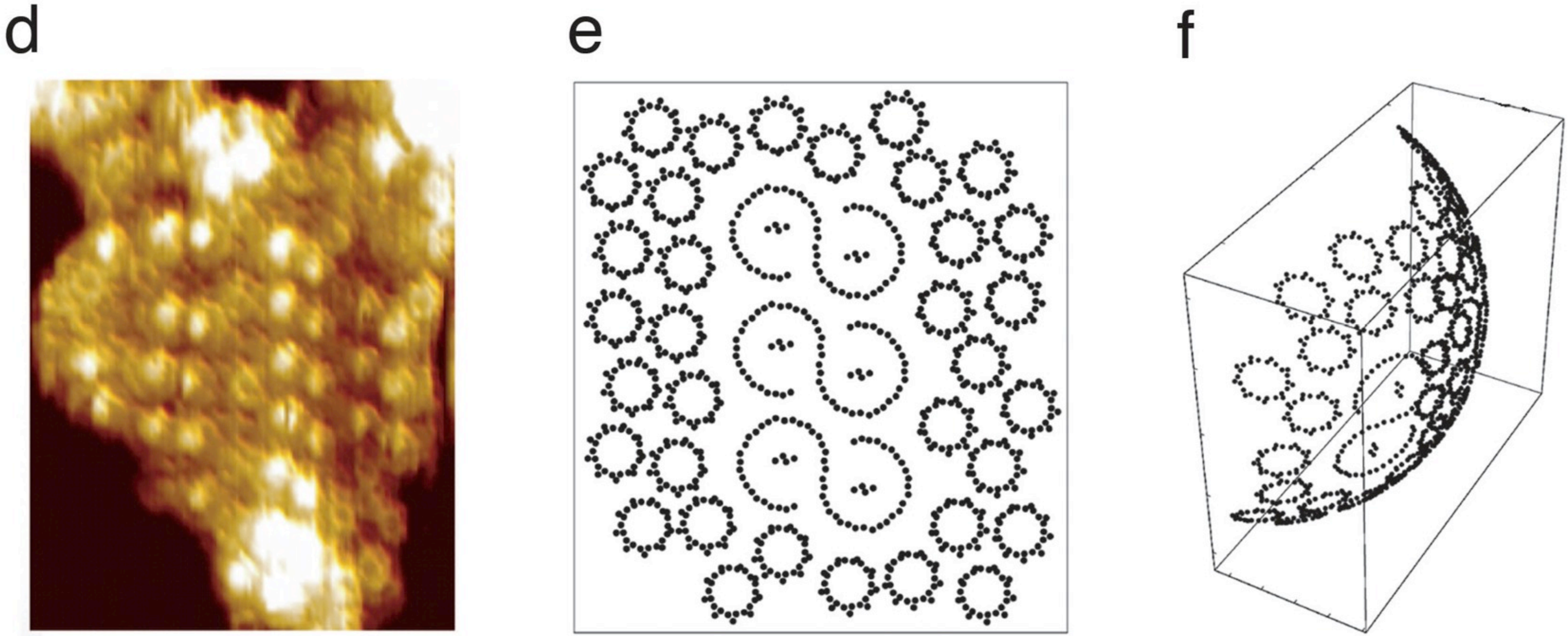

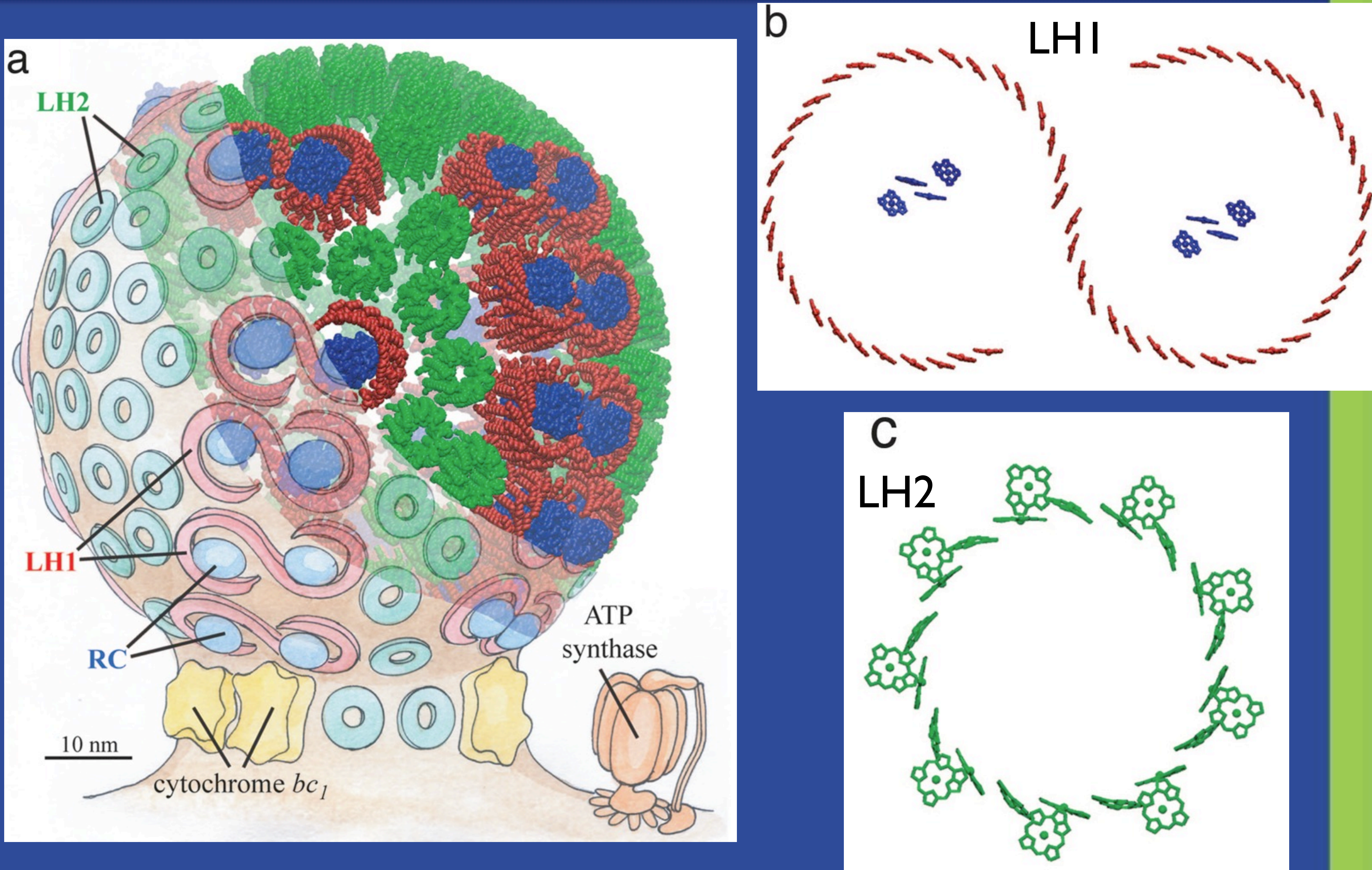
a
LH2
LH1
RC
ATP synthase
10 nm
cytochrome bc_1
b
LH1
c
LH2

Reaction Center from purple sulfur bacteria

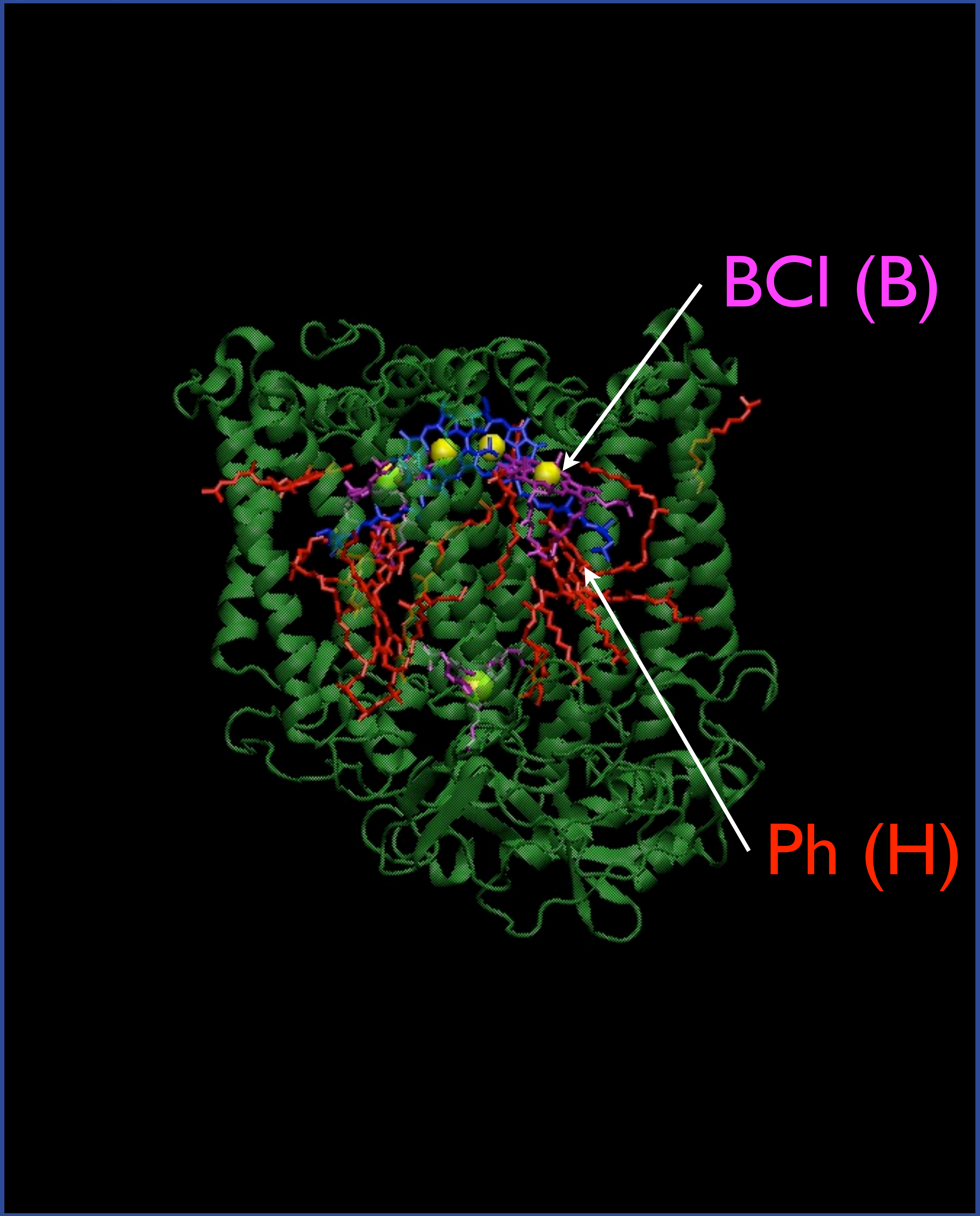

Coherence Dynamics in Photosynthesis: Protein Protection of Excitonic Coherence

Hohjai Lee, Yuan-Chung Cheng, Graham R. Fleming*

Science, 316, 1462 (2007)

states. We applied the method to the coherence between bacteriopheophytin and accessory bacteriochlorophyll in the purple bacteria reaction center (RC). The measurement quantifies dephasing dynamics in the system and provides strong evidence that the collective long-range electrostatic response of the protein environment to the electronic excitations is responsible for the long-lasting quantum coherence. In other words, the protein environment protects electronic coherences and plays a role in the optimization of excitation energy transfer in photosynthetic complexes.

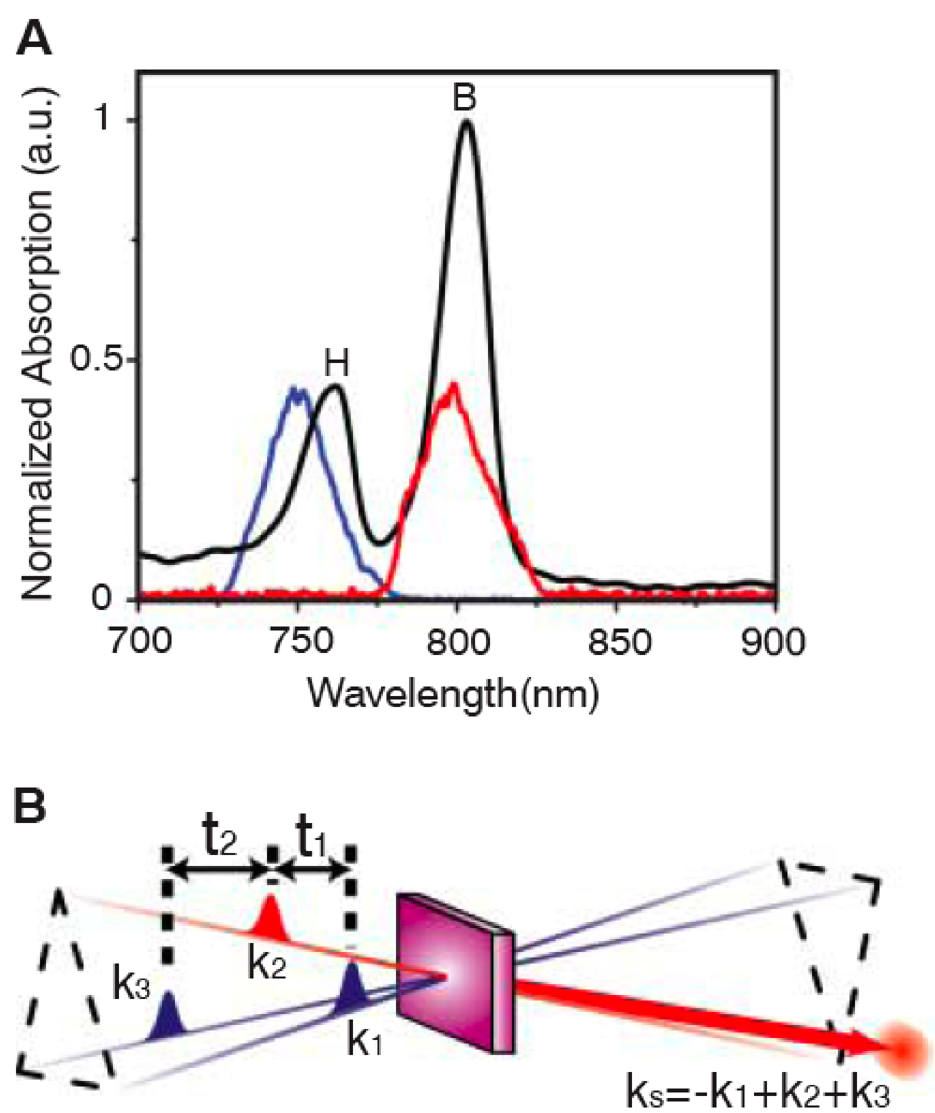

Fig. 1. The 2CECPE experiment. (**A**) The 77 K absorption spectrum (black) of the P-oxidized RC from the photosynthetic purple bacterium *R. sphaeroides* and the spectral profiles of the ~40-fs laser pulses (blue, 750 nm; red, 800 nm) used in the experiment. (**B**) The pulse sequence for the 2CECPE experiment. We detect the integrated intensity in the phase-matched direction $k_s = -k_1 + k_2 + k_3$. a.u., arbitrary units.

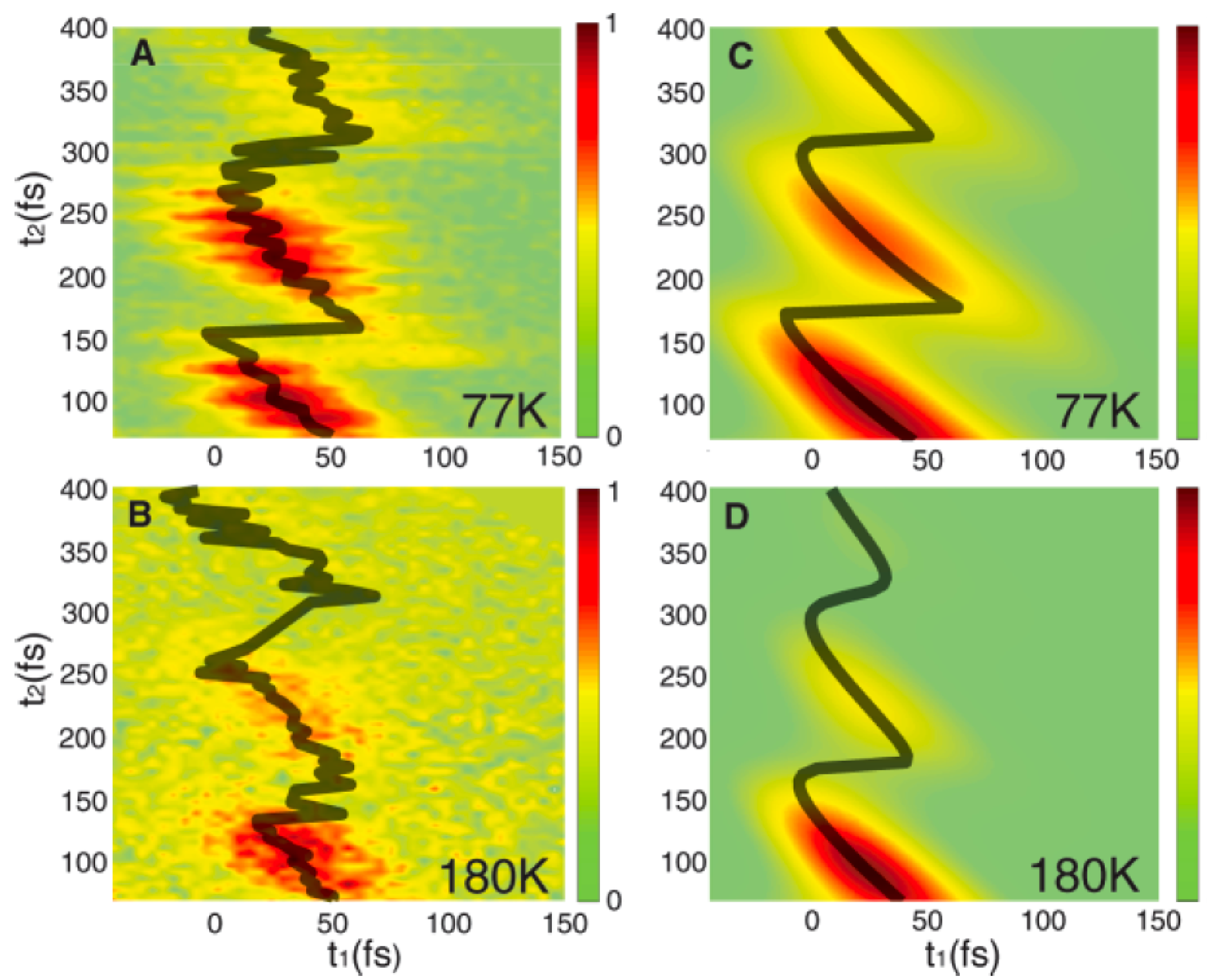

Fig. 2. Two-dimensional maps of experimental (**A** and **B**) and simulated (**C** and **D**) integrated echo signals as a function of the two delay times, t_1 and t_2, from the RC. The black lines follow the maximum of the echo signal at a given t_2. The data at $t_2 < 75$ fs are not shown because the conventional two-color three-pulse photon echo signal (750-750-800 nm) overwhelms the 2CECPE signal in this region, due to the pulse overlap effect.

Science, 323, 369 (2009)

Coherent Intrachain Energy Migration in a Conjugated Polymer at Room Temperature

Elisabetta Collini and Gregory D. Scholes*

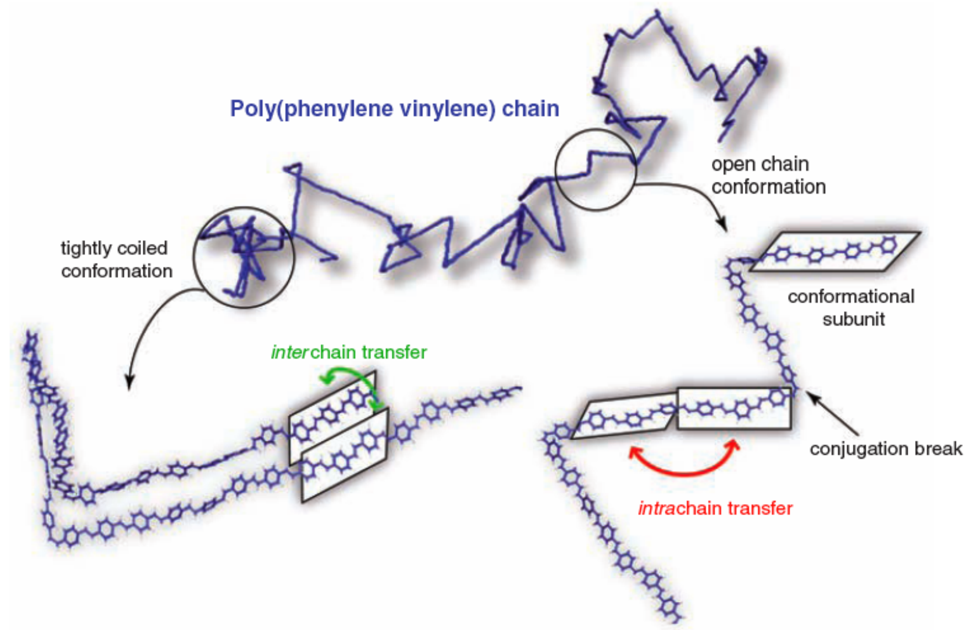

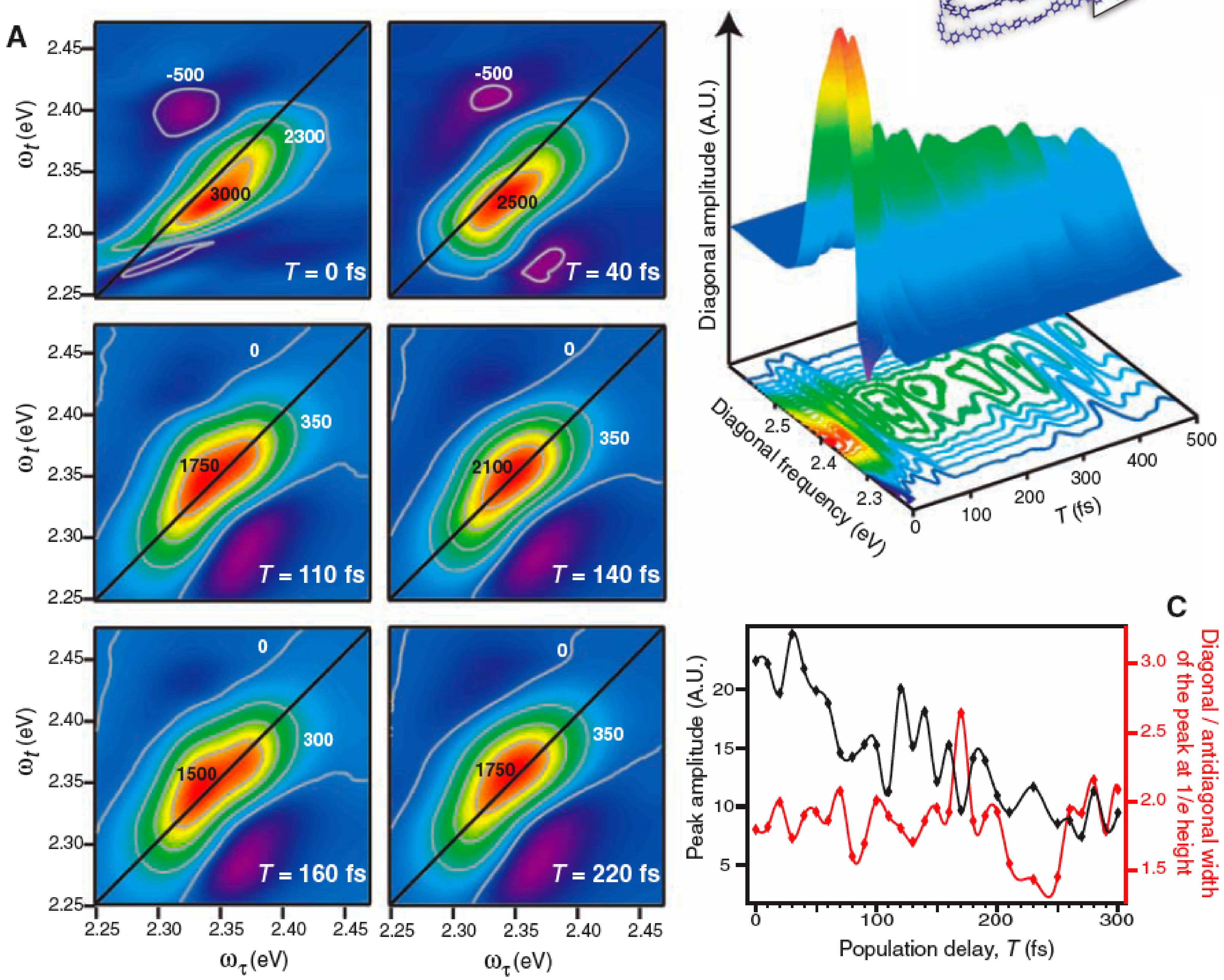

Fig. 4. (**A**) Selected 2DPE spectra (real part) of MEH-PPV in chloroform solution at $T = 0$, 40, 110, 140, 160, and 220 fs, demonstrating the oscillation in the amplitude and in the shape of the diagonal peak. The color scale indicates the signal value; deep blue denotes zero, and other values (arbitrary units) are shown by the contour lines and corresponding labels. (**B**) Three-dimensional plot of the amplitude of the spectra along the diagonal line as a function of frequency and population time. A cubic spline interpolation is used to connect the experimental points and generate a smooth surface. (**C**) Comparison between the amplitude of the diagonal peak (left axis, black line) and the ratio between the diagonal and antidiagonal widths of the peak at 1/*e* height (right axis, red line). These data are an average of three independent experiments. The lines show the characteristic anticorrelation theoretically predicted for oscillations caused by electronic coherences.

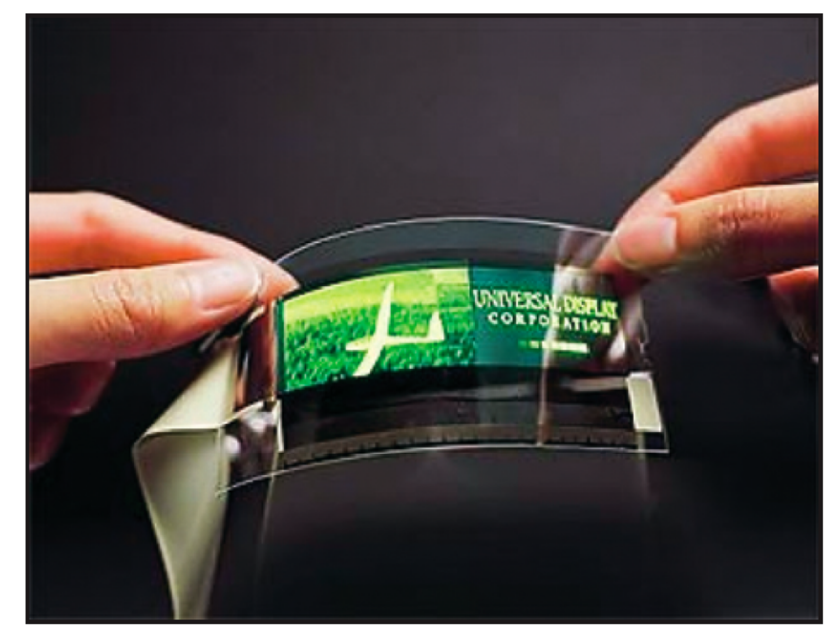

FIGURE 3.6. A prototype OLED (organic light-emitting diode) utilizes flexible organic materials for hole and electron transport and recombination to achieve efficient light emission. Advances in materials design and understanding should lead to more energy-efficient displays and solid-state lighting.

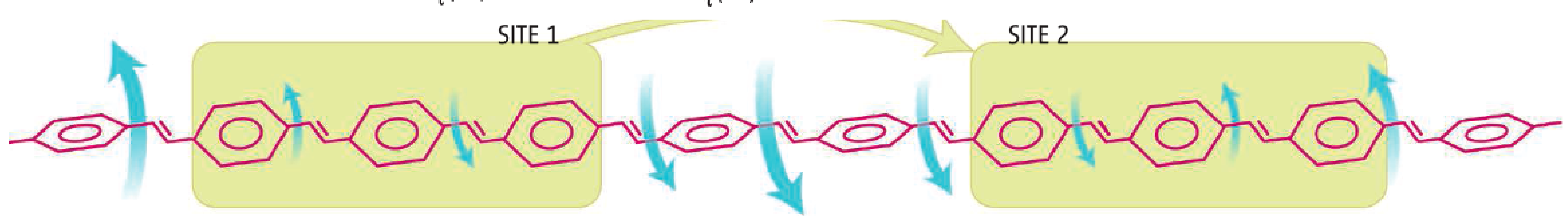

Surf, don't hop. Pictorial representation of exciton transfer from site 1 to site 2 along a poly(*p*-phenylenevinylene) conjugated polymer chain. Coherence could be preserved upon exciton transfer by coupling of the excitation to a vibrational mode (taken here for the sake of illustration to be a rotational mode, as suggested by the arrows) with a correlation length longer than the spacing between sites 1 and 2.

LHC2 B800-B850

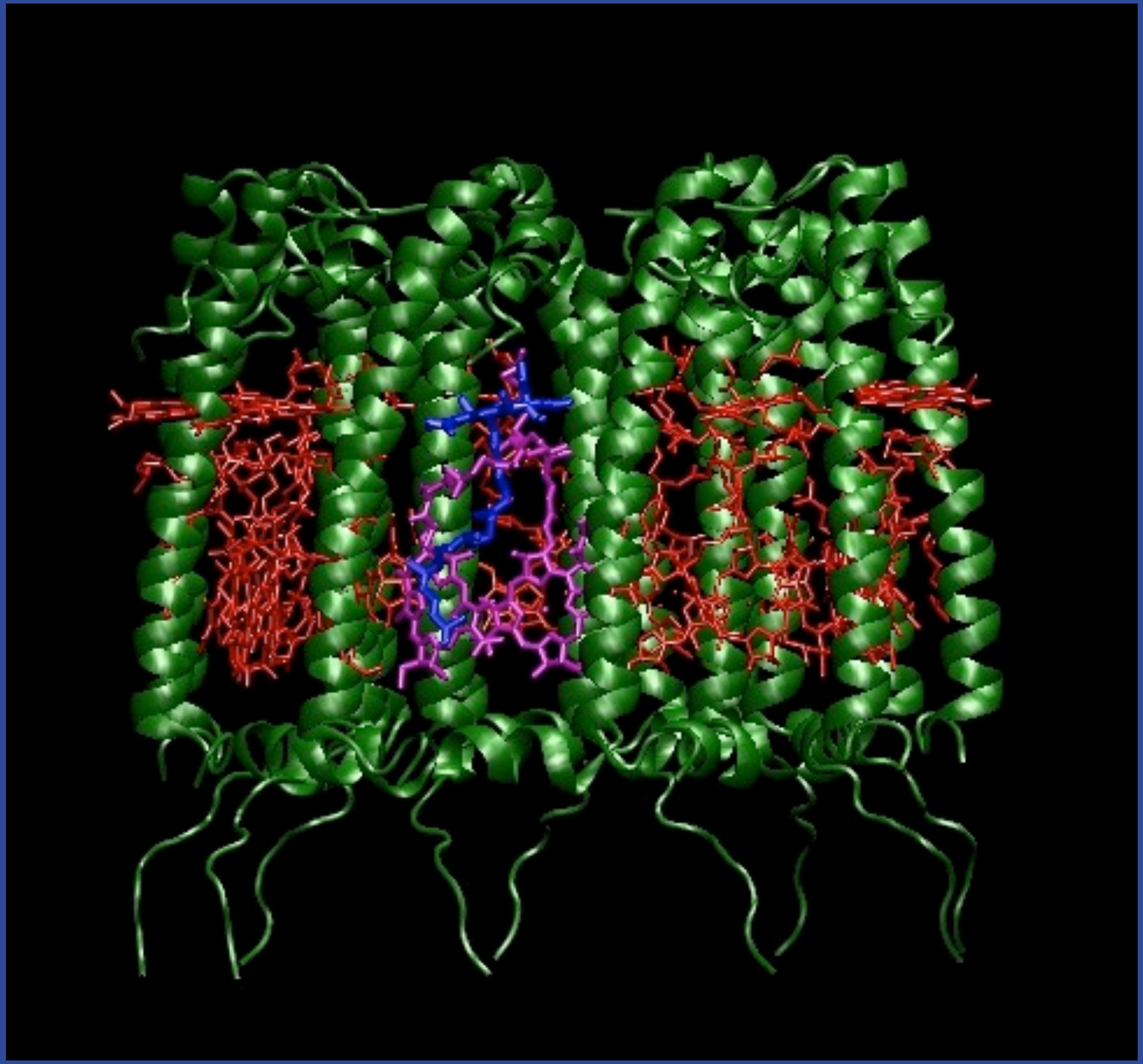

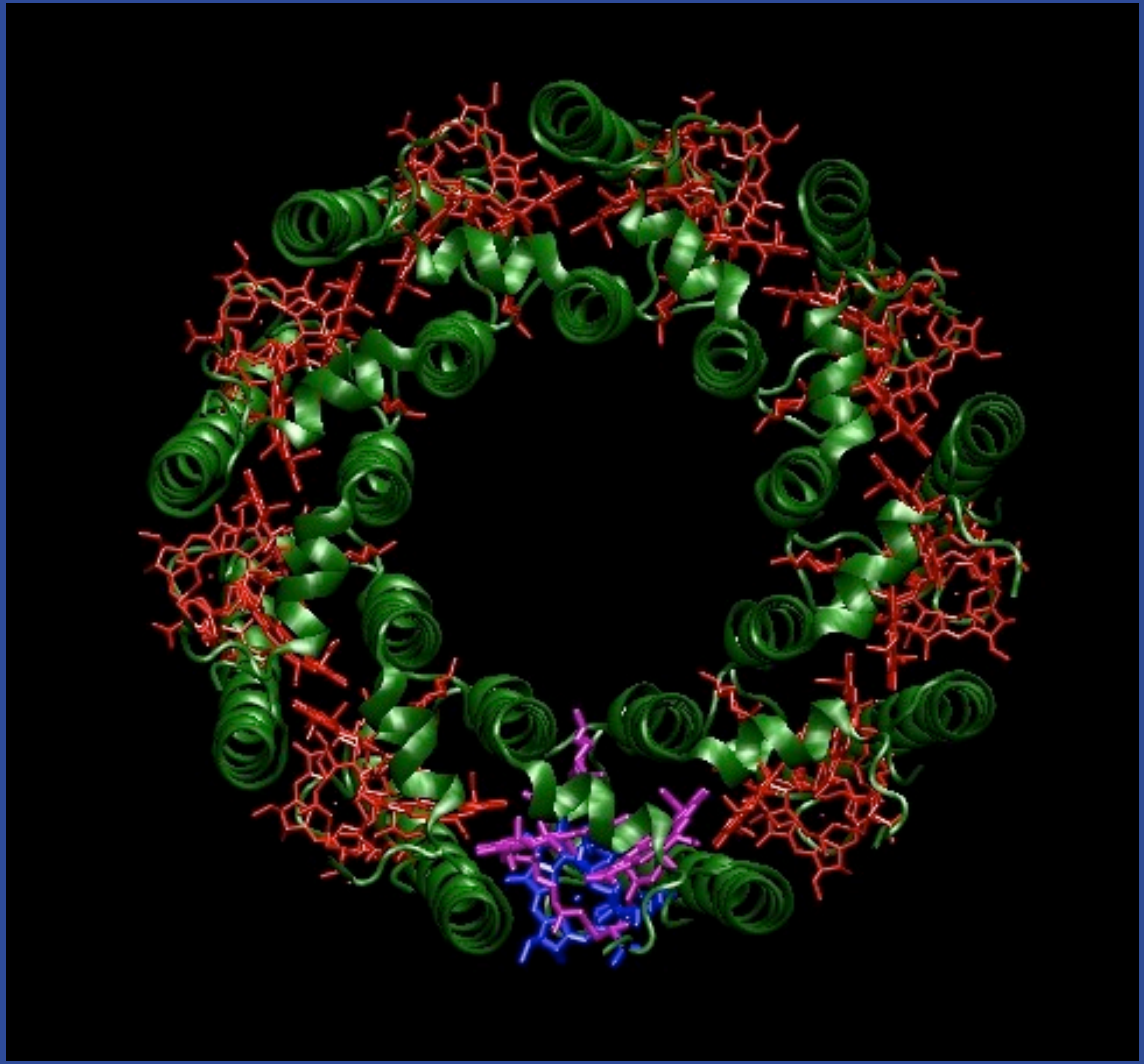

"Spin-Boson" model for exciton transport, dissipation, and decoherence in antenna arrays

$$
\begin{aligned}
\hat{H} &= \sum_n \hbar\omega_n(\hat{b}_n^\dagger \hat{b}_n + 1/2) \\
&+[\epsilon_D + \sum_n \hbar g_{n,D}(\hat{b}_n + \hat{b}_n^\dagger)]|D\rangle\langle D| \\
&+[\epsilon_\alpha + \sum_n \hbar g_{n,\alpha}(\hat{b}_n + \hat{b}_n^\dagger)]|A_\alpha\rangle\langle A_\alpha| \\
&+[\epsilon_\beta + \sum_n \hbar g_{n,\beta}(\hat{b}_n + \hat{b}_n^\dagger)]|A_\beta\rangle\langle A_\beta| \\
&+[\Delta_{\alpha\beta} + \sum_n \hbar g^\Delta_{n,\alpha\beta}(\hat{b}_n + \hat{b}_n^\dagger)](|A_\alpha\rangle\langle A_\beta| + |A_\beta\rangle\langle A_\alpha|) \\
&+[J_{D\alpha} + \sum_n \hbar g^J_{n,\alpha}(\hat{b}_n + \hat{b}_n^\dagger)](|D\rangle\langle A_\alpha| + |A_\alpha\rangle\langle D|) \\
&+[J_{D\beta} + \sum_n \hbar g^J_{n,\beta}(\hat{b}_n + \hat{b}_n^\dagger)](|D\rangle\langle A_\beta| + |A_\beta\rangle\langle D|)
\end{aligned}
$$

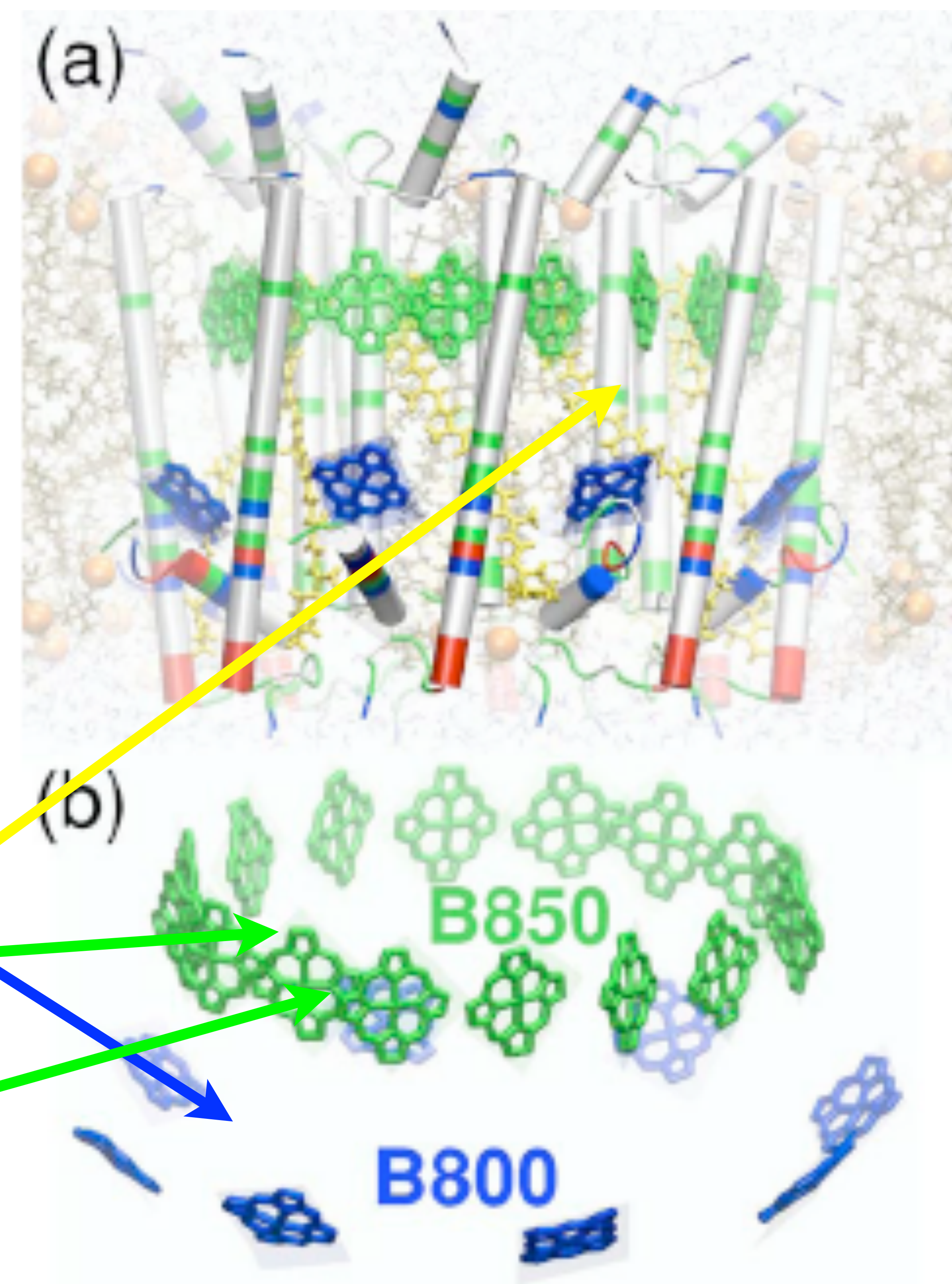

LHC2

c.f. Jang, Newton, Silbey
J. Phys. Chem. B, 111, 6807 (2007)

$$J_{D\alpha} = \frac{\mu_D \cdot \mu_\alpha - 3(\mu_D \cdot \hat{R}_{D\alpha})(\mu_\alpha \cdot \hat{R}_{D\alpha})}{\epsilon R^3_{D\alpha}}$$

Two perturbative limits for photosynthetic EET

Electronic coupling between pigments		Electron environment coupling
J_{Dn}	<<	g_n

(1) Forster Resonance Energy Transfer (FRET)
incoherent hopping between pigments

Electronic coupling between pigments		Electron environment coupling
J_{Dn}	>>	g_n

(2) Master equation approaches e.g. Redfield theory

Two perturbative limits for photosynthetic EET

Electronic coupling between pigments J_{Dn} << Electron environment coupling g_n

(1) Forster Resonance Energy Transfer (FRET) incoherent hopping between pigments

Unfortunately for typical Photosynthetic EET $J_{Dn} \sim g_n$

Electronic coupling between pigments J_{Dn} >> Electron environment coupling g_n

(2) Master equation approaches e.g. Redfield theory

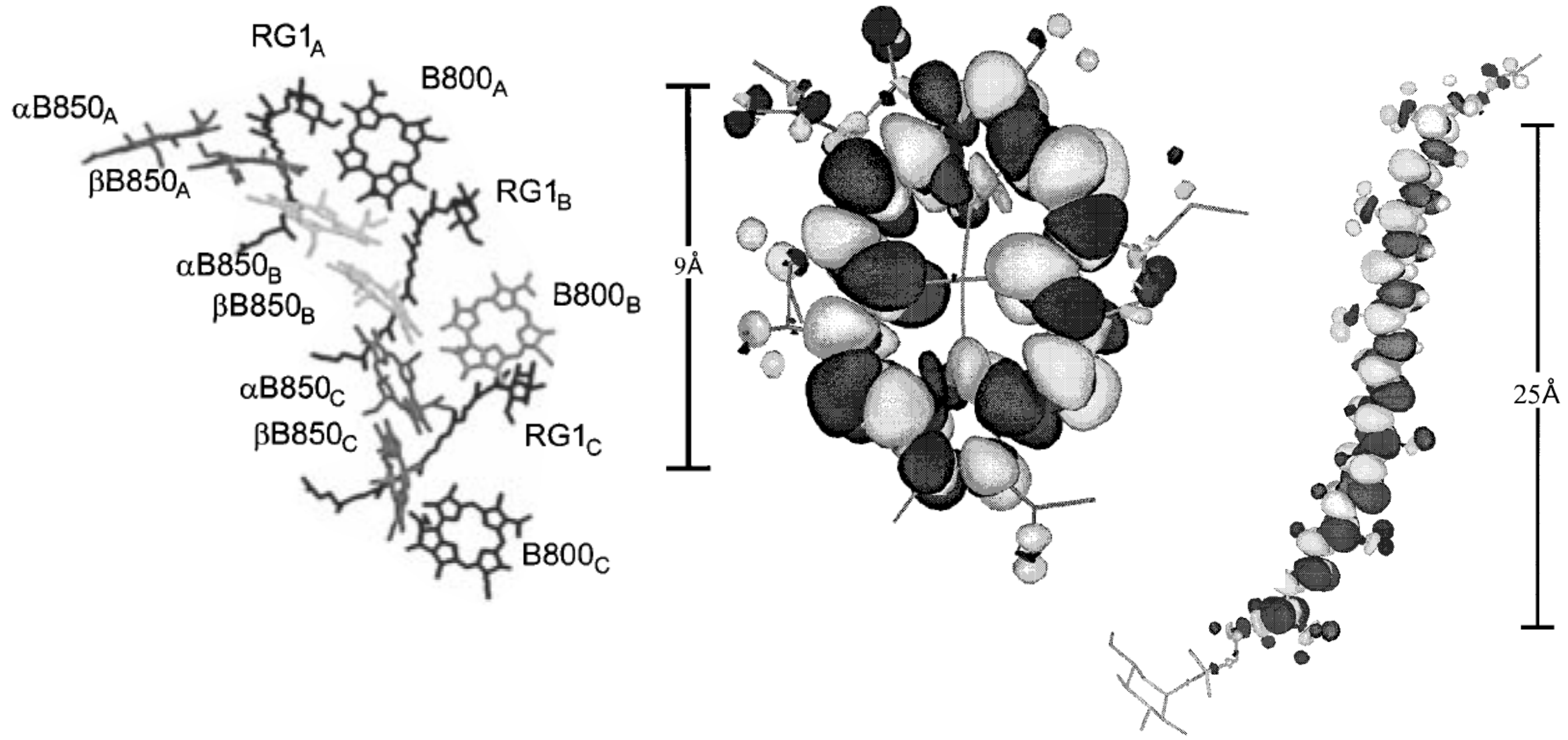

5378 J. Phys. Chem. B 1998, 102, 5378−5386

Calculation of Couplings and Energy-Transfer Pathways between the Pigments of LH2 by the ab Initio Transition Density Cube Method

Brent P. Krueger, Gregory D. Scholes, and Graham R. Fleming*

Parameters for models for use in approximate theories Obtained from detailed spectroscopy and ab initio calculations

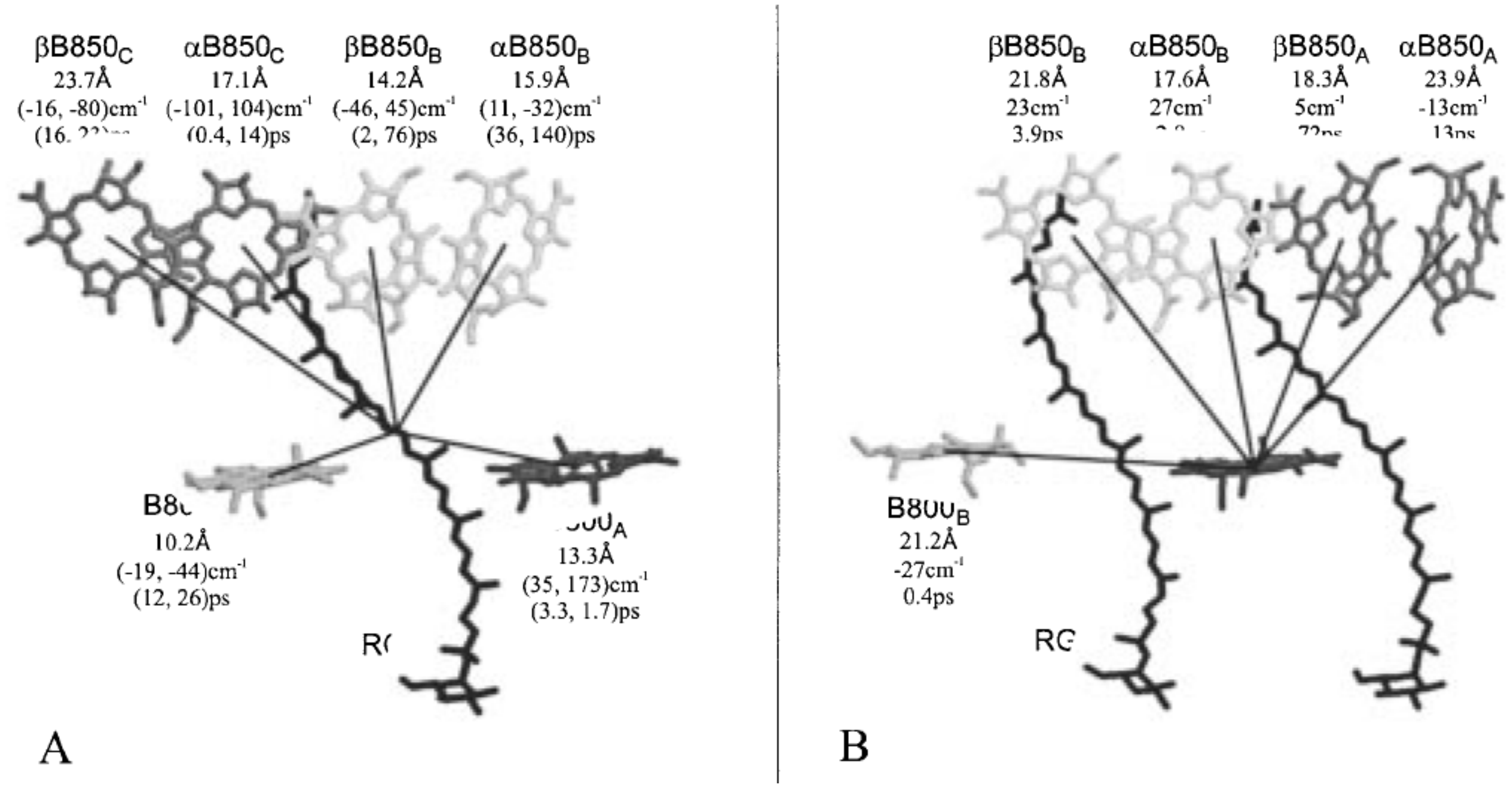

Coupling strengths and energy transfer times from the RG1B S2 (A) and B800A Q*y* (B) transitions to nearby Bchla transitions. Shading of the chromophores is as in Figure 2. Near each acceptor pigment is given the label, center-to-center separation, coupling strength *V*Coul, and transfer time. For transfer from RG S2, the interaction with both the Q*x* and Q*y* transitions of the acceptor is given (Q*x*, Q*y*), whereas for B800 Q*y* only interaction with the acceptor Q*y* transition is given.

PREVIOUS METHODS: 1/3

- **Forster resonance energy transfer (FRET) theory**

Multi-Chromophore FRET

$$k^{\mathrm{MC}}(t) = \sum_{j'j''}\sum_{k'k''} \frac{J_{j'k'}J_{j''k''}}{2\pi\hbar^2}\int_{-\infty}^{\infty} d\omega\, E_D^{j''j'}(t,\omega) I_A^{k'k''}(\omega),$$

$$I_A^{k'k''}(\omega) \equiv \int_{-\infty}^{\infty} dt\, e^{i\omega}\mathrm{Tr}_A\{e^{iH_A^g t/\hbar}\langle A_{k'}|e^{-iH_A^e t/\hbar}|A_{k''}\rangle\rho_A^g\}$$

$$E_D^{j''j'}(t,\omega) = 2\mathrm{Re}\Big[\int_0^t dt'\, e^{-i\omega t'}\mathrm{Tr}_D\{e^{-iH_D^g t'/\hbar}\langle D_j| \times e^{-iH_D^e(t-t')/\hbar}|D_{\hat{\mathbf{e}}}\rangle\langle D_{\hat{\mathbf{e}}}|\rho_D^g e^{iH_D^e t/\hbar}|D_{j'}\rangle\}\Big],$$

- **Comments:**
  - Time dependent perturbation theory
  - May not valid for strong coupling situation

SJ Jang, MD Newton, and RJ Silbey. Multichromophoric Forster resonance energy transfer. *PHYSICAL REVIEW LETTERS*, 92(21), MAY 28 2004.

PREVIOUS METHODS: 2/3

- **Extension of Redfield theory**

Mukamel et al., Kleinekarthofer, ...

Nakajima-Zwanzig equation

$$\frac{\partial}{\partial t}\mathcal{P}W(t) = -i\mathcal{P}\mathcal{L}\mathcal{P}W(t) - \int_0^t d\tau \mathcal{P}\mathcal{L}e^{-i\mathcal{Q}\mathcal{L}(t-\tau)}\mathcal{Q}\mathcal{L}\mathcal{P}W(\tau)$$

$$\mathcal{P}W(t) = R_{\mathrm{eq}}\,\mathrm{tr}_B\{W(t)\} = R_{\mathrm{eq}}\rho(t) \qquad \mathcal{Q} = 1 - \mathcal{P}$$

- Redfield Equation :

$$\frac{d\sigma_{ab}}{dt} = -i\omega_{ab}\sigma_{ab} - \frac{i}{\hbar}\sum_c(\hat{V}_{ac}\sigma_{cb} - \sigma_{ac}\hat{V}_{cb})$$
$$-\sum_{c,d}(R_{ac,cd}(\omega_{dc})\sigma_{db}(t) + R^*_{bd,dc}(\omega_{cd})\sigma_{ac}(t))$$
$$-\left[R_{db,ac}(\omega_{ca}) + R^*_{ca,bd}(\omega_{db})\right]\sigma_{cd}(t))$$

$$R_{ab,cd}(\omega) + R^*_{dc,ba}(\omega) = \int_{-\infty}^{\infty} dt e^{i\omega t} M_{ab,cd}(t)$$

$$M_{ab,cd}(t) \equiv \frac{1}{\hbar^2}C(t)V^s_{ab}V^s_{cd} \qquad C(t) = \langle V(0)\cdot V(t)\rangle \qquad V = \hat{H}_B + \hat{H}_{s-B}$$

- Includes Markovian approximation
- Valid only for bath mode moving faster than exciton transfer time scale
- Does not necessarily conserve the positivity property

THE JOURNAL OF CHEMICAL PHYSICS **124**, 084903(2006)

PREVIOUS METHODS: 3/3

- Methods based on the **Lindblad master equation**

$$\dot{\hat{\sigma}} = -\frac{i}{\hbar}\left[\hat{H}_0, \hat{\sigma}\right] + \frac{1}{2}\sum_j \left(\left[\hat{V}_j \hat{\sigma}, \hat{V}_j^{+}\right] + \left[\hat{V}_j, \hat{\sigma}\hat{V}_j^{+}\right] \right)$$

- A liner Markovian time evolution
- Conserve the positivity

PHYSICAL REVIEW B **78**, 085115 2008

Various alternative approximations to evolve the reduced density matrix based on the **Liouville-von neuman equation**

[1] M. Mohseni, P. Robentrost, S. Lloyd, and A. Aspuru-Guzik, "Environment assisted quantum walks in photosynthetic energy transfer", J. Chem. Phys. 129, 174106 (2008)
[2] P. Rebentrost, M. Mohseni, and A. Aspuru-Guzik, "The role of quantum coherence in the chromophoric energy transfer efficiency", J. Phys. Chem. B (in press).
[3] A. Olaya-Castro, C.F. Lee, F. Fassioli-Olsen, and N.F. Johnson, "Efficiency of energy transfer in a light-harvesting system under quantum coherence", Phys. Rev. B, 78 (2008).

Iterative linearized density matrix dynamics

J. Chem. Phys. 114106 (2008)

$$\hat{\rho}(2t) = e^{-\frac{i}{\hbar}\hat{H}t} e^{-\frac{i}{\hbar}\hat{H}t} \hat{\rho}(0) e^{\frac{i}{\hbar}\hat{H}t} e^{\frac{i}{\hbar}\hat{H}t}$$

$$\hat{H} = \hat{P}^2/2M + \hat{h}(\hat{R}) = \hat{P}^2/2M + \sum_n \sum_m |n\rangle h_{nm}(\hat{R})\langle m|$$

$$\langle R_{2t} n_{2t}|\hat{\rho}(2t)|R'_{2t} n'_{2t}\rangle \; = $$

$$\sum_{n_t, n'_t} \int dR_t dR'_t \sum_{n_0, n'_0} \int dR_0 dR'_0 \langle R_{2t} n_{2t}| e^{-\frac{i}{\hbar}\hat{H}t} |R_t n_t\rangle \langle R_t n_t| e^{-\frac{i}{\hbar}\hat{H}t} |R_0 n_0\rangle$$

$$\times \langle R_0 n_0|\hat{\rho}(0)|R'_0 n'_0\rangle \langle R'_0 n'_0| e^{\frac{i}{\hbar}\hat{H}t} |R'_t n'_t\rangle \langle R'_t n'_t| e^{\frac{i}{\hbar}\hat{H}t} |R'_{2t} n'_{2t}\rangle$$

Mapping Hamiltonian formulation

Miller-Meyer
Stock-Thoss

$$|n\rangle \; \rightarrow \; |m_n\rangle \; = \; |0_1, ..., 1_n, ..0_{N_s}\rangle \qquad \hat{H}_m = \hat{P}^2/2M + \hat{h}_m(\hat{R})$$

$$\hat{h}_m(\hat{R}) \; = \; \frac{1}{2}\sum_\lambda h_{\lambda,\lambda}(\hat{R})(\hat{q}_\lambda^2 + \hat{p}_\lambda^2 - \hbar)$$

$$+\frac{1}{2}\sum_{\lambda,\lambda'} h_{\lambda,\lambda'}(\hat{R})(\hat{q}_{\lambda'}\hat{q}_\lambda + \hat{p}_{\lambda'}\hat{p}_\lambda)$$

Time slice forward and backward propagators

$$\epsilon = t/N$$

$$\langle R_k | e^{-\frac{i}{\hbar}\hat{H}_m \epsilon} | R_{k-1} \rangle = \int \frac{dP_k}{2\pi\hbar} e^{\frac{i}{\hbar}[P_k(R_k - R_{k-1}) - \epsilon \frac{P_k^2}{2M}]} e^{-\frac{i\epsilon}{\hbar}\hat{h}_m(R_{k-1})}$$

$$\langle R_N m_{n_t} | e^{-\frac{i}{\hbar}\hat{H}_m t} | R_0 m_{n_0} \rangle = \int \prod_{k=1}^{N-1} dR_k \frac{dP_k}{2\pi\hbar} \frac{dP_N}{2\pi\hbar} e^{\frac{i}{\hbar}S_0} \langle m_{n_t} | e^{-\frac{i}{\hbar}\epsilon \hat{h}_m(R_{N-1})} \ldots . e^{-\frac{i}{\hbar}\epsilon \hat{h}_m(R_0)} | m_{n_0} \rangle$$

$$S_0 = \epsilon \sum_{k=1}^{N} \left[P_k \frac{(R_k - R_{k-1})}{\epsilon} - \frac{P_k^2}{2M} \right]$$

Transition amplitudes

$$\langle m_{n_t}|e^{-\frac{i}{\hbar}\epsilon\hat{h}_m(R_{N-1})}....e^{-\frac{i}{\hbar}\epsilon\hat{h}_m(R_0)}|m_{n_0}\rangle =$$
$$\int dq_0 dp_0 r_{t,n_t}(\{R_k\})e^{-i\Theta_{t,n_t}(\{R_k\})} r_{0,n_0} e^{i\Theta_{0,n_0}} G_0$$

Magnitude

$$G_0 = e^{-\frac{1}{2}\sum_\lambda (q_{0,\lambda}^2 + p_{0,\lambda}^2)}$$

$$r_{t,n_t}(\{R_k\}) = \sqrt{q_{t,n_t}^2(\{R_k\}) + p_{t,n_t}^2(\{R_k\})}$$

Phase

$$\Theta_{t,n_t}(\{R_k\}) \; =$$
$$\tan^{-1}\left(\frac{p_{0,n_t}}{q_{0,n_t}}\right) + \int_0^t d\tau h_{n_t,n_t}(R_\tau) + \int_0^t d\tau \sum_{\lambda \neq n_t} \left[h_{n_t,\lambda}(R_\tau) \frac{(p_{\tau n_t} p_{\tau\lambda} + q_{\tau n_t} q_{\tau\lambda})}{(p_{\tau n_t}^2 + q_{\tau n_t}^2)} \right]$$
$$= \; \tan^{-1}\left(\frac{p_{0,n_t}}{q_{0,n_t}}\right) + \int_0^t \theta_{n_t}(R_\tau) d\tau$$

Density matrix propagation: First step

$$\langle R_N n_t|\hat{\rho}(t)|R'_N n'_t\rangle \;=\;$$
$$\sum_{n_0,n'_0}\int dq_0 dp_0 dq'_0 dp'_0 \int dR_0 dR'_0 \int \prod_{k=1}^{N-1} dR_k \frac{dP_k}{2\pi\hbar}\frac{dP_N}{2\pi\hbar}\int \prod_{k=1}^{N-1} dR'_k \frac{dP'_k}{2\pi\hbar}\frac{dP'_N}{2\pi\hbar}$$
$$\times e^{\frac{i}{\hbar}(S_0-S'_0)} r'_{0,n'_0} e^{-i\Theta'_{0,n'_0}} G'_0 r_{0,n_0} e^{i\Theta_{0,n_0}} G_0 \langle R_0 n_0|\hat{\rho}(0)|R'_0 n'_0\rangle$$
$$\times r_{t,n_t}(\{R_k\}) e^{-i\Theta_{t,n_t}(\{R_k\})} r'_{t,n'_t}(\{R'_k\}) e^{i\Theta'_{t,n'_t}(\{R'_k\})}$$

Mean and difference environmental path variables

$$\bar{R}_k \;=\; (R_k + R'_k)/2 \quad Z_k = R_k - R'_k$$
$$\bar{P}_k \;=\; (P_k + P'_k)/2 \quad Y_k = P_k - P'_k$$

Action difference linear in Z & Y

$$(S_0 - S'_0) \;=\; \bar{P}_N Z_N - \bar{P}_1 Z_0 - \sum_{k=1}^{N-1}(\bar{P}_{k+1} - \bar{P}_k) Z_k - \sum_{k=1}^{N}[\frac{\epsilon}{m}\bar{P}_k - (\bar{R}_k - \bar{R}_{k-1})]Y_k$$

truncate phase difference to linear order in path difference

$$\Theta_{t,n_t}(\{\bar{R}_k + Z_k/2\}) - \Theta'_{t,n'_t}(\{\bar{R}_k - Z_k/2\})$$

Sample initial conditions from Wigner density

$$(\hat{\rho})_W^{n_0,n_0'}(\bar{R}_0,\bar{P}_1) = \int dZ_0 \langle \bar{R}_0 + \frac{Z_0}{2} n_0 | \hat{\rho} | \bar{R}_0 - \frac{Z_0}{2} n_0' \rangle e^{-\frac{i}{\hbar}\bar{P}_1 Z_0}$$

First linearized density matrix propagation segment

$$\langle \bar{R}_N + \frac{Z_N}{2} n_t | \hat{\rho}(t) | \bar{R}_N - \frac{Z_N}{2} n_t' \rangle =$$

$$\sum_{n_0,n_0'} \int d\bar{R}_0 dq_0 dp_0 dq_0' dp_0' r'_{0,n_0'} e^{-i\Theta'_{0,n_0'}} G_0' r_{0,n_0} e^{i\Theta_{0,n_0}} G_0$$

$$\times \int \prod_{k=1}^{N-1} d\bar{R}_k \frac{d\bar{P}_k}{2\pi} \frac{d\bar{P}_N}{2\pi} [\hat{\rho}]_W^{n_0,n_0'}(\bar{R}_0,\bar{P}_1) e^{i\bar{P}_N Z_N}$$

$$\times r_{t,n_t}(\{\bar{R}_k\}) r'_{t,n_t'}(\{\bar{R}_k\}) e^{-i\epsilon \sum_{k=1}^{N} (\theta_{n_t}(\bar{R}_k) - \theta_{n_t'}(\bar{R}_k))}$$

$$\prod_{k=1}^{N-1} \delta\left(\frac{\bar{P}_{k+1}-\bar{P}_k}{\epsilon} - F_k^{n_t,n_t'}\right) \prod_{k=1}^{N} \delta\left(\frac{\bar{P}_k}{M} - \frac{\bar{R}_k - \bar{R}_{k-1}}{\epsilon}\right)$$

Different trajectory forces for different final density matrix elements

$$F_k^{n_t,n'_t} = -\frac{1}{2}\left\{\nabla_{\bar{R}_k} h_{n_t,n_t}(\bar{R}_k) + \nabla_{\bar{R}_k} h_{n'_t,n'_t}(\bar{R}_k)\right\}$$
$$-\frac{1}{2}\sum_{\lambda\neq n_t}\nabla_{\bar{R}_k} h_{n_t,\lambda}(\bar{R}_k)\left\{\frac{(p_{n_t k}p_{\lambda k} + q_{n_t k}q_{\lambda k})}{(p^2_{n_t k} + q^2_{n_t k})}\right\}$$
$$-\frac{1}{2}\sum_{\lambda\neq n'_t}\nabla_{\bar{R}_k} h_{n'_t,\lambda}(\bar{R}_k)\left\{\frac{(p'_{n'_t k}p'_{\lambda k} + q'_{n'_t k}q'_{\lambda k})}{(p'^2_{n'_t k} + q'^2_{n'_t k})}\right\}$$

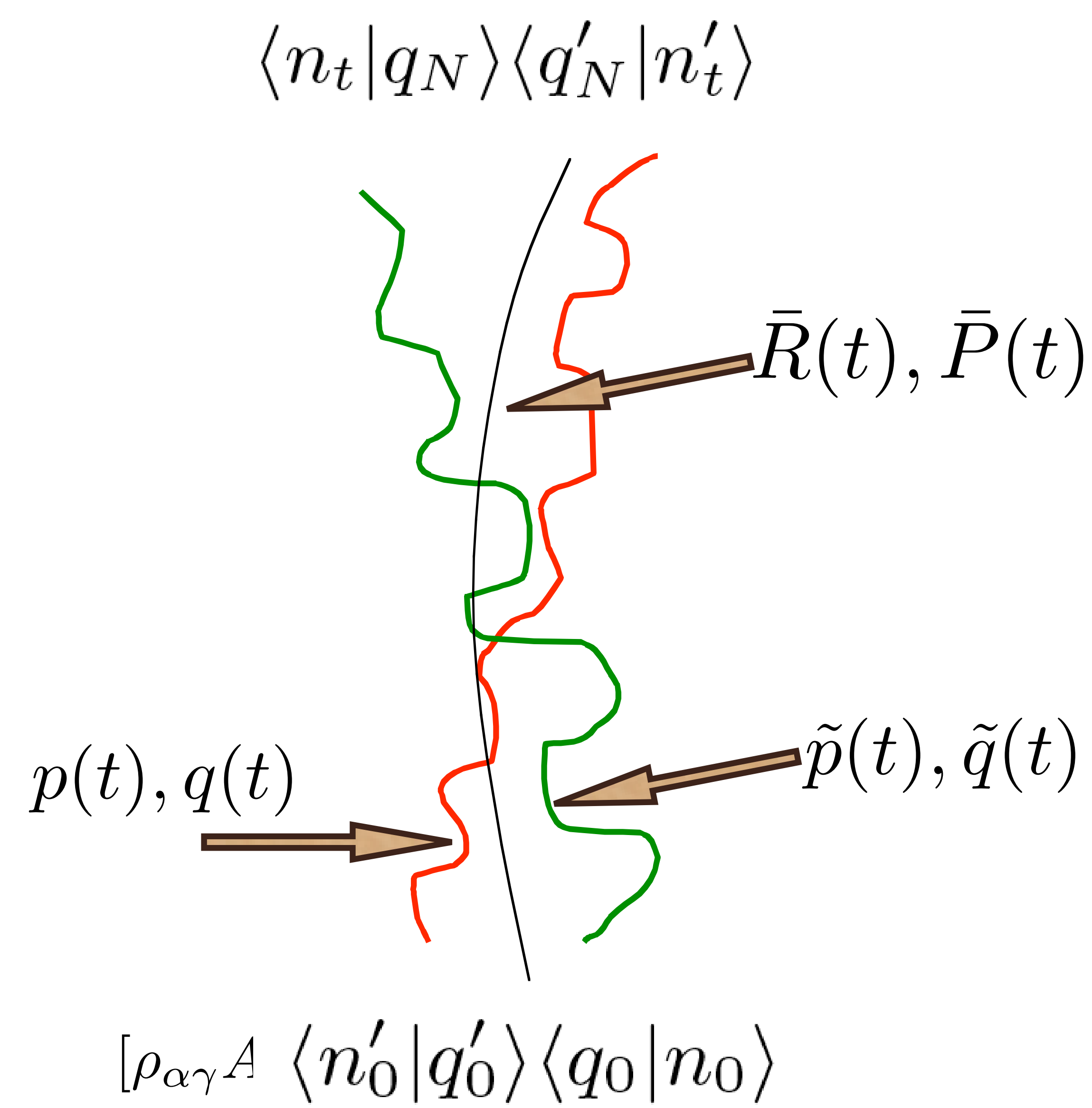

$$\langle \bar{R}_{2N} + \frac{Z_{2N}}{2} n_{2t}|\hat{\rho}(2t)|\bar{R}_{2N} - \frac{Z_{2N}}{2} n'_{2t}\rangle =$$
$$\sum_{n_t,n'_t}\int d\bar{R}_N dZ_N dq_N dp_N dq'_N dp'_N r'_{t,n'_t} e^{-i\Theta'_{t,n'_t}} G'_t r_{t,n_t} e^{i\Theta_{t,n_t}} G_t$$
$$\times\int\prod_{k=N+1}^{2N-1} d\bar{R}_k \frac{d\bar{P}_k}{2\pi}\frac{d\bar{P}_{2N}}{2\pi}\langle \bar{R}_N + \frac{Z_N}{2} n_t|\hat{\rho}(t)|\bar{R}_N - \frac{Z_N}{2} n'_t\rangle e^{i\bar{P}_{N+1}Z_N}$$
$$\times e^{-i\bar{P}_{2N+1}Z_{2N}} r_{2t,n_{2t}}(\{\bar{R}_k\}) r'_{2t,n'_{2t}}(\{\bar{R}_k\}) e^{-i\epsilon\sum_{k=N+1}^{2N}(\theta_{n_{2t}}(\bar{R}_k) - \theta_{n'_{2t}}(\bar{R}_k))}$$
$$\times\prod_{k=N+1}^{2N-1}\delta\left(\frac{\bar{P}_{k+1} - \bar{P}_k}{\epsilon} - F_k^{n_{2t},n'_{2t}}\right)\prod_{k=N+1}^{2N}\delta\left(\frac{\bar{P}_k}{M} - \frac{\bar{R}_k - \bar{R}_{k-1}}{\epsilon}\right)$$

Second linearized density matrix propagation segment

$$
\begin{aligned}
\langle \bar{R}_{2N} + \frac{Z_{2N}}{2} n_{2t} | \hat{\rho}(2t) | \bar{R}_{2N} - \frac{Z_{2N}}{2} n'_{2t} \rangle = \int \prod_{k=N+1}^{2N-1} d\bar{R}_k \frac{d\bar{P}_k}{2\pi} \frac{d\bar{P}_{2N}}{2\pi} e^{i\bar{P}_{2N} Z_{2N}} \\
\times r_{2t,n_{2t}}(\{\bar{R}_k\}) r'_{2t,n'_{2t}}(\{\bar{R}_k\}) e^{-i\epsilon \sum_{k=N+1}^{2N} (\theta_{n_{2t}}(\bar{R}_k) - \theta_{n'_{2t}}(\bar{R}_k))} \\
\times \prod_{k=N+1}^{2N-1} \delta\left(\frac{\bar{P}_{k+1} - \bar{P}_k}{\epsilon} - F_k^{n_{2t},n'_{2t}} \right) \prod_{k=N+1}^{2N} \delta\left(\frac{\bar{P}_k}{M} - \frac{\bar{R}_k - \bar{R}_{k-1}}{\epsilon} \right) \\
\sum_{n_t,n'_t} \int d\bar{R}_N \frac{d\bar{P}_N}{2\pi} dq_N dp_N dq'_N dp'_N r'_{t,n'_t} e^{-i\Theta'_{t,n'_t}} G'_t r_{t,n_t} e^{i\Theta_{t,n_t}} G_t \\
\times \delta(\bar{P}_N - \bar{P}_{N+1}) \delta\left(\frac{\bar{P}_N}{M} - \frac{\bar{R}_N - \bar{R}_{N-1}}{\epsilon} \right) \\
\times \int \prod_{k=1}^{N-1} d\bar{R}_k \frac{d\bar{P}_k}{2\pi} r_{t,n_t}(\{\bar{R}_k\}) r'_{t,n'_t}(\{\bar{R}_k\}) e^{-i\epsilon \sum_{k=1}^{N} (\theta_{n_t}(\bar{R}_k) - \theta_{n'_t}(\bar{R}_k))} \\
\times \prod_{k=1}^{N-1} \delta\left(\frac{\bar{P}_{k+1} - \bar{P}_k}{\epsilon} - F_k^{n_t,n'_t} \right) \prod_{k=1}^{N} \delta\left(\frac{\bar{P}_k}{M} - \frac{\bar{R}_k - \bar{R}_{k-1}}{\epsilon} \right) \\
\times \sum_{n_0,n'_0} \int d\bar{R}_0 dq_0 dp_0 dq'_0 dp'_0 r'_{0,n'_0} e^{-i\Theta'_{0,n'_0}} G'_0 r_{0,n_0} e^{i\Theta_{0,n_0}} G_0 [\hat{\rho}]_W^{n_0,n'_0}(\bar{R}_0, \bar{P}_1)
\end{aligned}
$$

An Algorithm:

$$(\sum_{n_t,n'_t} \int dq_N dp_N dq'_N dp'_N)_{n_{2t},n'_{2t}}$$

Intermediate mapping integrals performed by steepest descent

$$(p^o_{n_0}, q^o_{n_0}) \;=\; (1/\sqrt{2}, 1/\sqrt{2}) \quad (p^u_{n_0}, q^u_{n_0}) \;=\; (0,0)$$

Intermediate state sums performed by importance sampled MC

$$r_{\tau,n_t} r'_{\tau,n'_t} \exp[-i \int_0^\tau d\tau' (\theta_{n_t}(\tau') - \theta_{n'_t}(\tau'))]$$

$$M_{n_t,n'_t} = r_{t,n_t} r'_{t,n'_t} / \mathcal{N}(t) \qquad \mathcal{N}(t) = \sum_{n_t,n'_t} r_{t,n_t} r'_{t,n'_t}$$

Trajectory weights

$$\Omega_K \;=\; \left\{ \prod_{k=1}^{K-1} \mathcal{N}(kt) \exp[-i \int_{(k-1)t}^{kt} d\tau' (\theta_{n_{kt}}(\tau') - \theta_{n_{kt'}}(\tau'))] \right\}$$

$$\times \;\; r_{Kt,n_{Kt}} r'_{Kt,n'_{Kt}} \exp[-i \int_{(K-1)t}^{Kt} d\tau' (\theta_{n_{Kt}}(\tau') - \theta_{n'_{Kt}}(\tau'))]$$

J. Chem. Phys. 114106 (2008)

Iterative Scheme LAND-Map

Dunkel et.al 2008

$$\langle \hat{O} \rangle_{2t} = Tr\{\hat{\rho}(2t)\hat{O}\}$$
$$= \int dR_{2t} \int dR'_{2t} \sum_{n_{2t}} \sum_{n'_{2t}} \langle R_{2t} n_{2t} | \hat{\rho}(2t) | R'_{2t} n'_{2t} \rangle \langle R'_{2t} n'_{2t} | \hat{O} | R_{2t} n_{2t} \rangle$$

$$\hat{\rho}(2t) = e^{-\frac{i}{\hbar}\hat{H}t} e^{-\frac{i}{\hbar}\hat{H}t} \hat{\rho}(0) e^{\frac{i}{\hbar}\hat{H}t} e^{\frac{i}{\hbar}\hat{H}t}$$

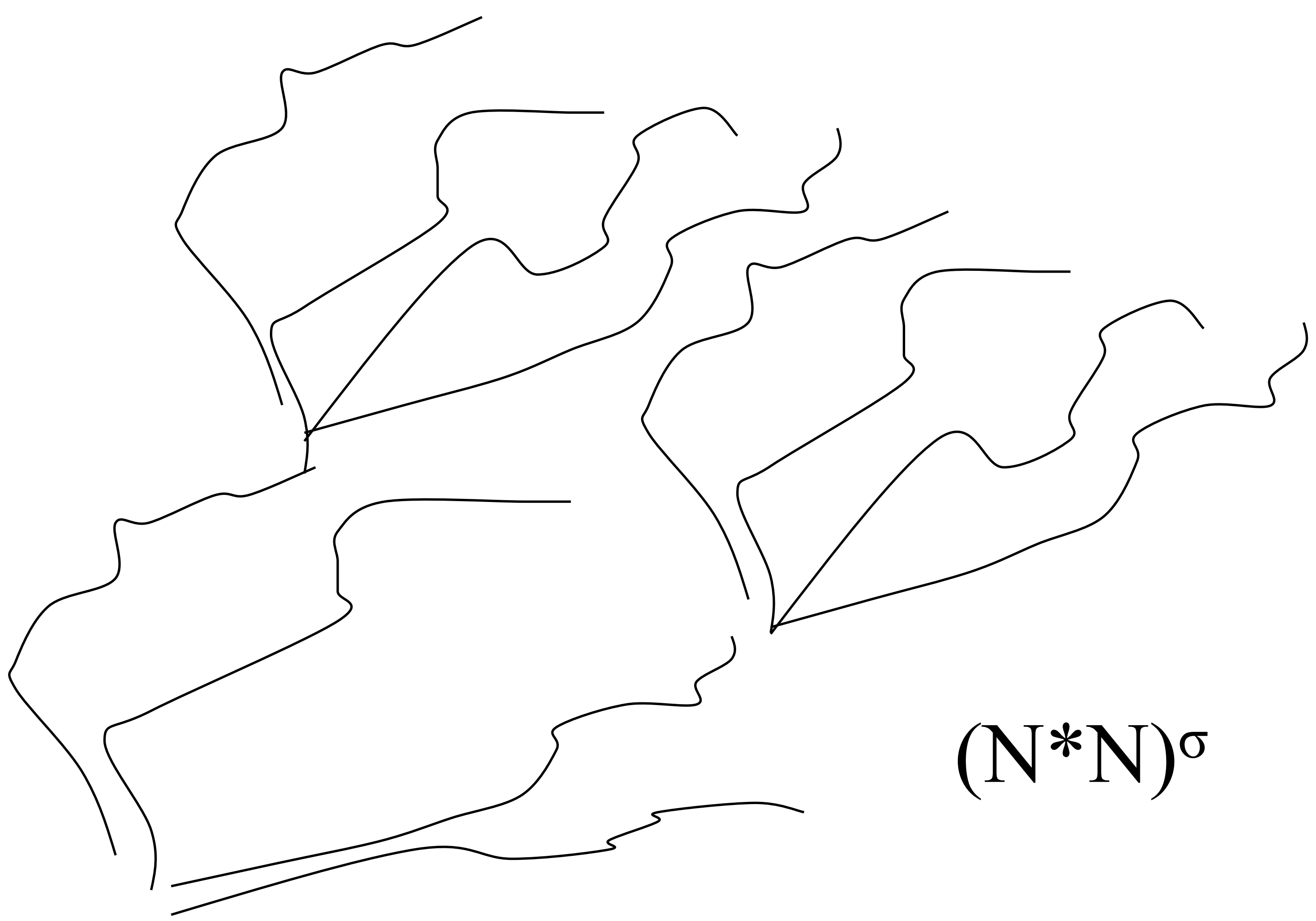

$(N*N)^{\sigma}$

$$\langle \hat{O} \rangle_{2t} = \sum_{n_{2t}, n'_{2t}} \int \prod_{k=N+1}^{2N} d\bar{R}_k \frac{d\bar{P}_k}{2\pi\hbar} O^W_{n'_{2t}, n_{2t}}(\bar{R}_{2N}, \bar{P}_{2N})$$
$$\times \quad r_{2t,n_{2t}}(\{\bar{R}_k\}) r'_{2t,n'_{2t}}(\{\bar{R}_k\}) e^{-i\epsilon \sum_{k=N+1}^{2N} (\theta_{n_{2t}}(\bar{R}_k) - \theta_{n'_{2t}}(\bar{R}_k))}$$
$$\times \quad \prod_{k=N+1}^{2N-1} \delta\left(\frac{\bar{P}_{k+1} - \bar{P}_k}{\epsilon} - F_k^{n_{2t}, n'_{2t}}\right) \prod_{k=N+1}^{2N} \delta\left(\frac{\bar{P}_k}{M} - \frac{\bar{R}_k - \bar{R}_{k-1}}{\epsilon}\right)$$
$$\sum_{n_t, n'_t} \int d\bar{R}_N \frac{d\bar{P}_N}{2\pi\hbar} dq_N dp_N dq'_N dp'_N r'_{t,n'_t} e^{i\Theta'_{t,n'_t}} G'_t r_{t,n_t} e^{-i\Theta_{t,n_t}} G_t$$
$$\times \quad \delta(\bar{P}_N - \bar{P}_{N+1}) \delta\left(\frac{\bar{P}_N}{M} - \frac{\bar{R}_N - \bar{R}_{N-1}}{\epsilon}\right)$$
$$\times \quad \int \prod_{k=1}^{N-1} d\bar{R}_k \frac{d\bar{P}_k}{2\pi\hbar} r_{t,n_t}(\{\bar{R}_k\}) r'_{t,n'_t}(\{\bar{R}_k\}) e^{-i\epsilon \sum_{k=1}^{N} (\theta_{n_t}(\bar{R}_k) - \theta_{n'_t}(\bar{R}_k))}$$
$$\times \quad \prod_{k=1}^{N-1} \delta\left(\frac{\bar{P}_{k+1} - \bar{P}_k}{\epsilon} - F_k^{n_t, n'_t}\right) \prod_{k=1}^{N} \delta\left(\frac{\bar{P}_k}{M} - \frac{\bar{R}_k - \bar{R}_{k-1}}{\epsilon}\right)$$
$$\times \quad \sum_{n_0, n'_0} \int d\bar{R}_0 dq_0 dp_0 dq'_0 dp'_0 r'_{0,n'_0} e^{i\Theta'_{0,n'_0}} G'_0 r_{0,n_0} e^{-i\Theta_{0,n_0}} G_0(\hat{\rho})_W^{n_0, n'_0}(\bar{R}_0, \bar{P}_1)$$

Algorithm: Iterative Scheme LAND-Map

$$M_{n_t,n'_t} = r_{t,n_t} r'_{t,n'_t} / \sum_{n_t,n'_t} r_{t,n_t} r'_{t,n'_t}$$

$$C_{m_t,m'_t} = \sum_{n_t=1}^{m_t} \sum_{n'_t=1}^{m'_t} M_{n_t,n'_t}$$

$$\xi \in (0,1]$$

$$> C_{m_t,m'_t} \qquad \xi$$

$$m_t = n_t^* \text{ and } m'_t = n'^*_t$$

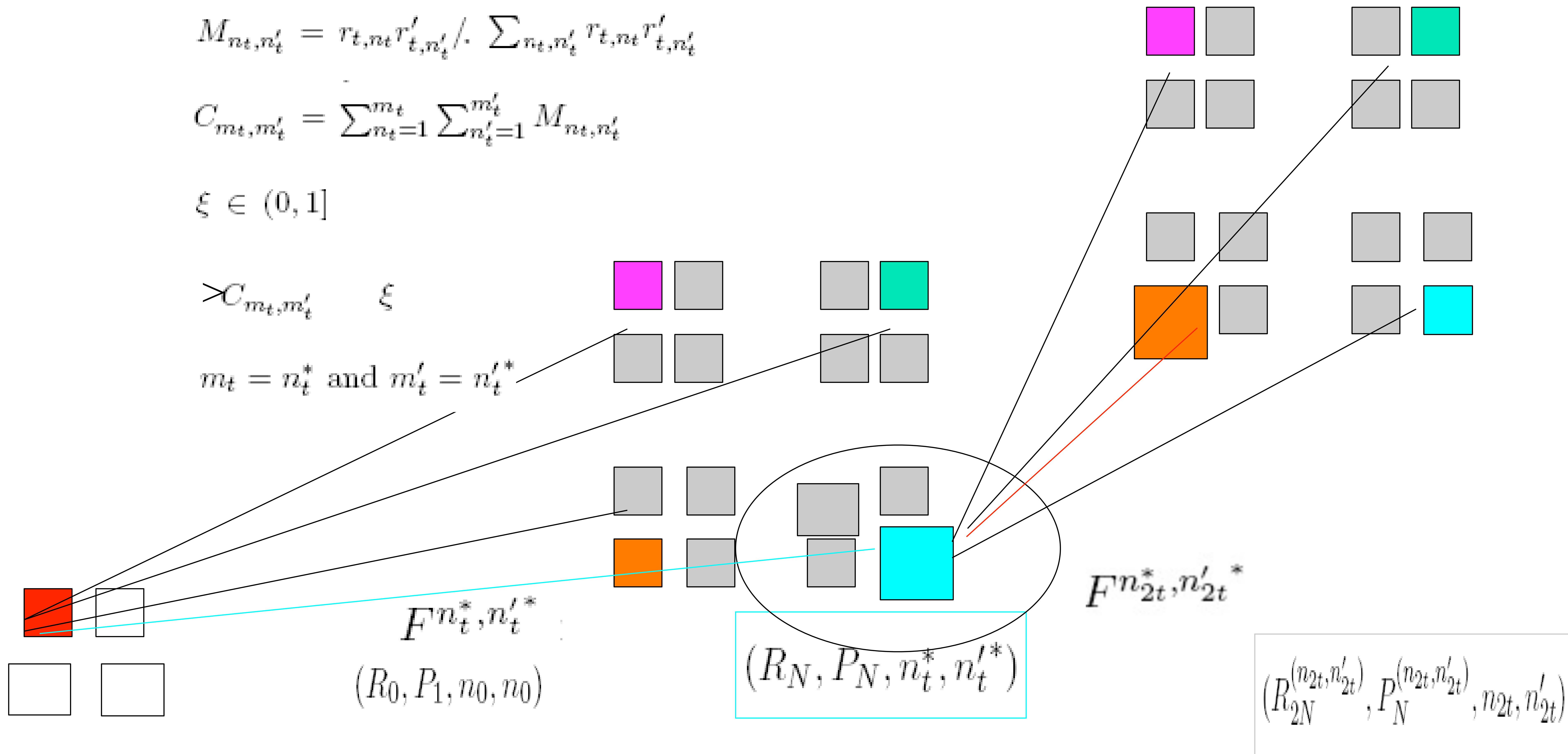

Algorithm: Iterative Scheme LAND-Map

$$M_{n_t,n'_t} = r_{t,n_t} r'_{t,n'_t} / \sum_{n_t,n'_t} r_{t,n_t} r'_{t,n'_t}$$

$$C_{m_t,m'_t} = \sum_{n_t=1}^{m_t} \sum_{n'_t=1}^{m'_t} M_{n_t,n'_t}$$

$$\xi \in (0,1]$$

$$> C_{m_t,m'_t} \qquad \xi$$

$$m_t = n_t^* \text{ and } m'_t = n'^*_t$$

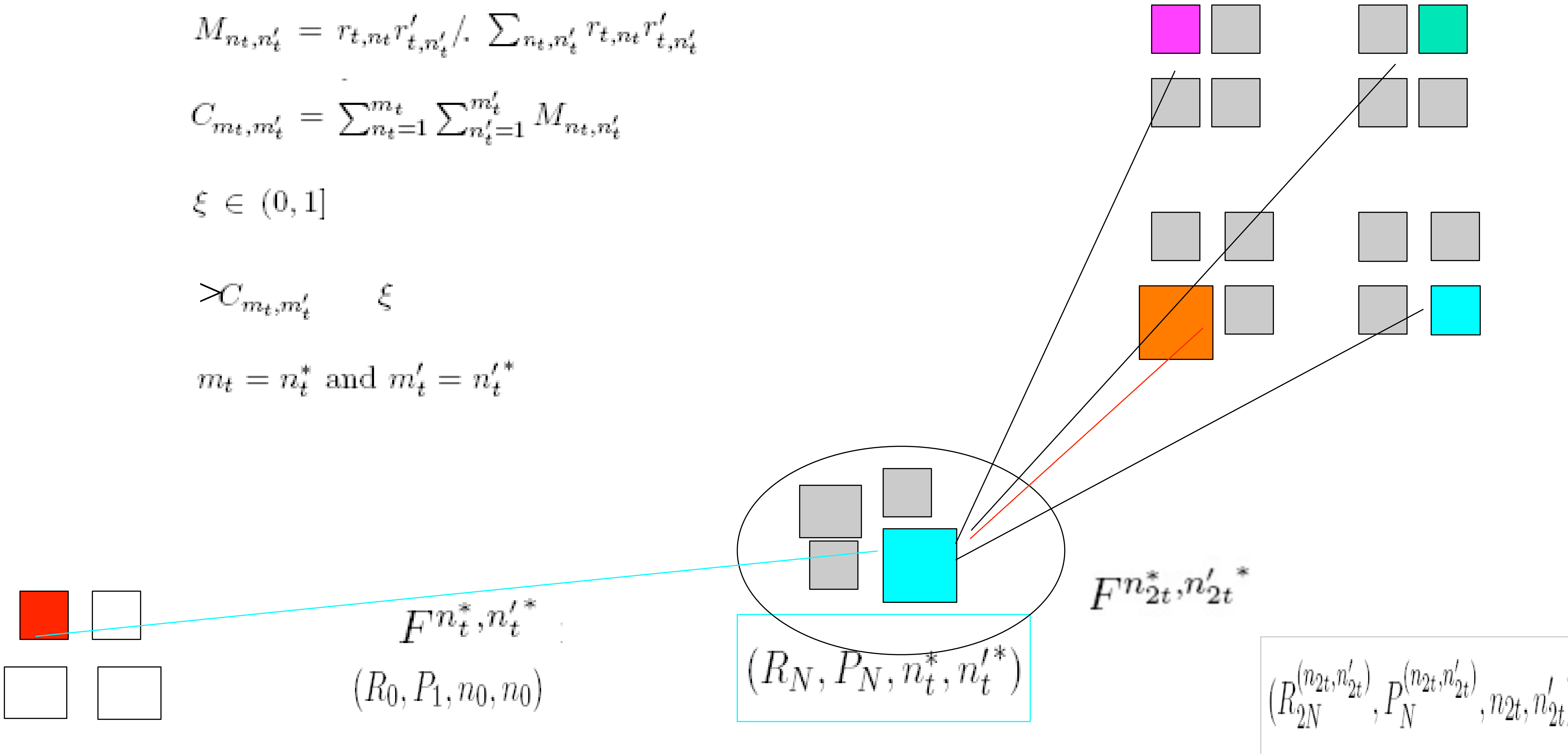

Algorithm: Iterative Scheme LAND-Map

$M_{n_t,n'_t} = r_{t,n_t} r'_{t,n'_t} / \sum_{n_t,n'_t} r_{t,n_t} r'_{t,n'_t}$

$C_{m_t,m'_t} = \sum_{n_t=1}^{m_t} \sum_{n'_t=1}^{m'_t} M_{n_t,n'_t}$

$\xi \in (0,1]$

$> C_{m_t,m'_t} \quad \xi$

$m_t = n_t^*$ and $m'_t = n'^*_t$

$\mathcal{N}(t) \exp[-i \int_0^t d\tau (\theta_{n_t}(\tau) - \theta_{n'_t}(\tau))$

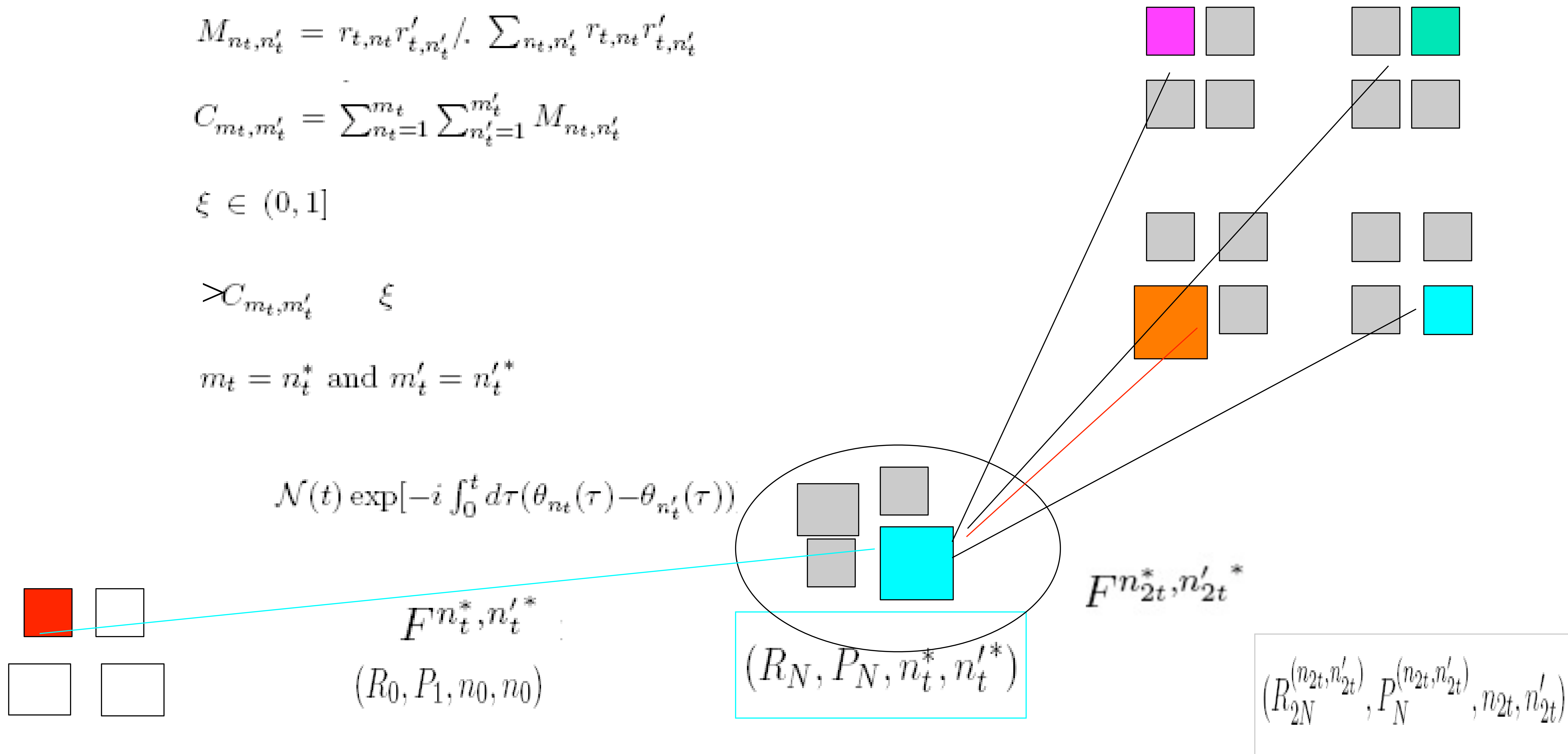

Algorithm: Iterative Scheme LAND-Map

$$M_{n_t,n'_t} = r_{t,n_t} r'_{t,n'_t} / \sum_{n_t,n'_t} r_{t,n_t} r'_{t,n'_t}$$

$$C_{m_t,m'_t} = \sum_{n_t=1}^{m_t} \sum_{n'_t=1}^{m'_t} M_{n_t,n'_t}$$

$$\xi \in (0,1]$$

$$> C_{m_t,m'_t} \qquad \xi$$

$$m_t = n^*_t \text{ and } m'_t = n'^*_t$$

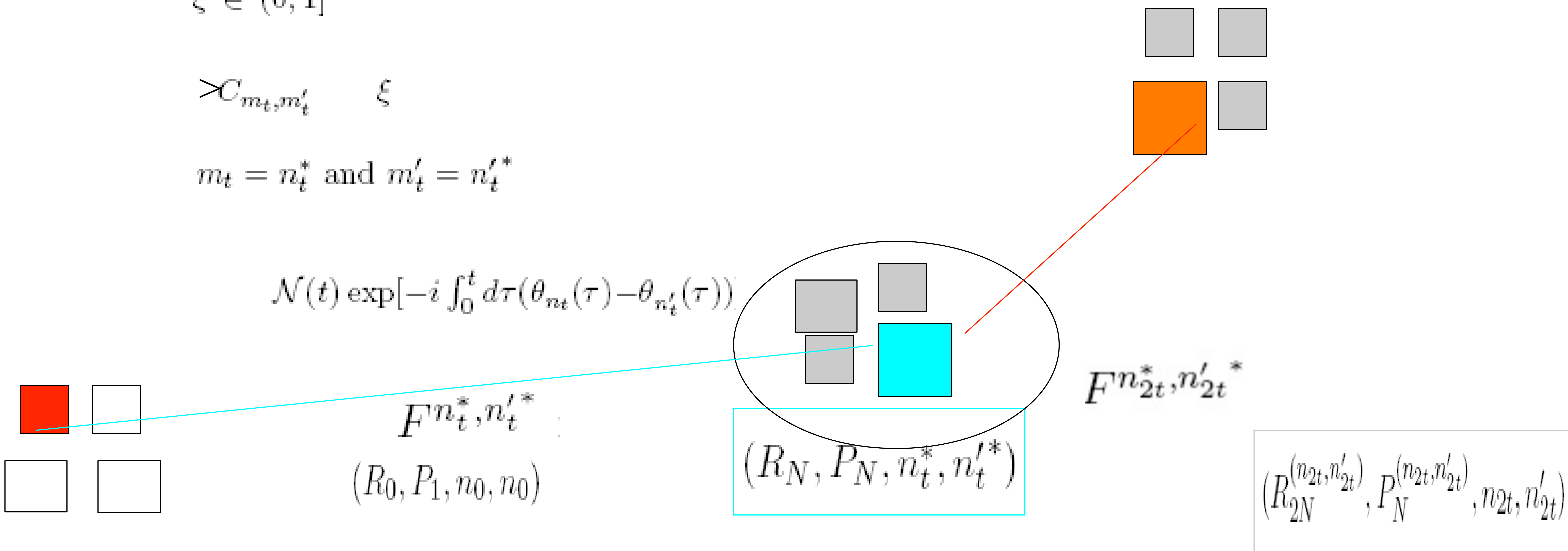

Algorithm: Iterative Scheme LAND-Map

$$M_{n_t,n'_t} = r_{t,n_t} r'_{t,n'_t} / \sum_{n_t,n'_t} r_{t,n_t} r'_{t,n'_t}$$

$$C_{m_t,m'_t} = \sum_{n_t=1}^{m_t} \sum_{n'_t=1}^{m'_t} M_{n_t,n'_t}$$

$$\xi \in (0,1]$$

$$> C_{m_t,m'_t} \qquad \xi$$

$$m_t = n_t^* \text{ and } m'_t = n'^*_t$$

$$\mathcal{N}(2t)\mathcal{N}(t)\exp[-i\int_t^{2t} d\tau(\theta_{n^*_{2t}}(\tau) - \theta_{n^{*\prime}_{2t}}(\tau))]\exp[-i\int_0^t d\tau(\theta_{n^*_t}(\tau) - \theta_{n^{*\prime}_t}(\tau))]$$

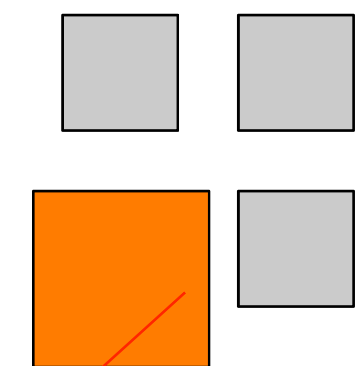

$$\mathcal{N}(t)\exp[-i\int_0^t d\tau(\theta_{n_t}(\tau) - \theta_{n'_t}(\tau))$$

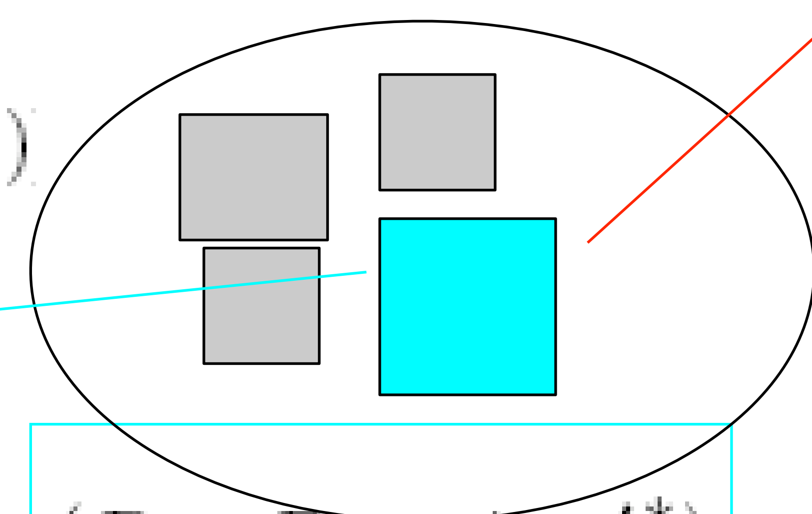

$$F^{n^*_{2t}, n'^*_{2t}}$$

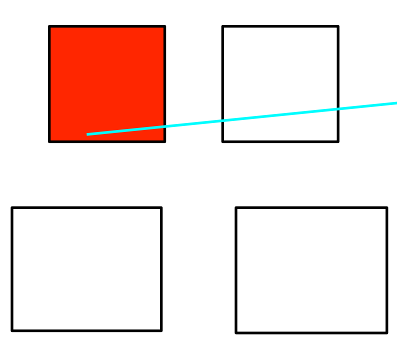

$$F^{n^*_t, n'^*_t}$$

$$(R_0, P_1, n_0, n_0)$$

$$(R_N, P_N, n^*_t, n'^*_t)$$

$$(R_{2N}^{(n_{2t},n'_{2t})}, P_N^{(n_{2t},n'_{2t})}, n_{2t}, n'_{2t})$$

Sampling different density matrix elements allows forward and backward paths to deviate at longer times when phases of different trajectory segment combinations are added coherently

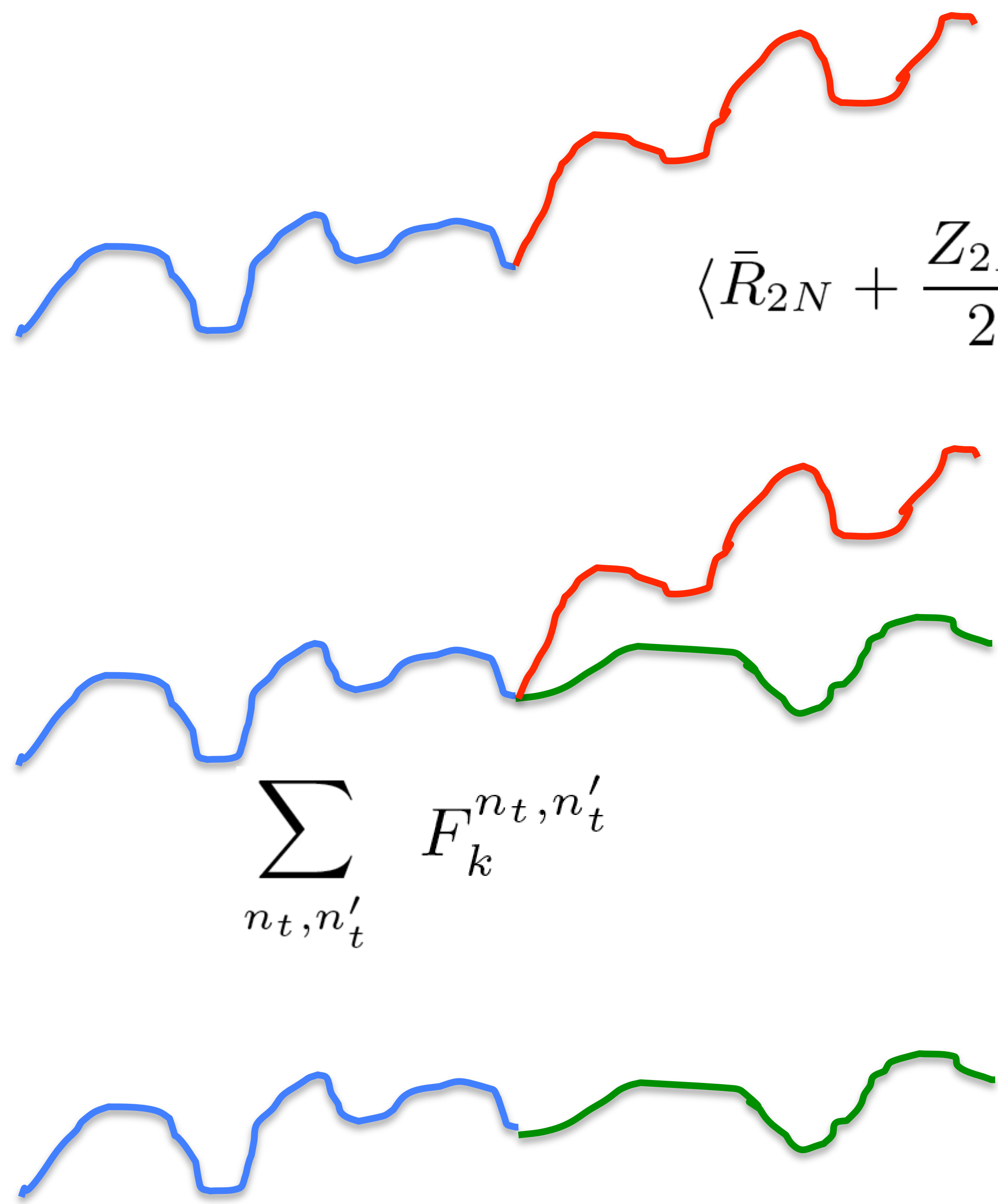

$$\langle \bar{R}_{2N} + \frac{Z_{2N}}{2} n_{2t} | \hat{\rho}(2t) | \bar{R}_{2N} - \frac{Z_{2N}}{2} n'_{2t} \rangle$$

$$F_k^{n_{2t}, n'_{2t}}$$

$$\sum_{n_t, n'_t} F_k^{n_t, n'_t}$$

1D Nonadiabatic scattering models

Tully I: 5-15 hop attempt, $N_{traj} = 5\times10^{5}$

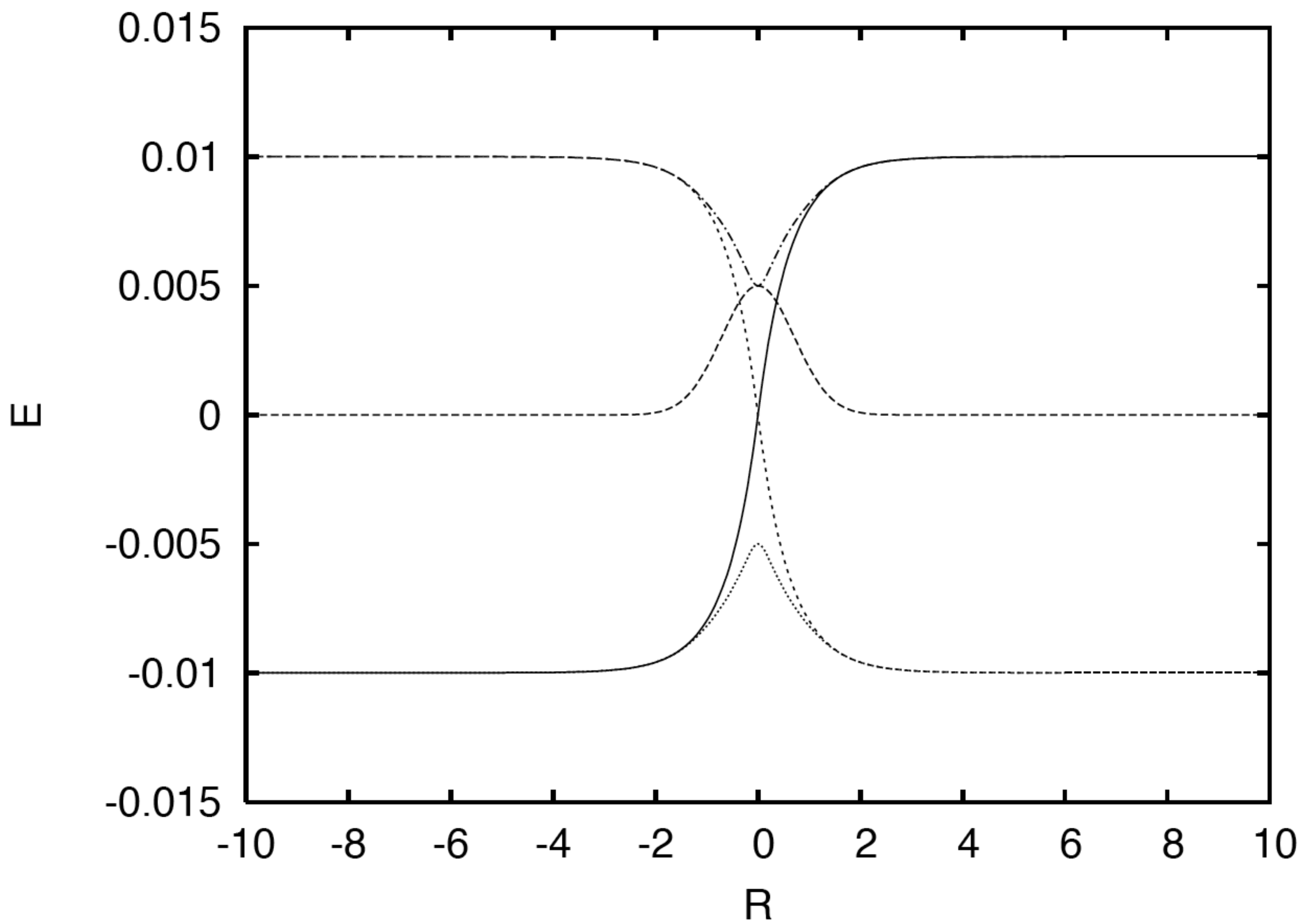

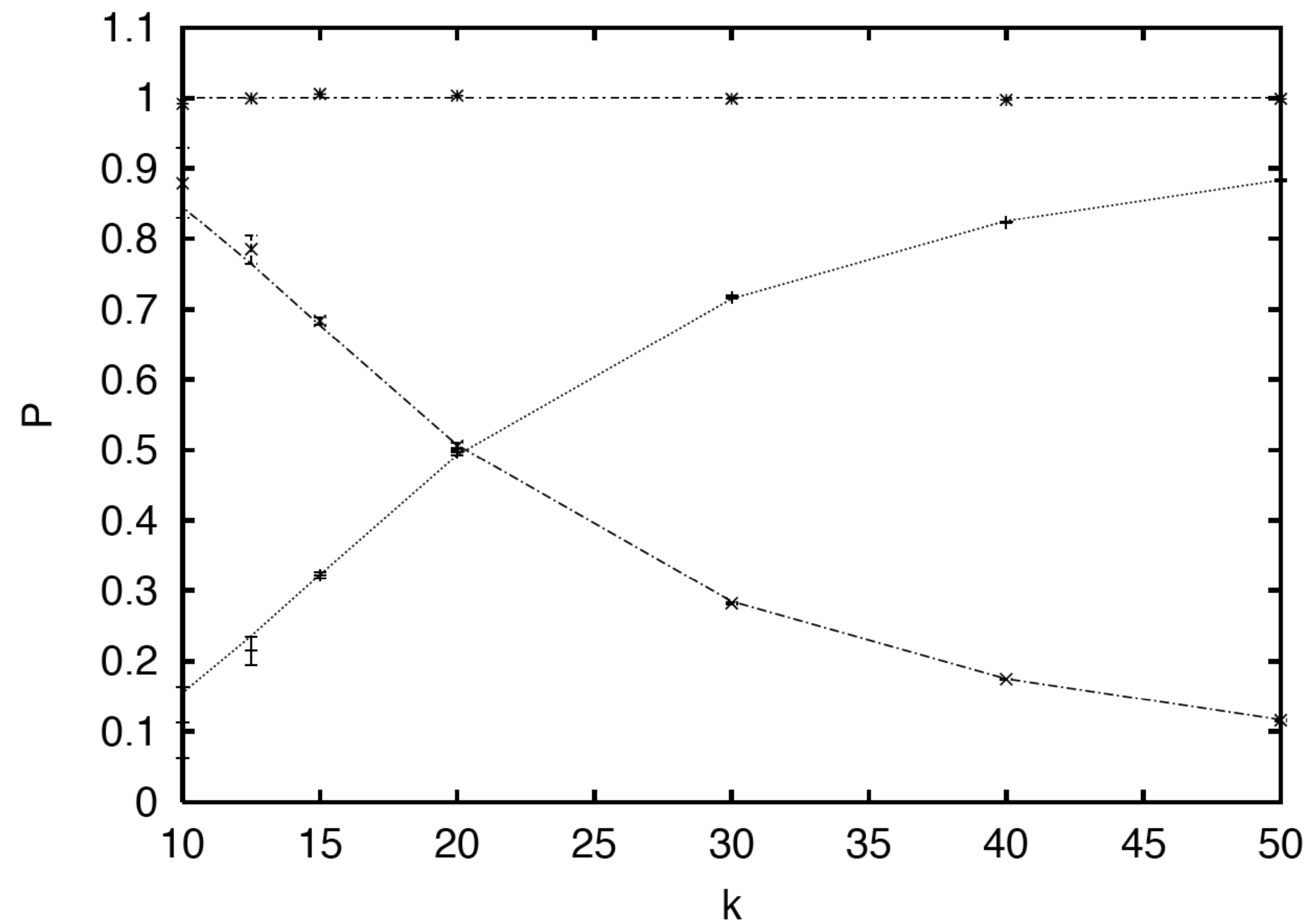

Stuckelberg Scattering model

Tully II: 10-20 hop attempt, N_{traj}= 1x10 ^{6}

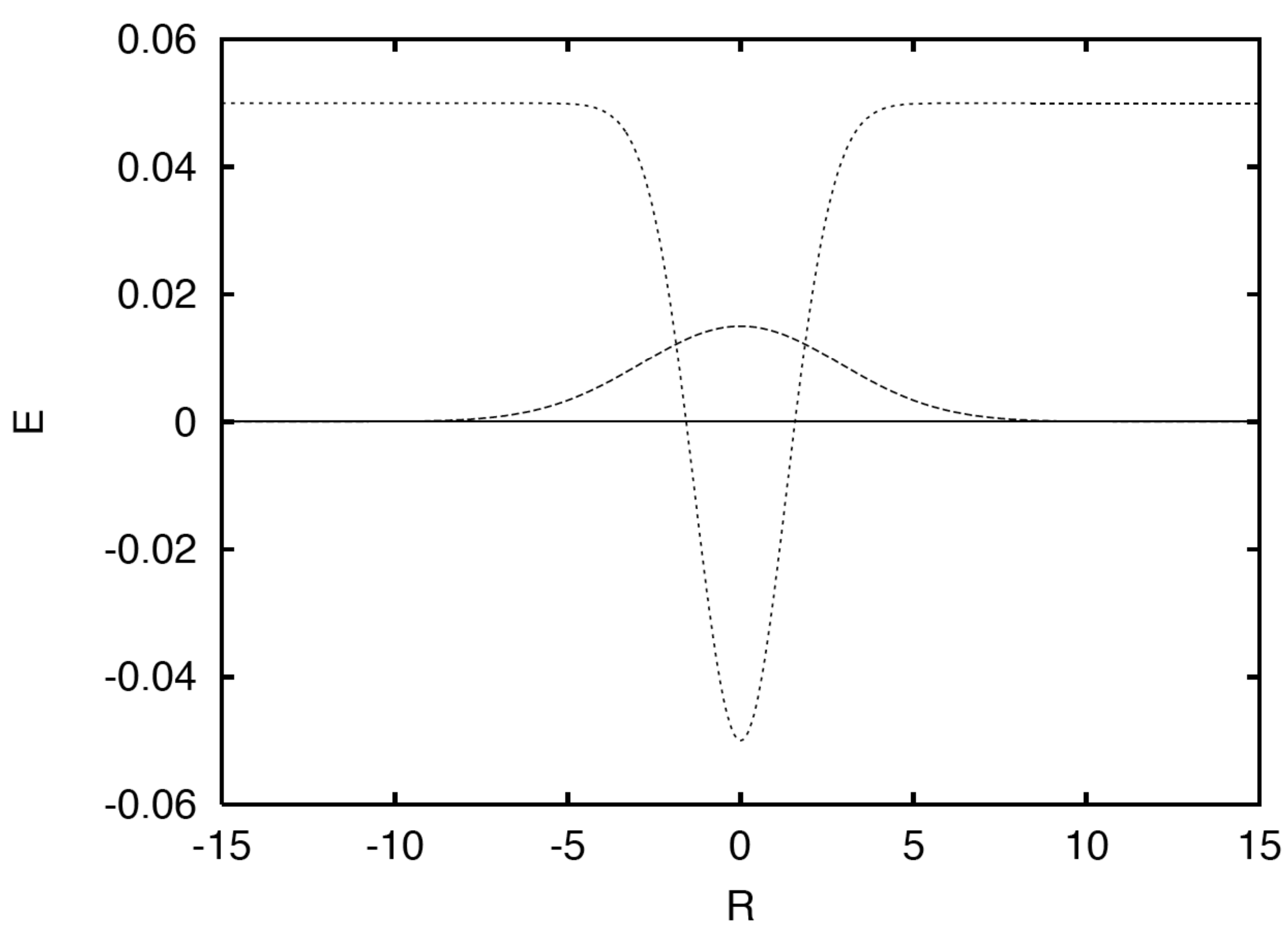

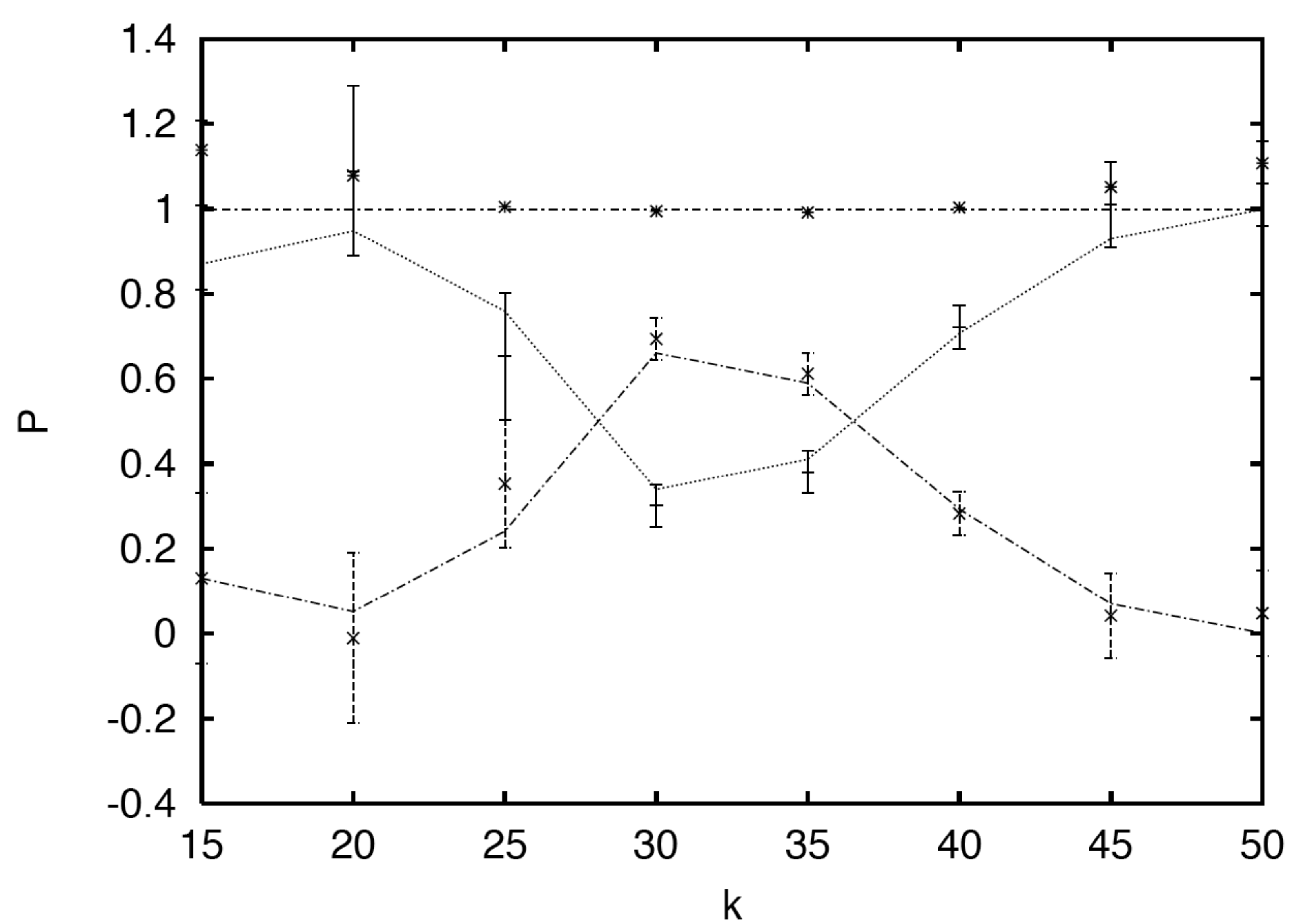

Time dependence of density matrix elements for Stuekelberg scattering k=30

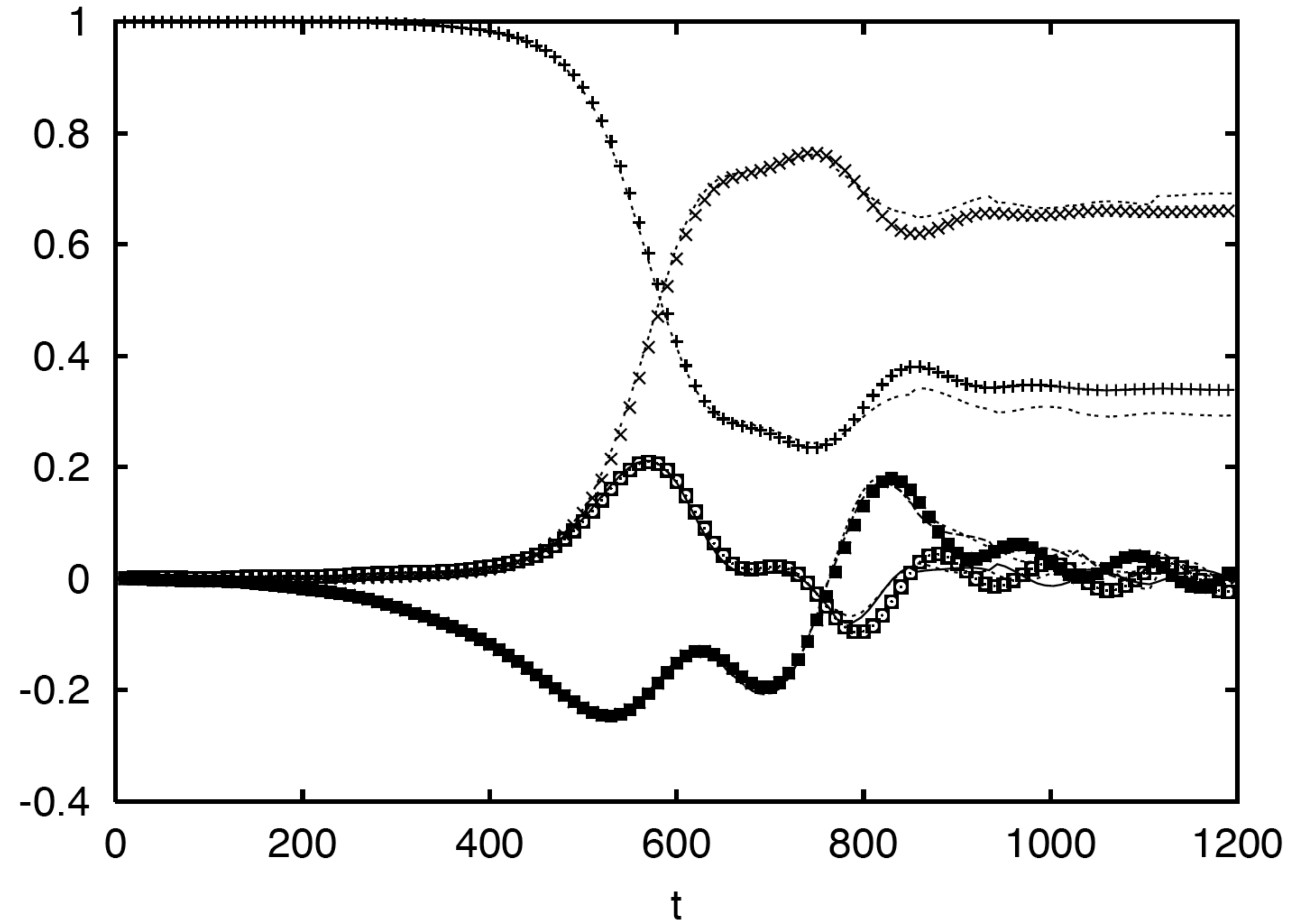

Trajectory weight distributions for Stuekelberg scattering k=30

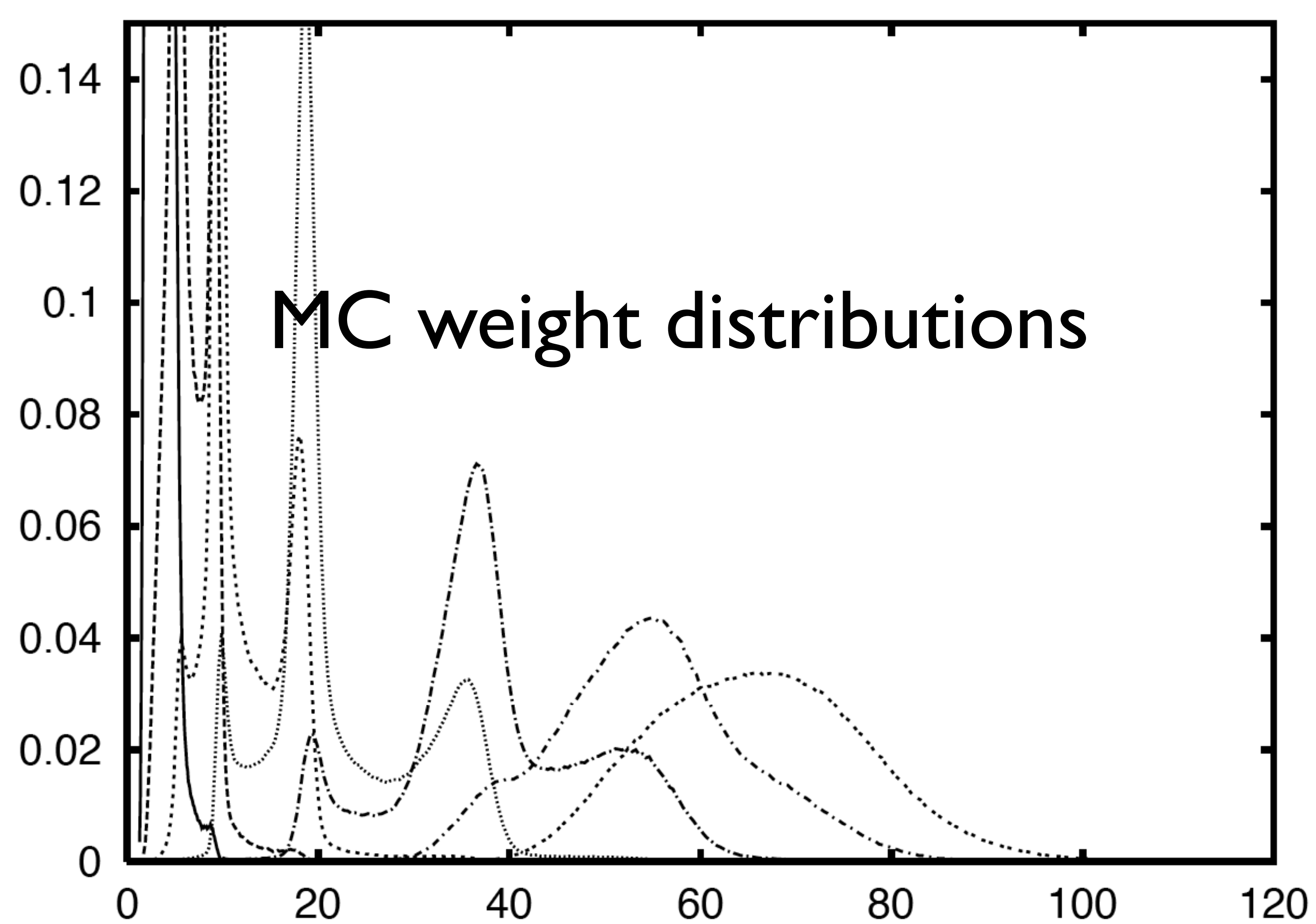

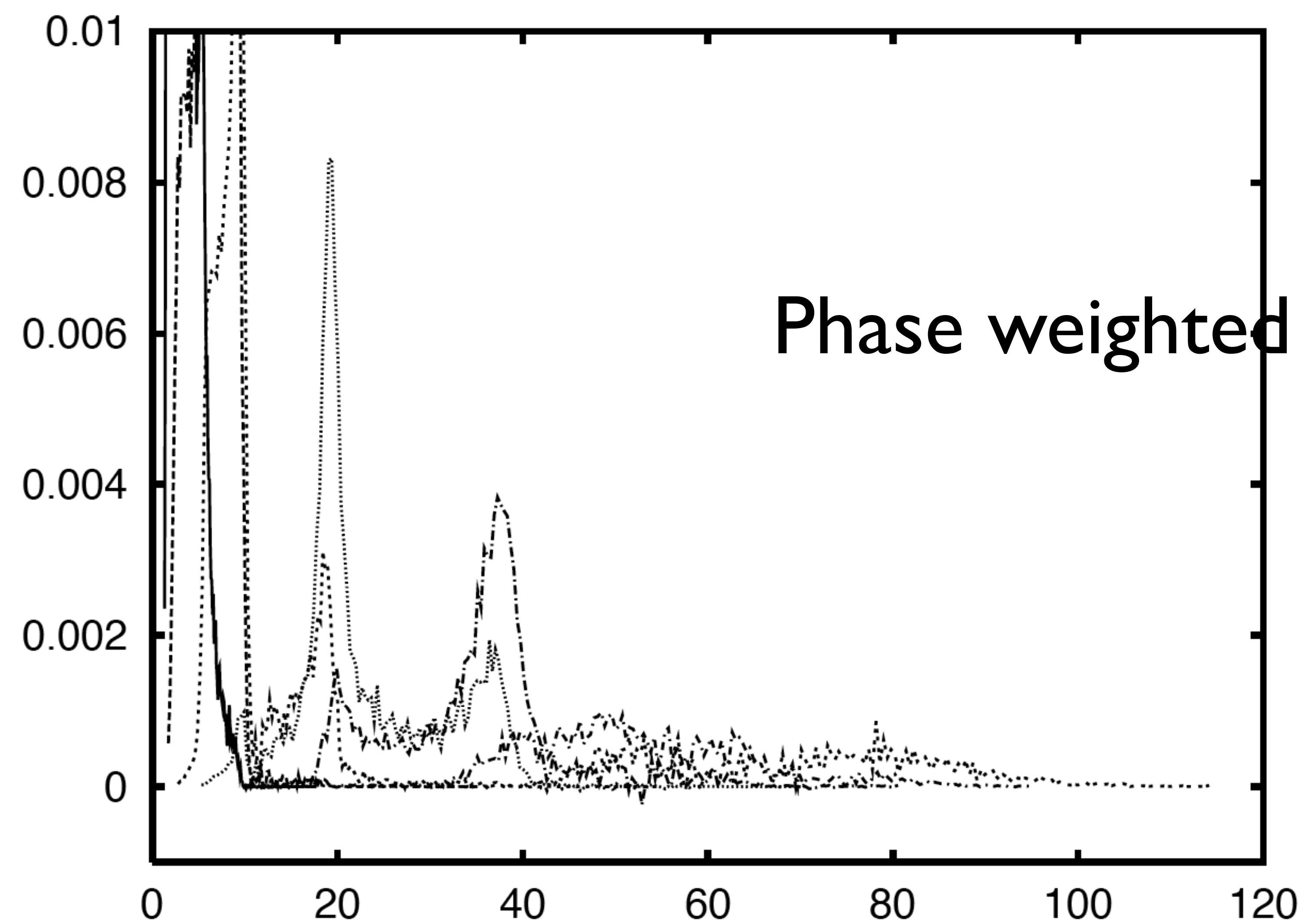

Three Coupled Morse Molecular Photodissociation Model

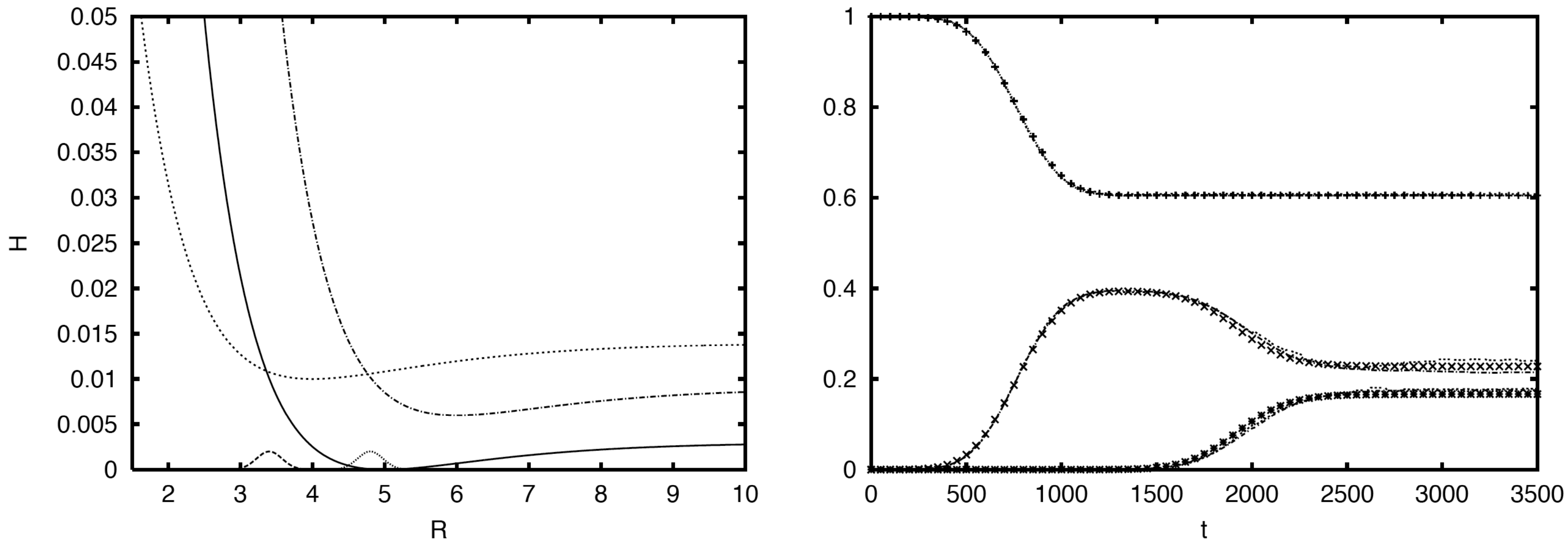

40 hop attempts, $N_{traj} = 5x10^4, 5x10^5$

Asymmetric spin Boson

$$\hat{\rho}(0) = \hat{\rho}_s(0)\hat{\rho}_b(0)$$

$$H = \frac{1}{2}\sum_{j=1}^{M}(P^2 + \omega^2 R^2) + \epsilon\hat{\sigma}_z + \hat{\sigma}_z\sum_{j=1}^{M} \mathsf{C_j} R_j - \Omega\hat{\sigma}_x$$

$$J(\omega) = \xi\omega e^{-\omega/\omega_c}$$

$$J(\omega) = \frac{\pi}{2}\sum_k \frac{C_k^2}{M_B \Omega_k}\delta(\omega - \Omega_k)$$

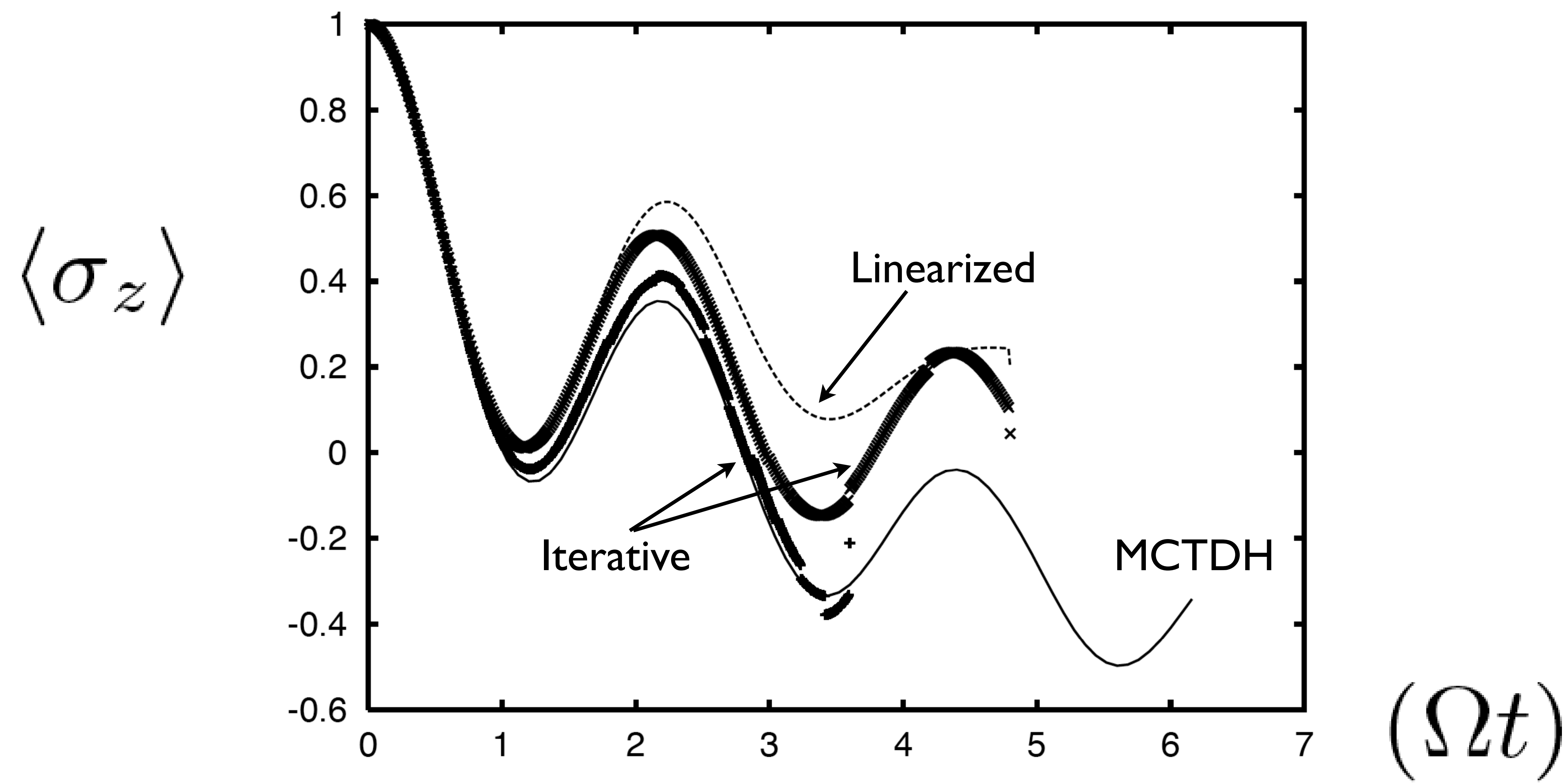

FIG. 9: Population difference $\langle\sigma_z\rangle$ as a function of reduced time (Ωt) for the asymmetric spin-boson with $\xi = 0.13$, $\Omega = 0.4$, $\beta = 12.5$, and $\epsilon = 0.4$, modeled using a discrete bath of 10 oscillators with frequencies sampled from the exponential distribution $\omega_c = 1$ and $\omega_{max} = 3$ (see text). Solid curve gives exact results obtained from MCTDH calculations, dashed curve are linearized dynamics calculations for the full time interval. "×" symbols present results obtained with the iterative linearized scheme using a hop attempt rate of ~ 1.6, "+" symbols give results using a hop attempt rate of ~ 5.5

Symmetric spin Boson

$$H = \frac{1}{2}\sum_{j=1}^{M}(P^2 + \omega^2 R^2) + \cancel{\epsilon}\hat{\sigma}_z + \hat{\sigma}_z \sum_{j=1}^{M} C_j R_j - \Omega\hat{\sigma}_x$$

$$\hat{\rho}(0) = \hat{\rho}_s(0)\hat{\rho}_b(0)$$

Equilibrium Perturbation Theory

$$1/T_2 = 1/2T_1 + 1/T_2^*$$

$\xi = 0.09,\ \Omega = 0.4,\ \beta = 12.5$ $\quad\quad$ $\xi = 0.5,\ \Omega = 0.333,\ \beta = 3.$

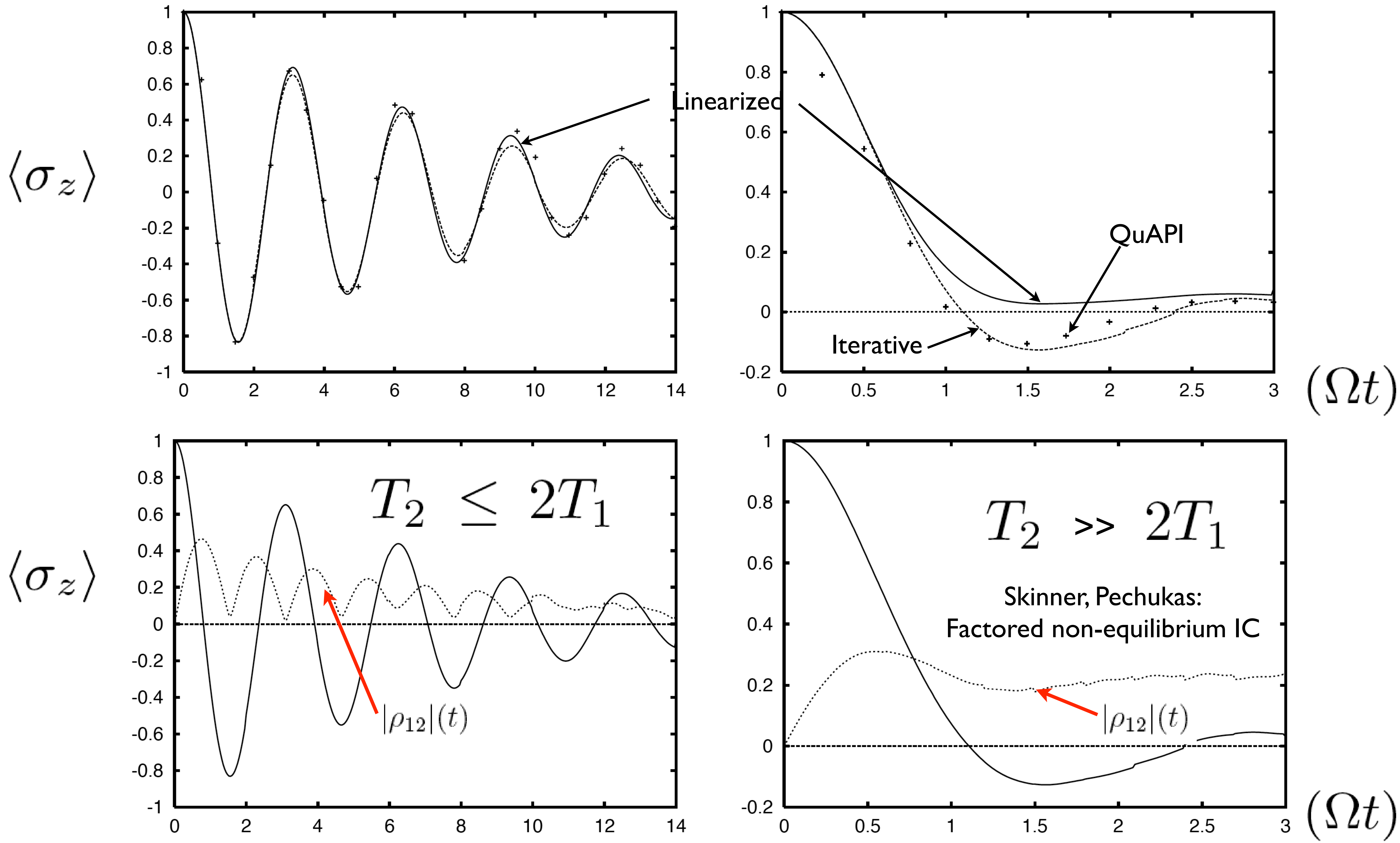

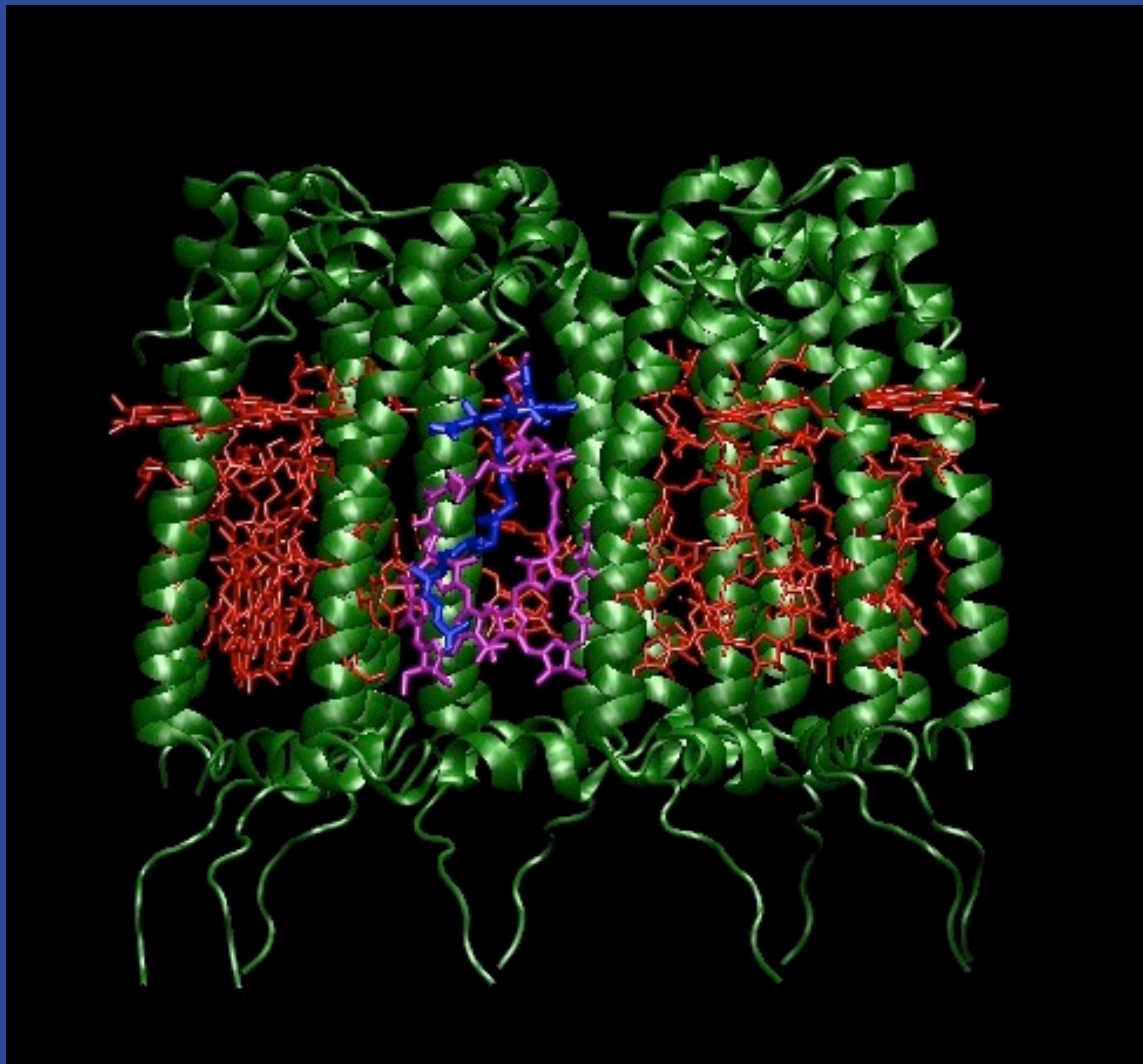

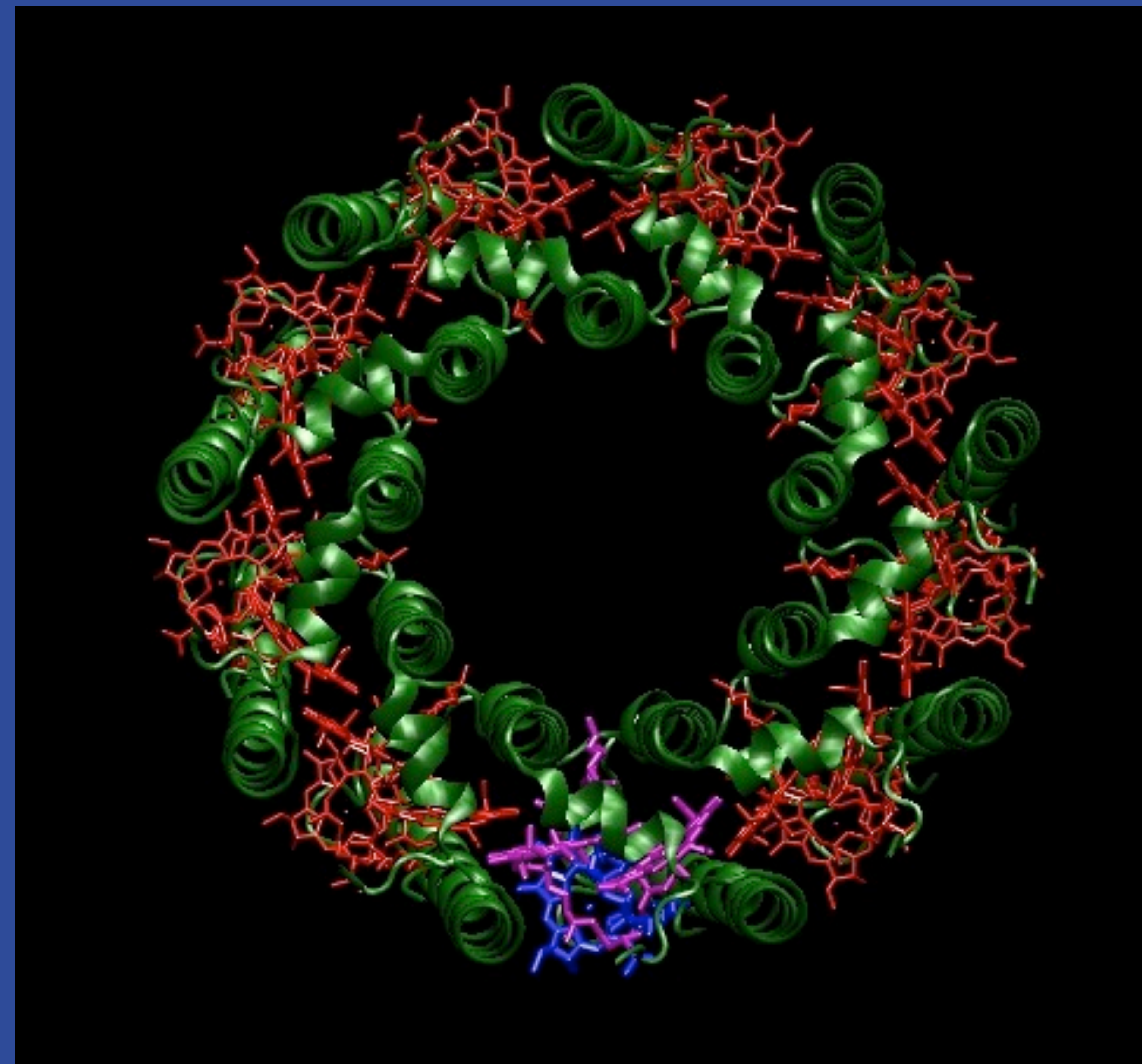

"Spin-Boson" model for exciton transport, dissipation, and decoherence in antenna arrays

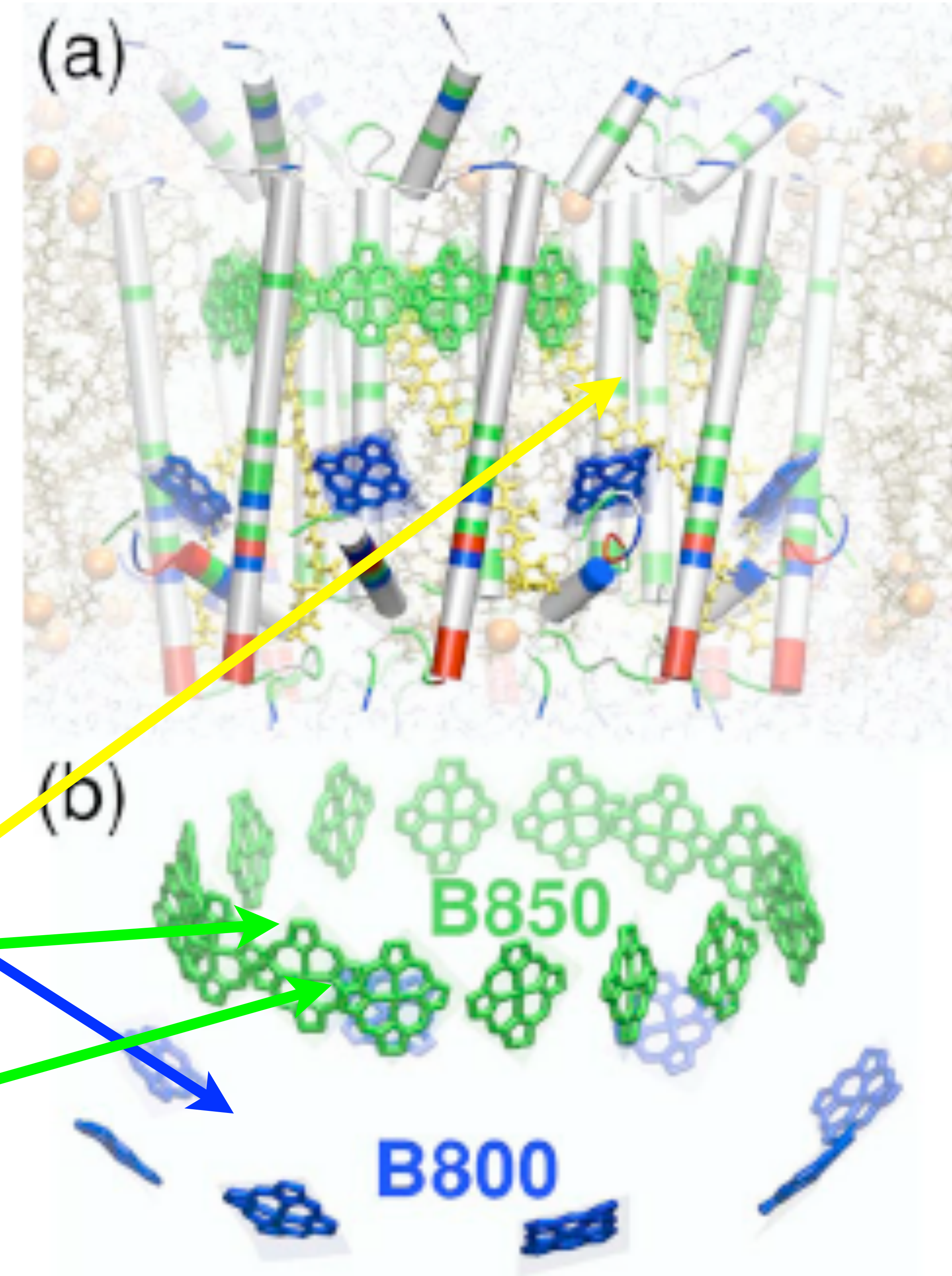

$$
\begin{aligned}
\hat{H} \;=\; & \sum_n \hbar\omega_n(\hat{b}_n^\dagger \hat{b}_n + 1/2) \\
& +[\epsilon_D + \sum_n \hbar g_{n,D}(\hat{b}_n + \hat{b}_n^\dagger)]|D\rangle\langle D| \\
& +[\epsilon_\alpha + \sum_n \hbar g_{n,\alpha}(\hat{b}_n + \hat{b}_n^\dagger)]|A_\alpha\rangle\langle A_\alpha| \\
& +[\epsilon_\beta + \sum_n \hbar g_{n,\beta}(\hat{b}_n + \hat{b}_n^\dagger)]|A_\beta\rangle\langle A_\beta| \\
& +[\Delta_{\alpha\beta} + \sum_n \hbar g^{\Delta}_{n,\alpha\beta}(\hat{b}_n + \hat{b}_n^\dagger)](|A_\alpha\rangle\langle A_\beta| + |A_\beta\rangle\langle A_\alpha|) \\
& +[J_{D\alpha} + \sum_n \hbar g^{J}_{n,\alpha}(\hat{b}_n + \hat{b}_n^\dagger)](|D\rangle\langle A_\alpha| + |A_\alpha\rangle\langle D|) \\
& +[J_{D\beta} + \sum_n \hbar g^{J}_{n,\beta}(\hat{b}_n + \hat{b}_n^\dagger)](|D\rangle\langle A_\beta| + |A_\beta\rangle\langle D|)
\end{aligned}
$$

LHC2

c.f. Jang, Newton, Silbey
J. Phys. Chem. B, 111, 6807 (2007)

$$
J_{D\alpha} = \frac{\mu_D \cdot \mu_\alpha - 3(\mu_D \cdot \hat{R}_{D\alpha})(\mu_\alpha \cdot \hat{R}_{D\alpha})}{\epsilon R^3_{D\alpha}}
$$

Multichromophoric Főrster Resonance Energy Transfer from B800 to B850 in the Light Harvesting Complex 2: Evidence for Subtle Energetic Optimization by Purple Bacteria

Seogjoo Jang, Marshall D. Newton, and Robert J. Silbey

J. Phys. Chem. B, **2007**, 111 (24), 6807-6814• DOI: 10.1021/jp070111l • Publication Date (Web): 17 April 2007

Reduced 3 state model

MC-FRET rate distribution averaged over 40,000 realizations of site disorder

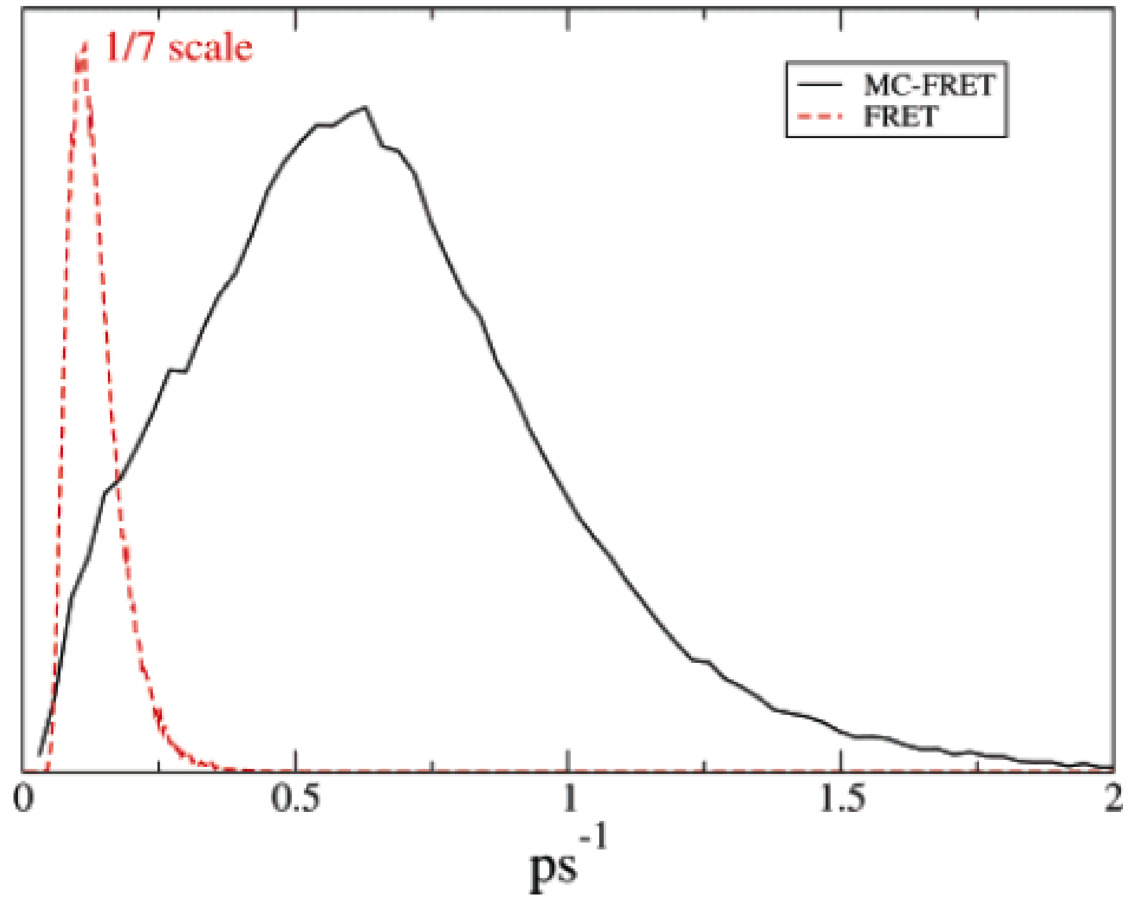

Figure 2. Distribution of rates (ps^{-1}). Solid line is the distribution of rates based on MC-FRET, and red dashed line is the distribution of rates based on FRET. The height of the FRET distribution is 1/7 of the actual height.

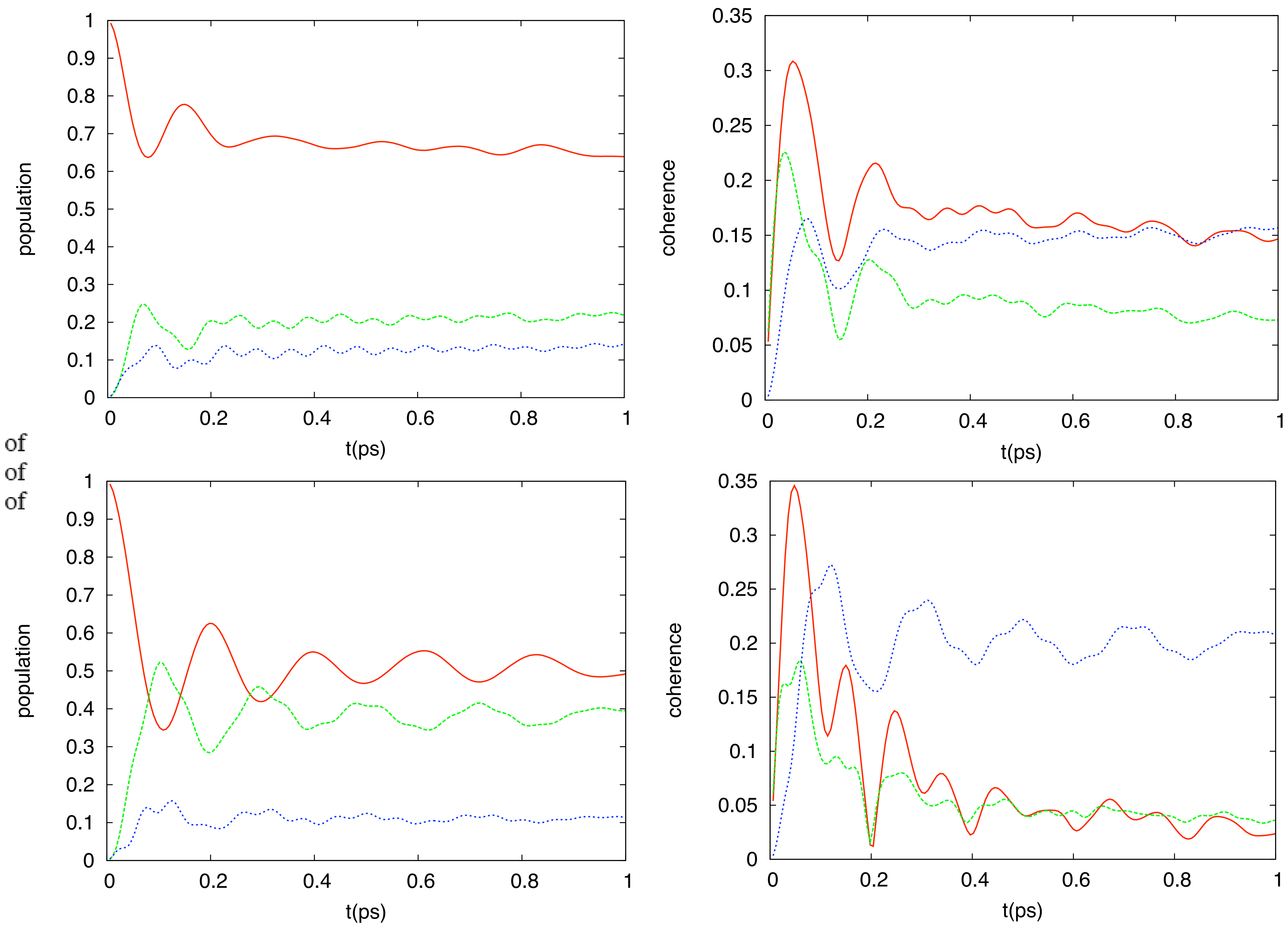

ISLAND-map rate distribution averaged over 1,000 realizations of site disorder (converged initial condition average)

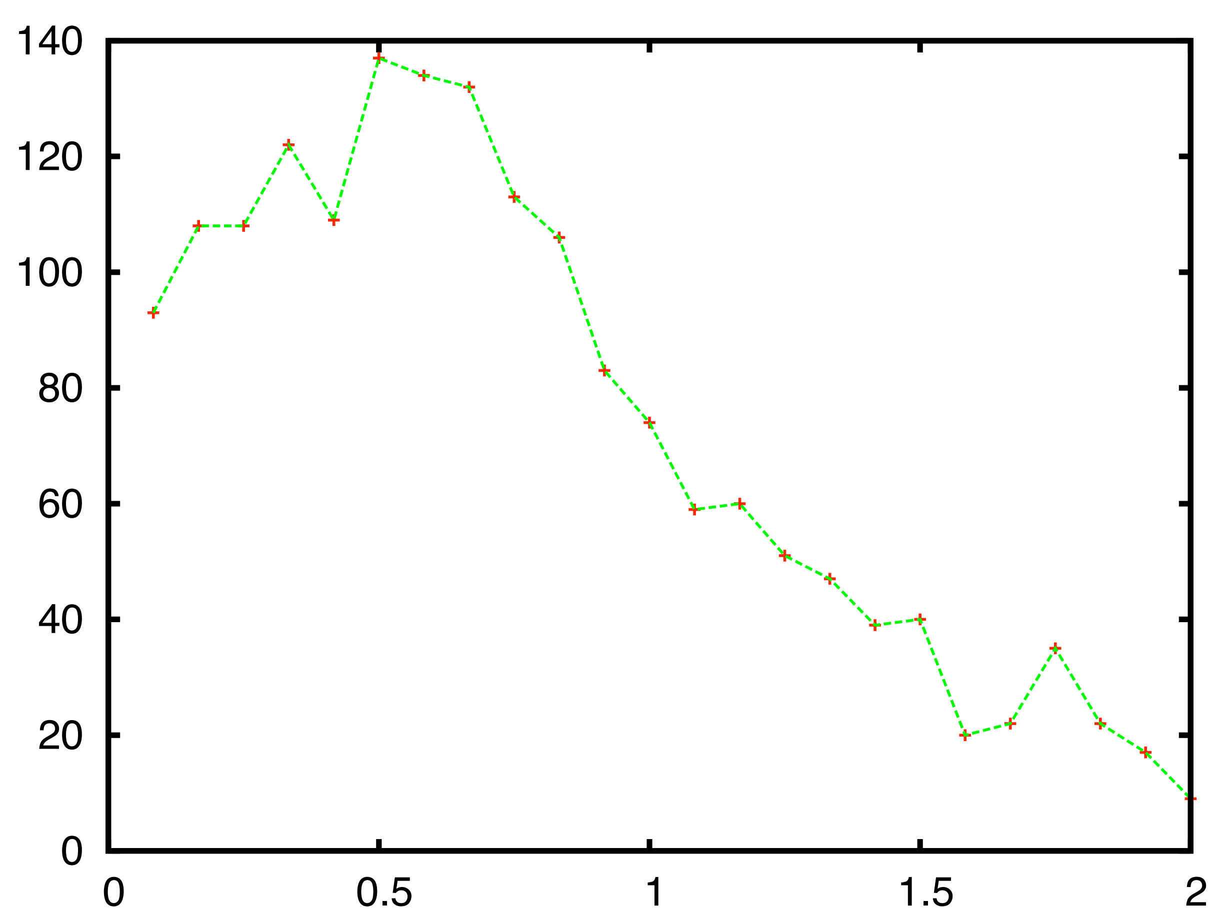

- -Dipole of donor and acceptors 5.3 D
- -Distance between donor and acceptor a 17.6 A
- -Distance between donor and acceptor b 16.6 A
- -Electronic coupling between acceptors 238 cm-1
- -Bias between donor and acceptors 260 cm-1
- -Temperature 10 cm-1

Converged Linearized dynamics, 18 state model
No site disorder

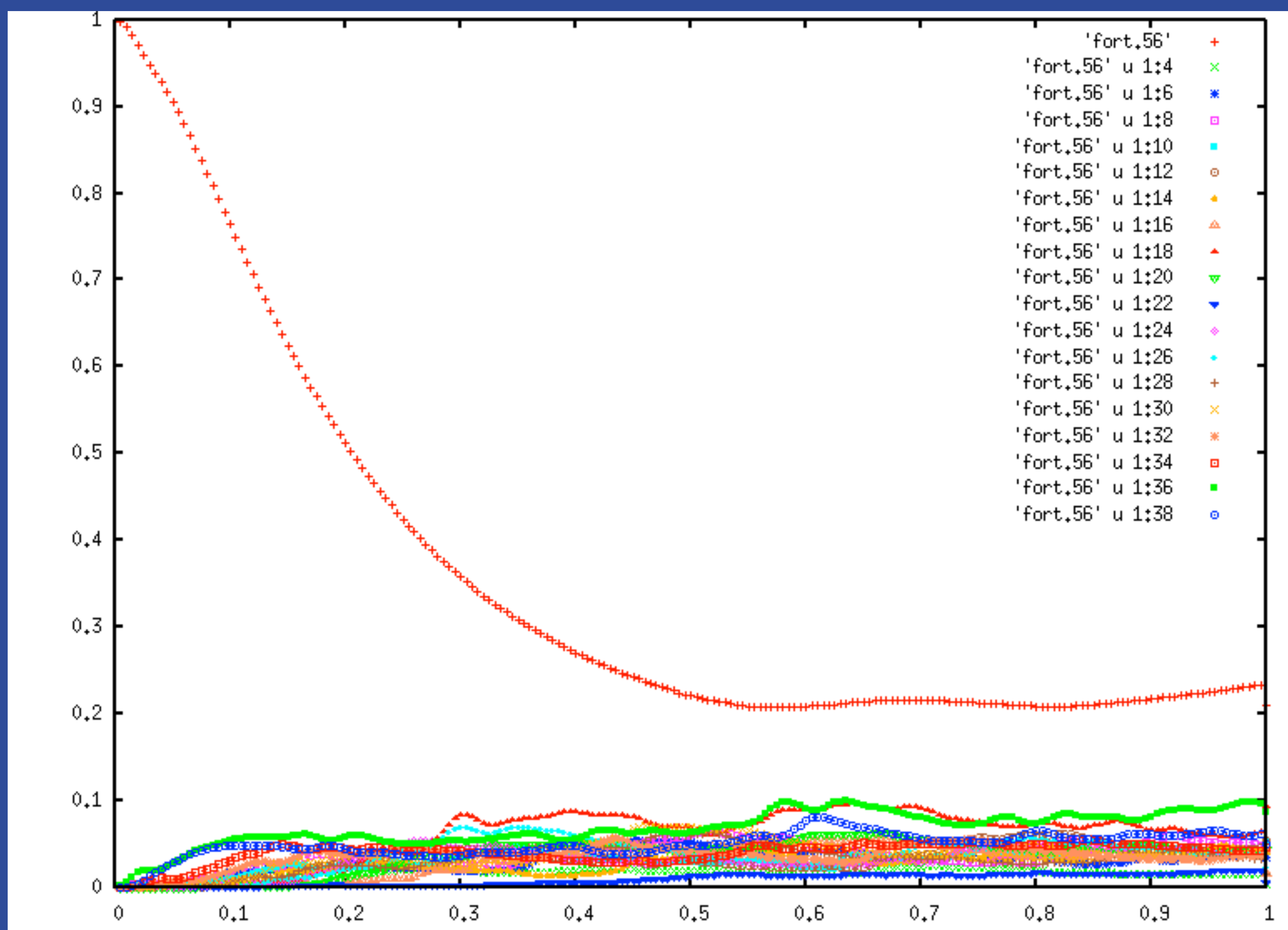

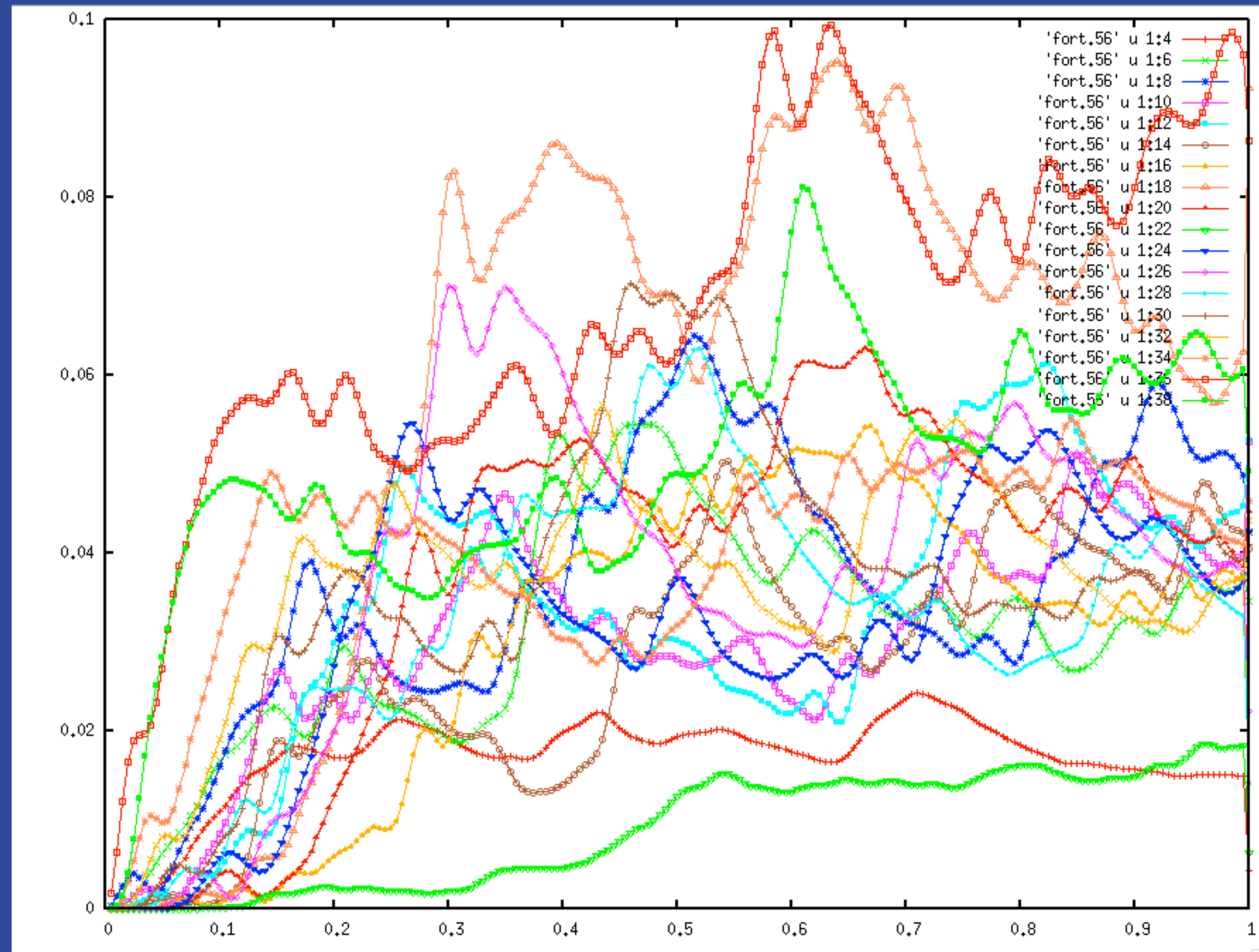

Pengfei (Frank) Huo

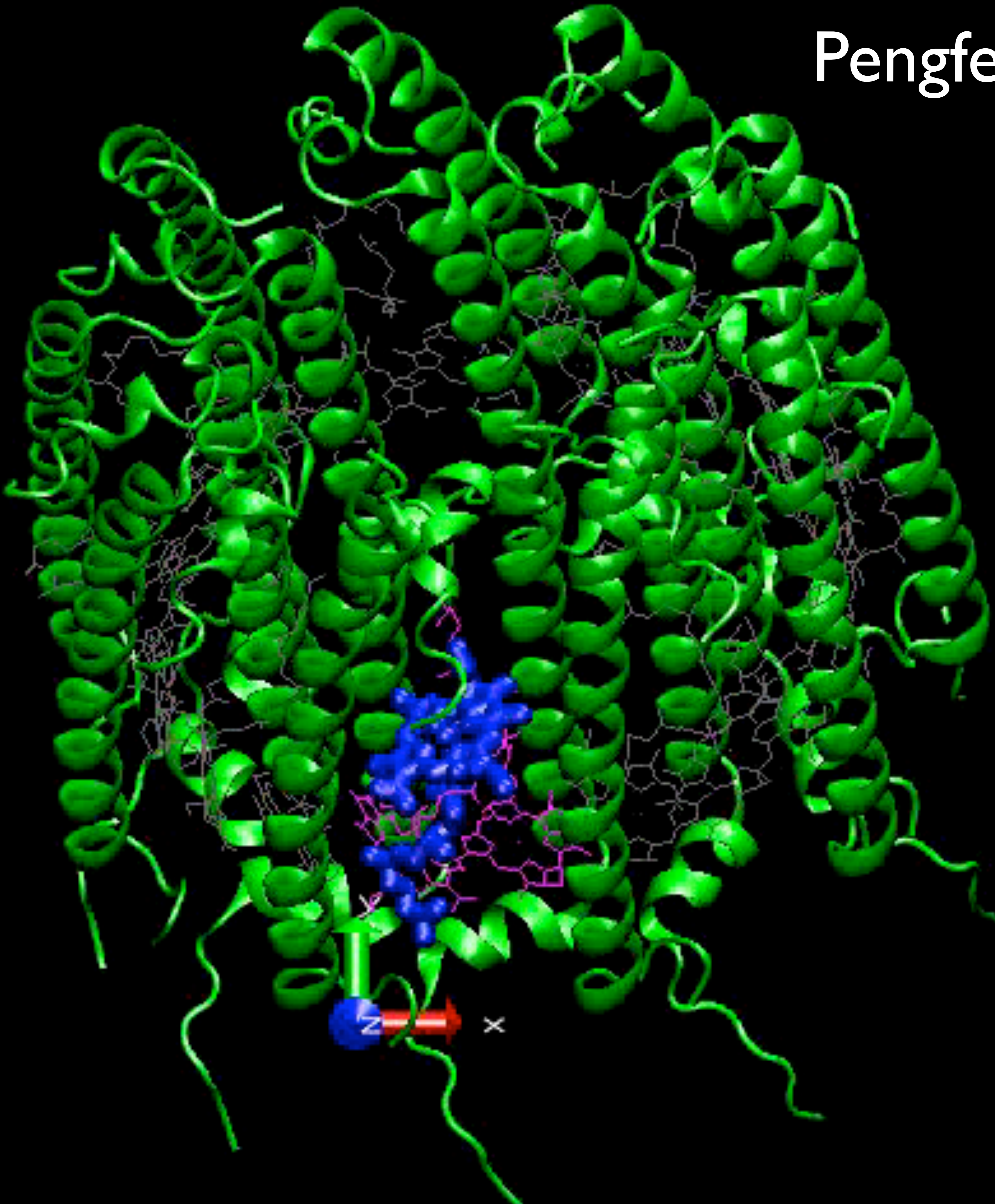

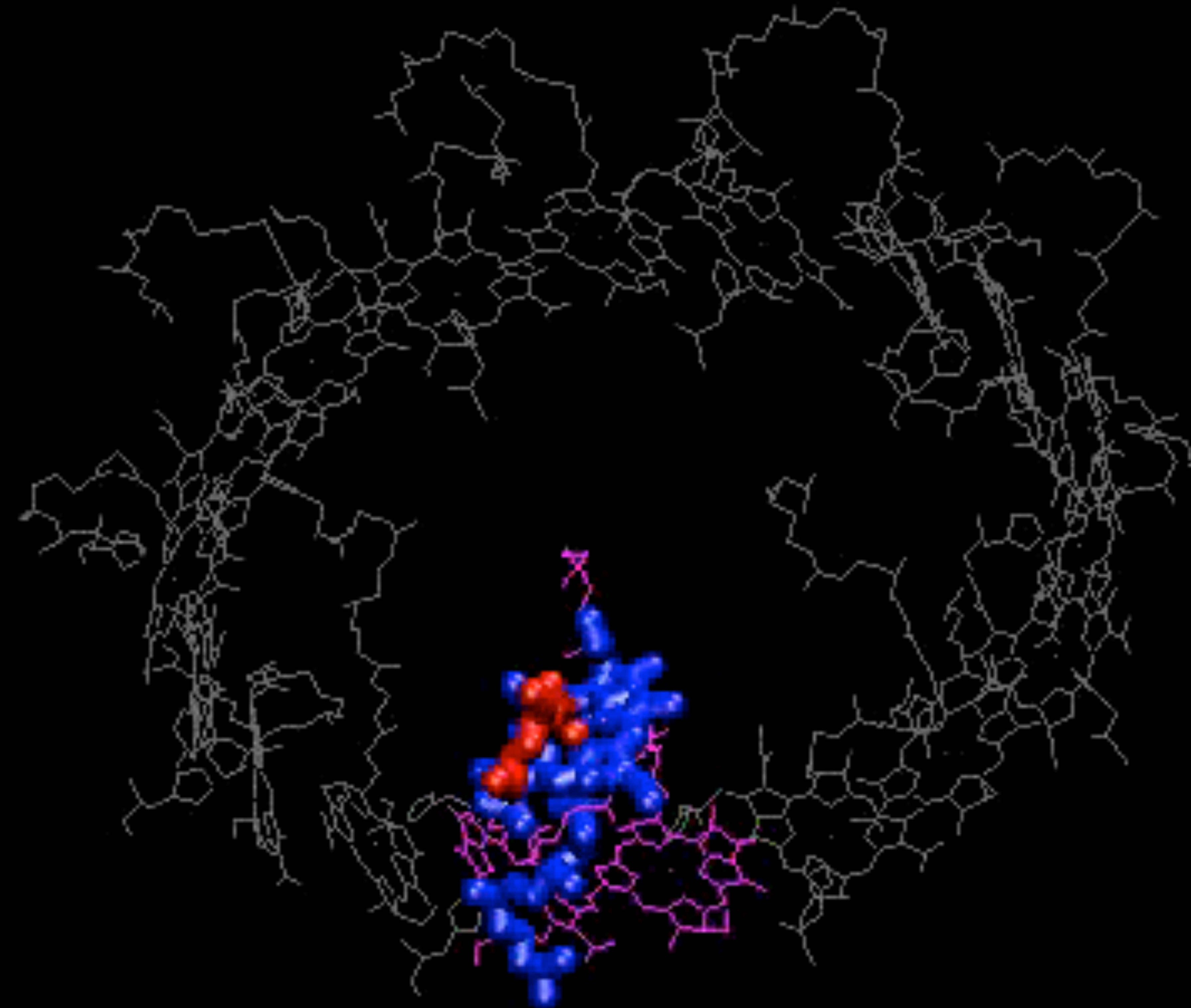

Converged Linearized dynamics,18 state model
1 realization of site disorder

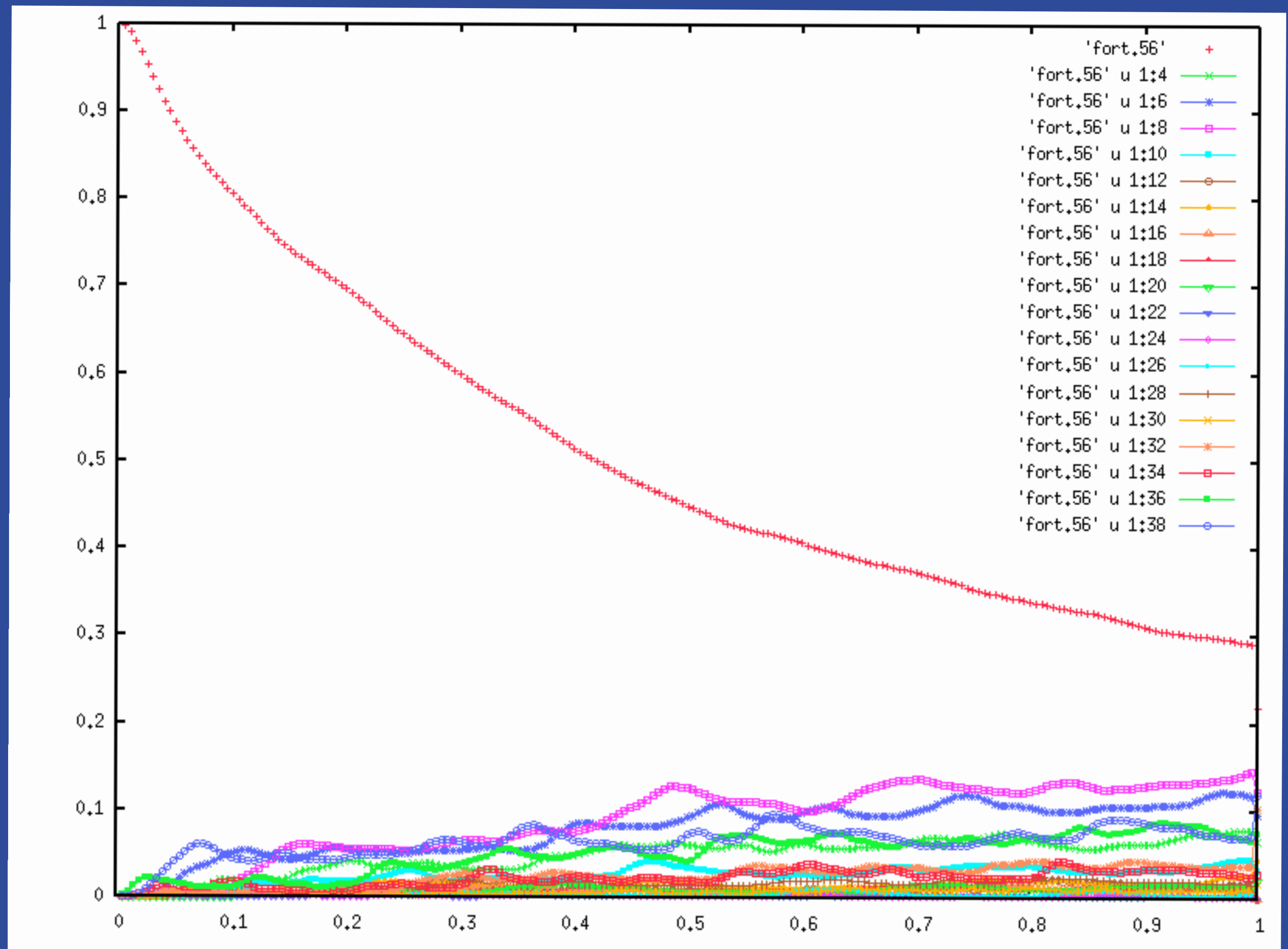

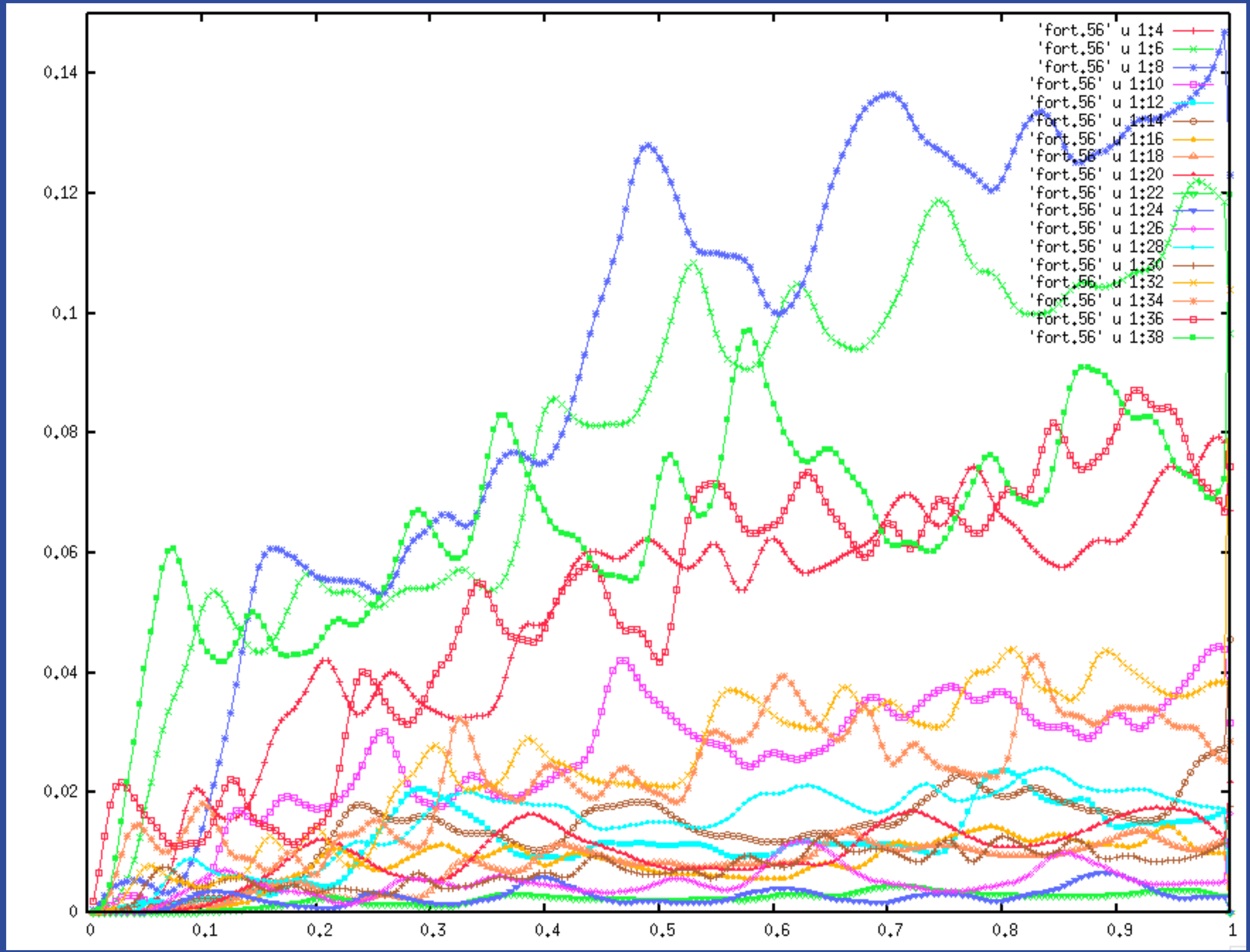

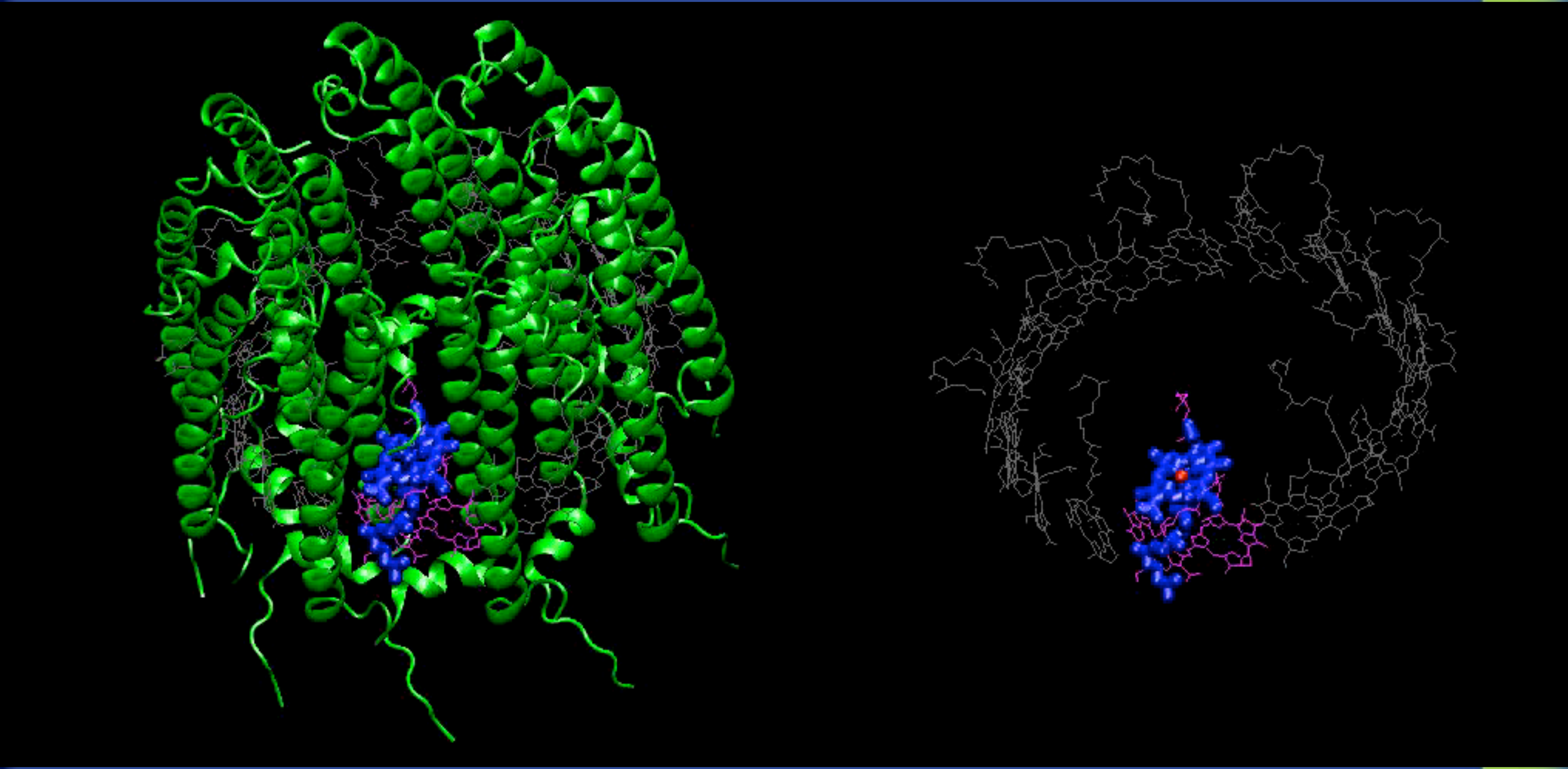

Converged Linearized dynamics, 18 state model another realization of site disorder

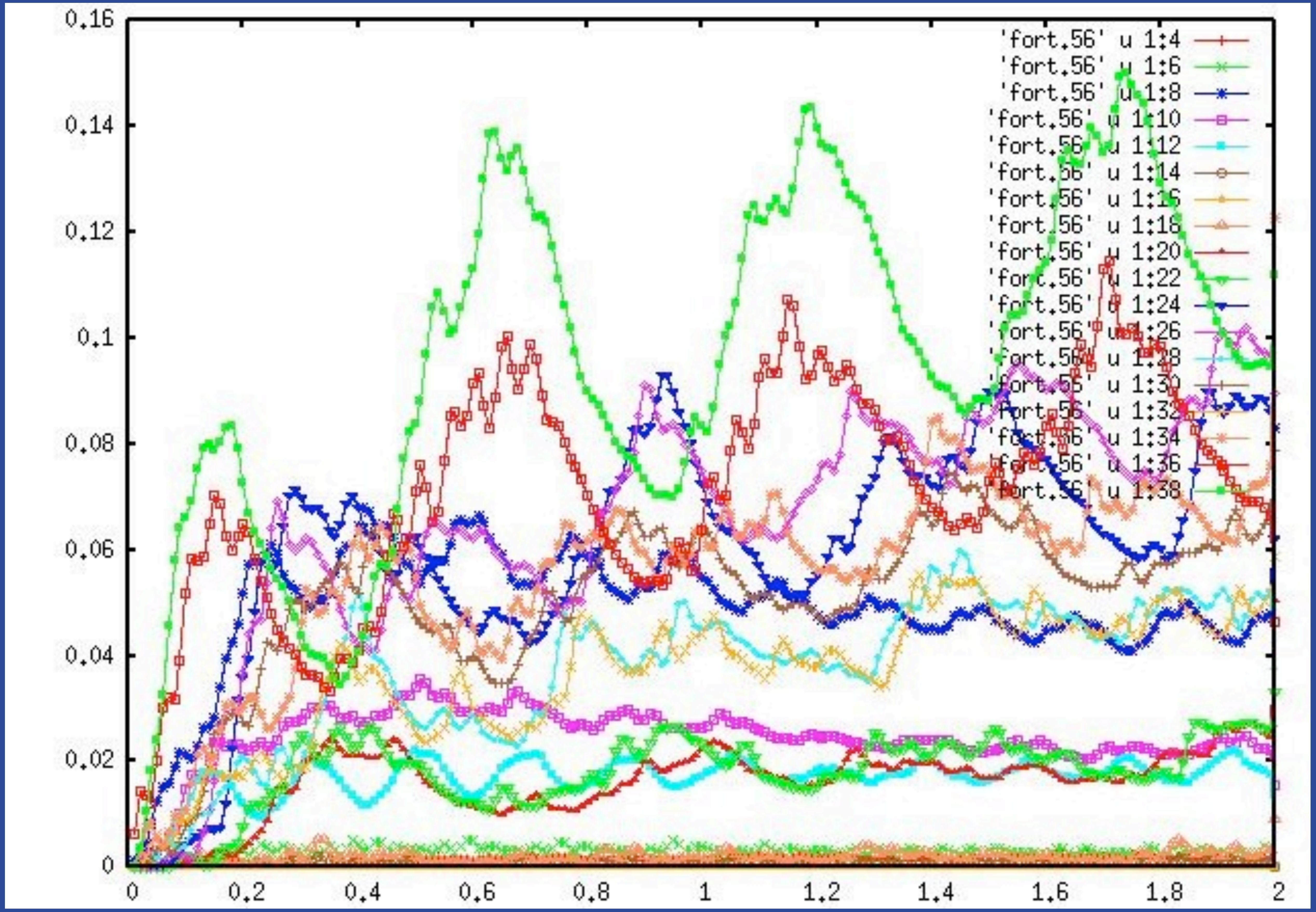

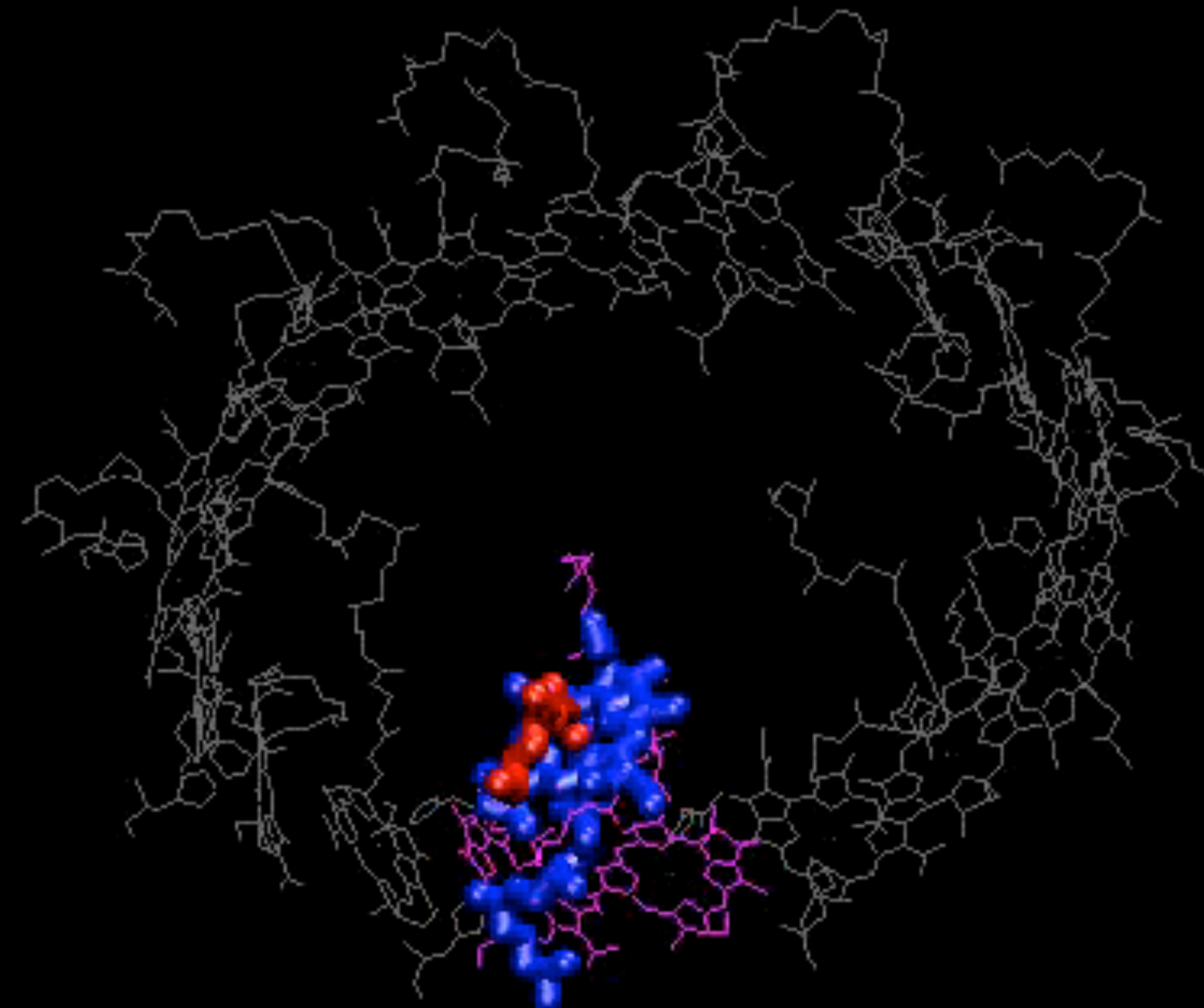

FMO complex from green sulfur bacteria

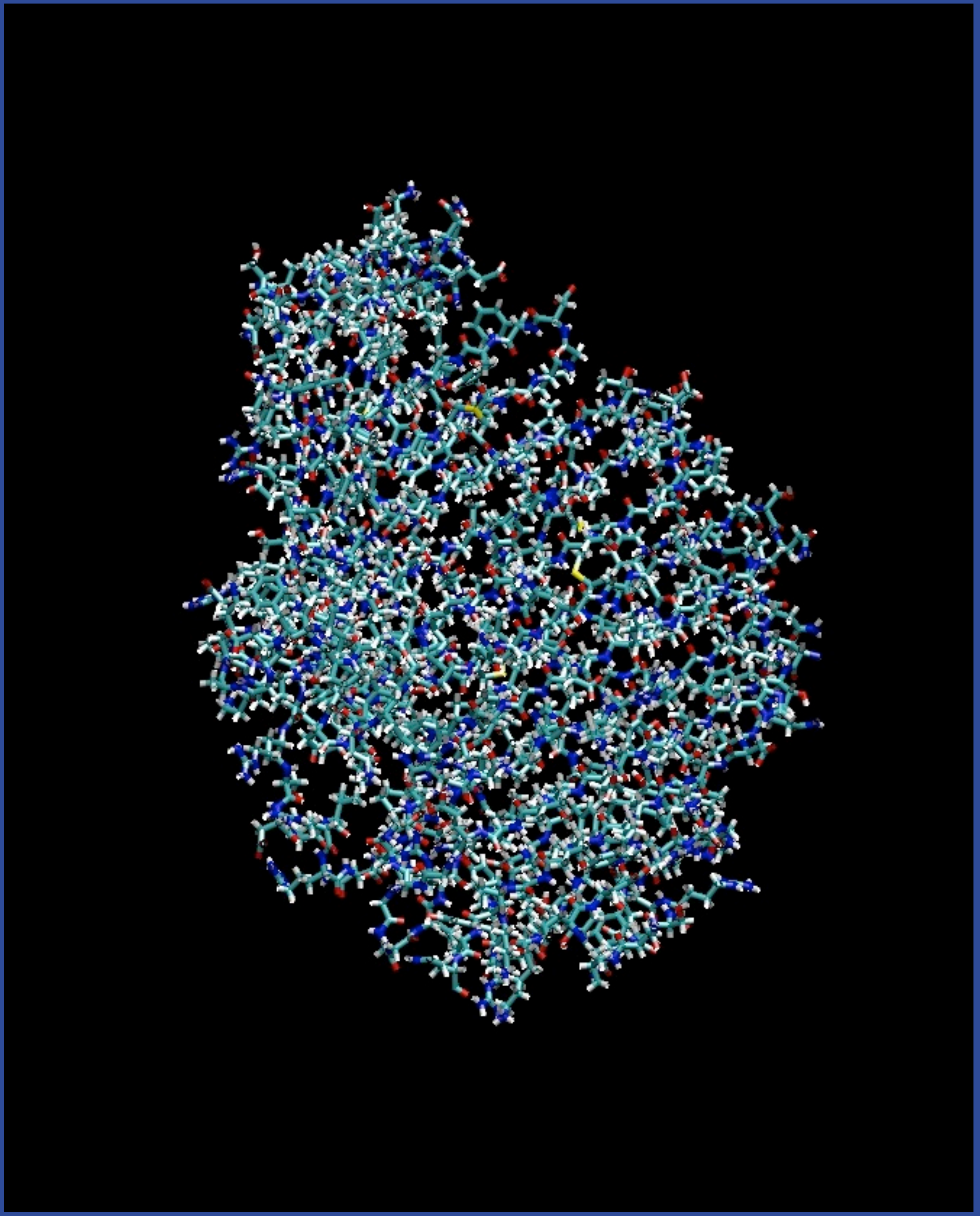

ACAM
Atlantic Centre for Atomistic Modelling

FMO complex from green sulfur bacteria

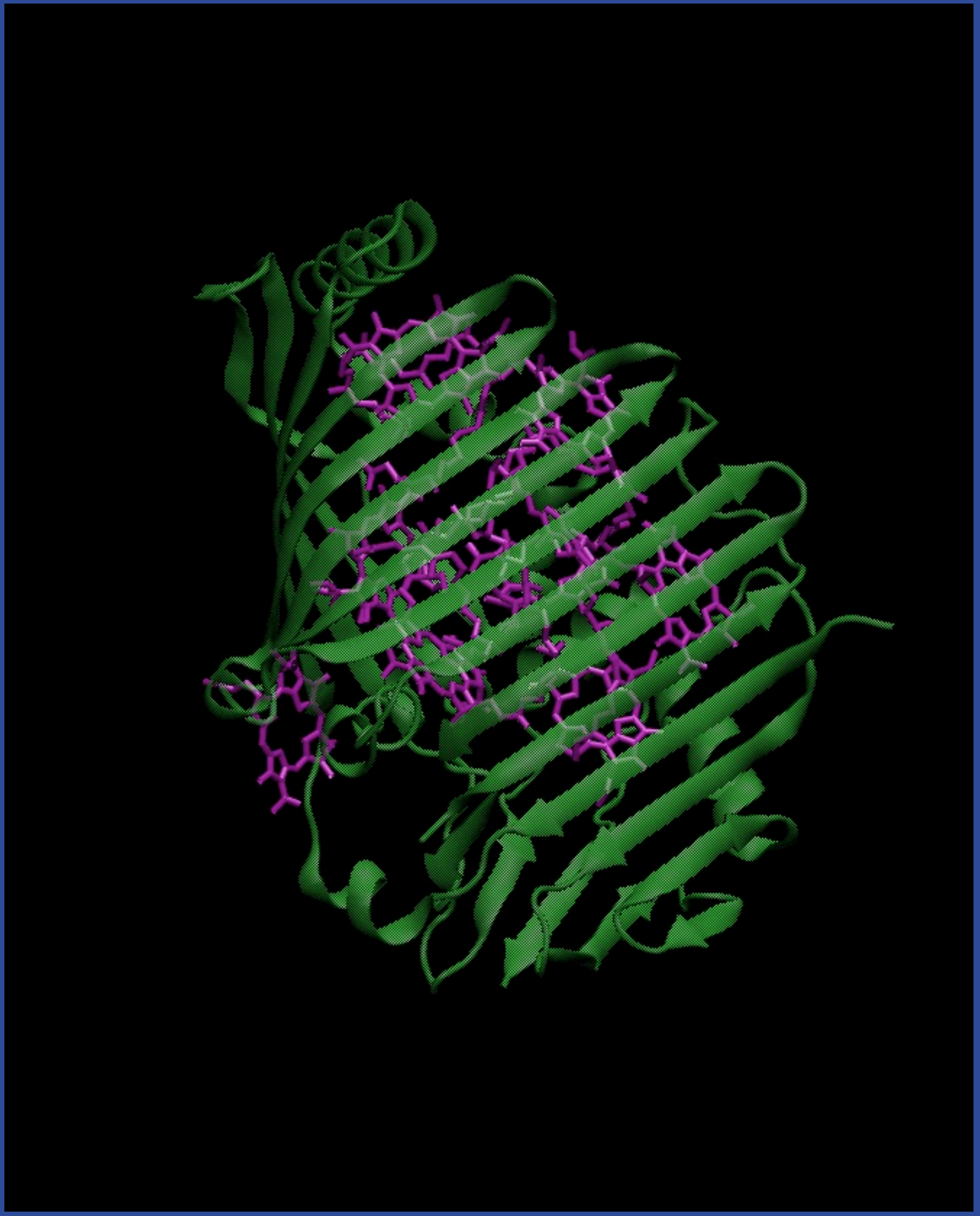

Atlantic Centre for Atomistic Modelling

FMO complex from green sulfur bacteria

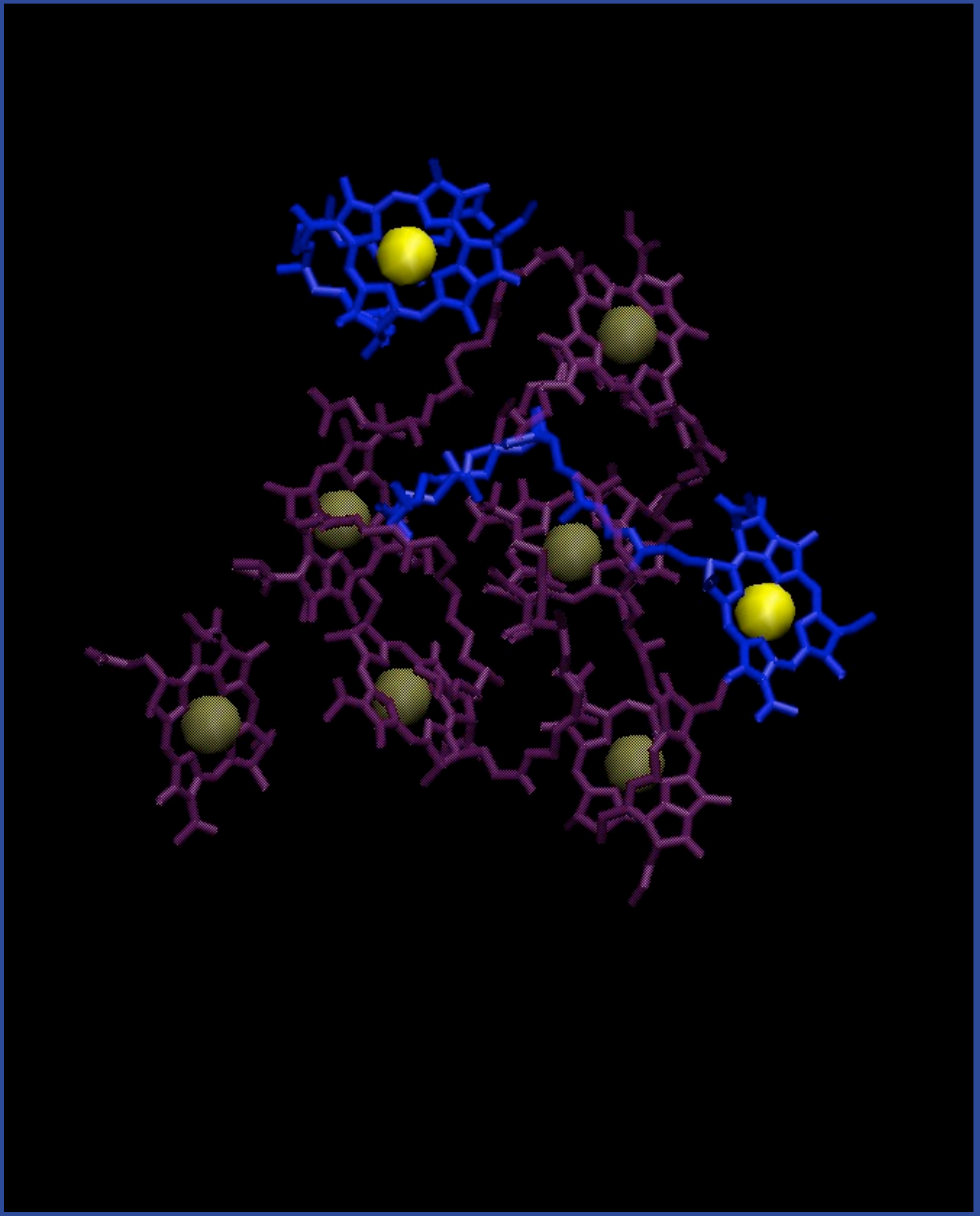

ACAM
Atlantic Centre for Atomistic Modelling

Two state model of FMO

$$J(\omega) = 2\lambda \frac{\omega \tau_c^{-1}}{\omega^2 + \tau_c^{-2}}$$

τ_c ← 500fs

200 Bath modes
Debye

$T=300K \quad J_{12} = 100cm^{-1} \quad E_1 - E_2 = 100cm^{-1}$

$\lambda = J_{12} / 50$

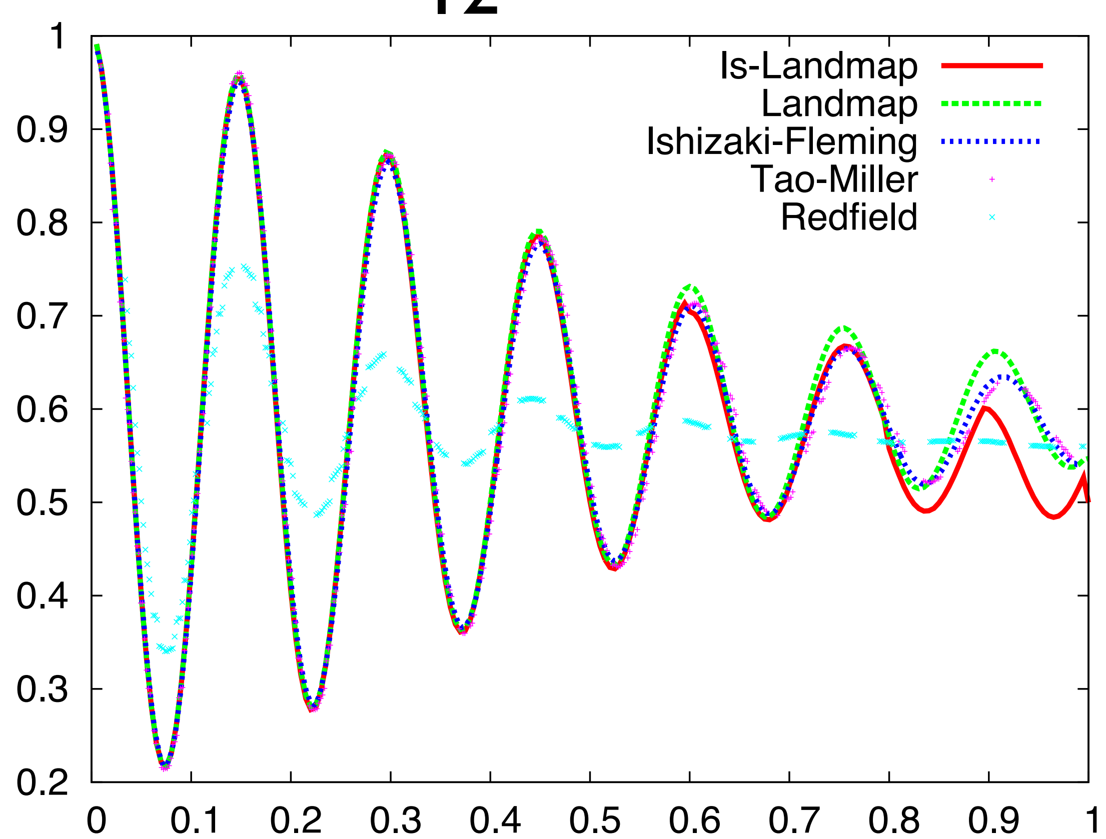

$\lambda = J_{12} / 5$

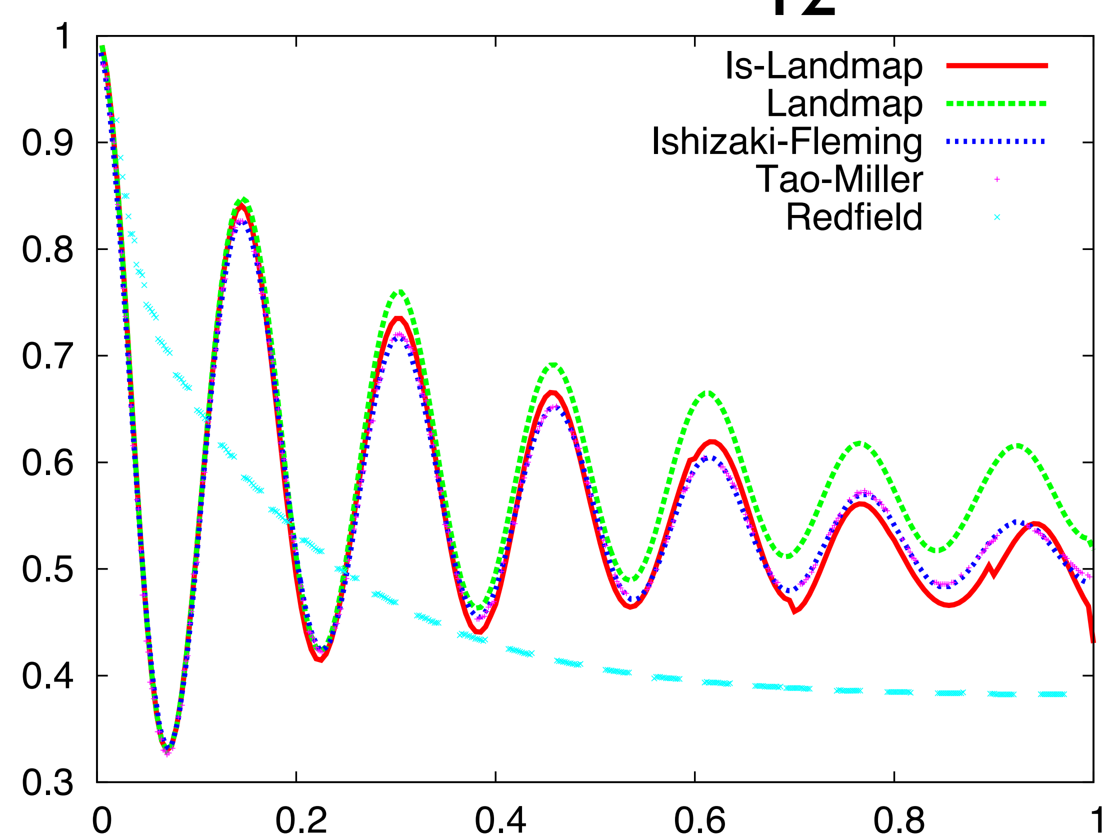

$\lambda = J_{12}$

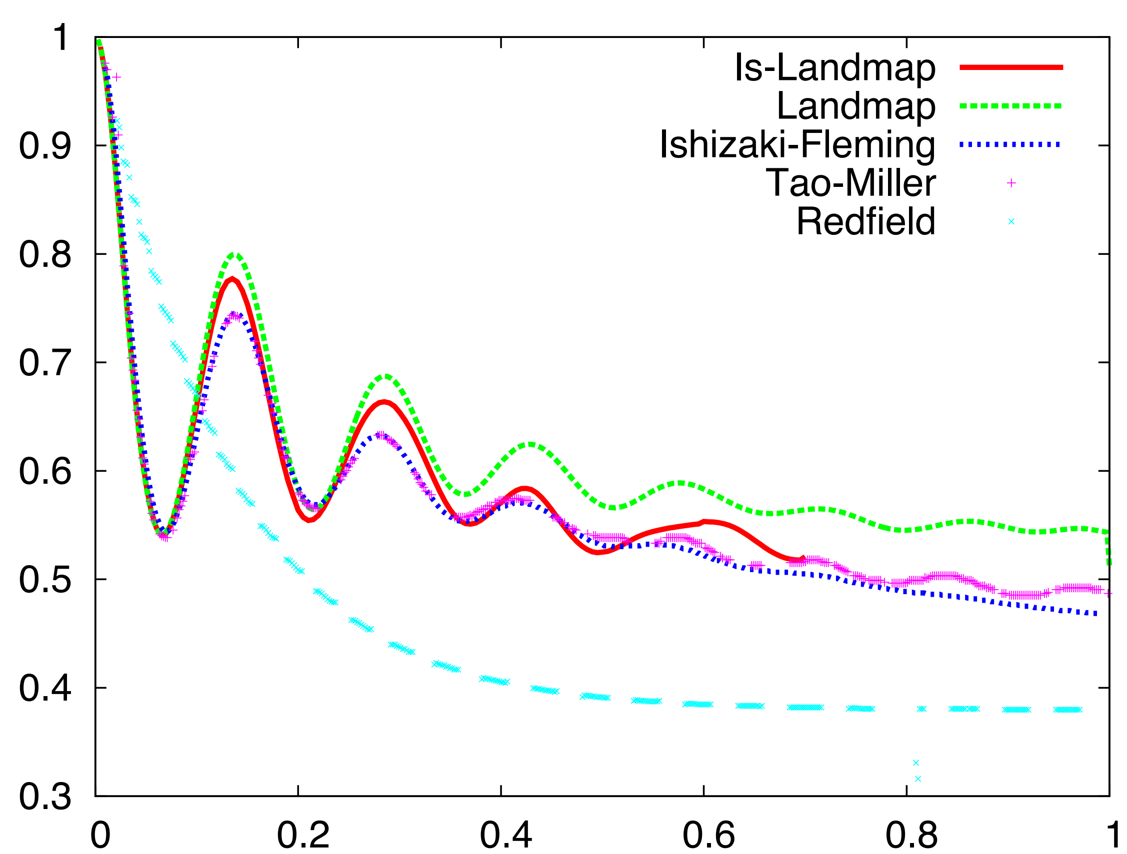

$\lambda = 5J_{12}$

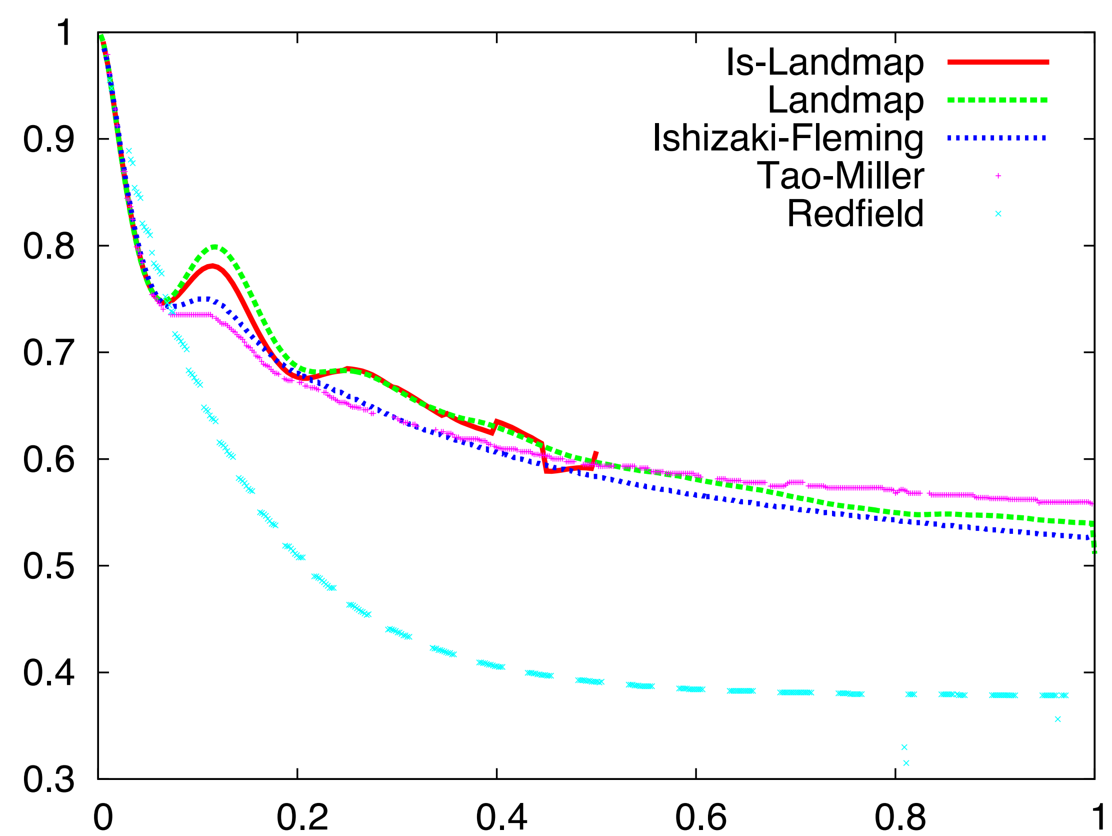

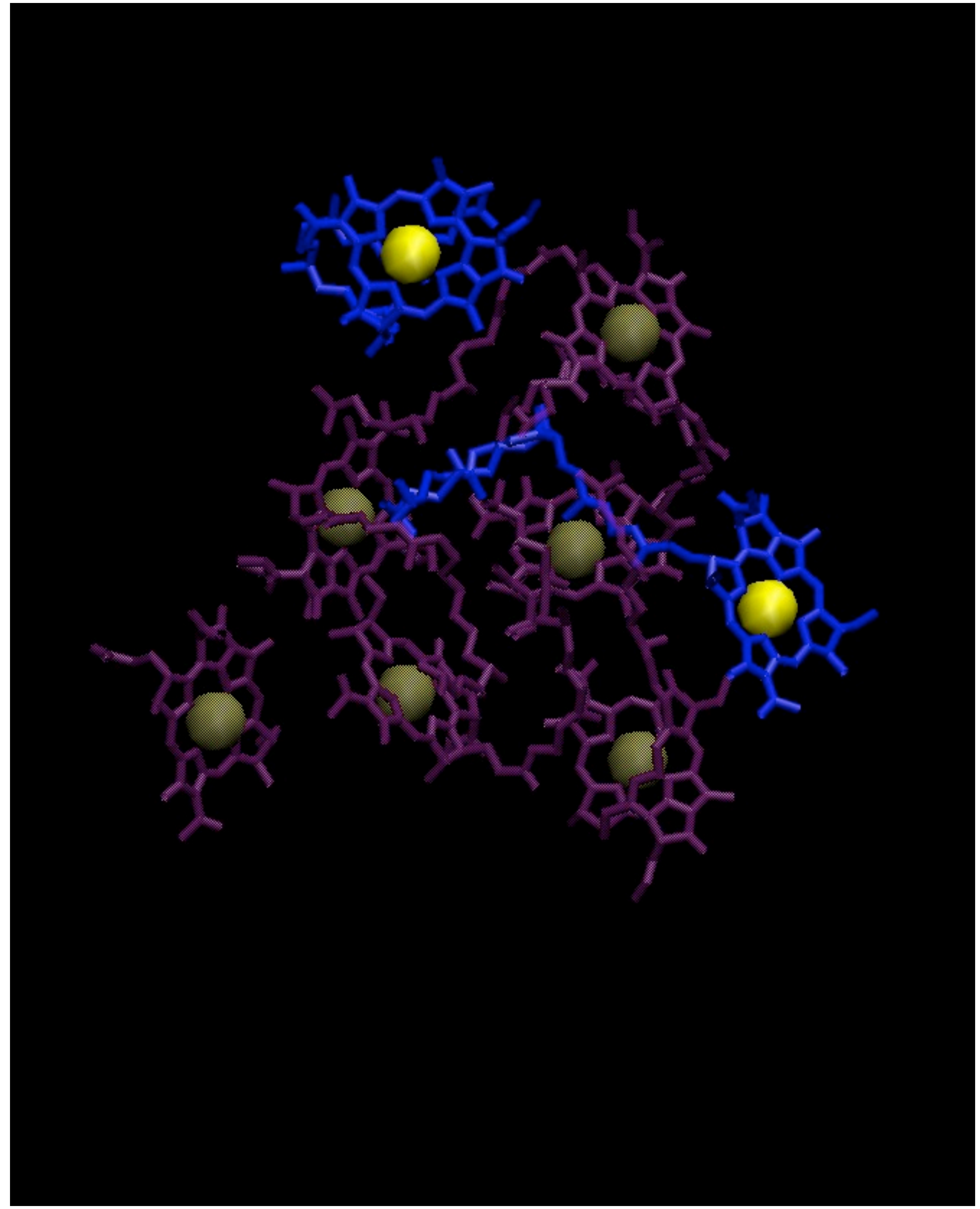

Full 7 state model of FMO

$$J(\omega) = 2\lambda \frac{\omega \tau_c^{-1}}{\omega^2 + \tau_c^{-2}}$$

← 50fs

200 Bath modes
Debye

T=77K λ = 35cm^{-1}

Reduced Hierarchy Equations: Ishizaki-Fleming, J.Chem. Phys. 130: 23411 (2009)

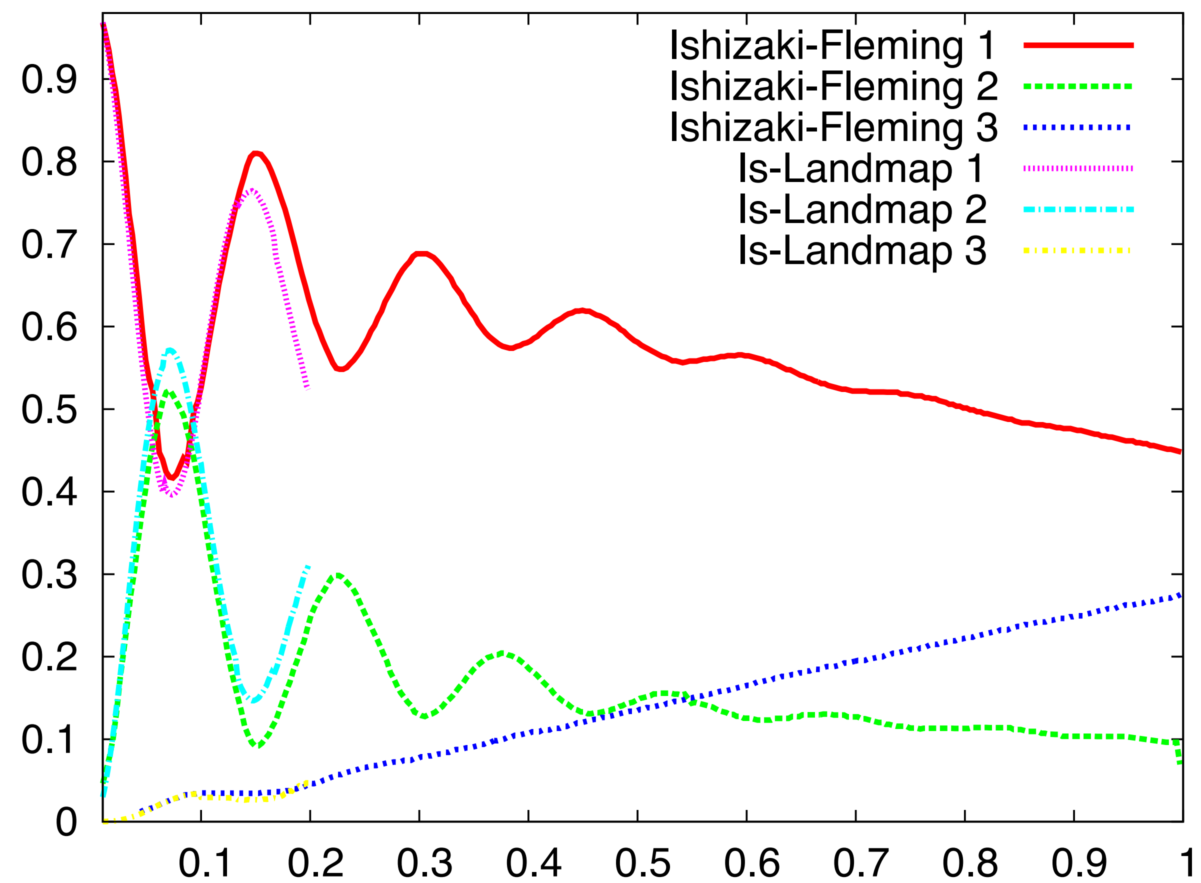

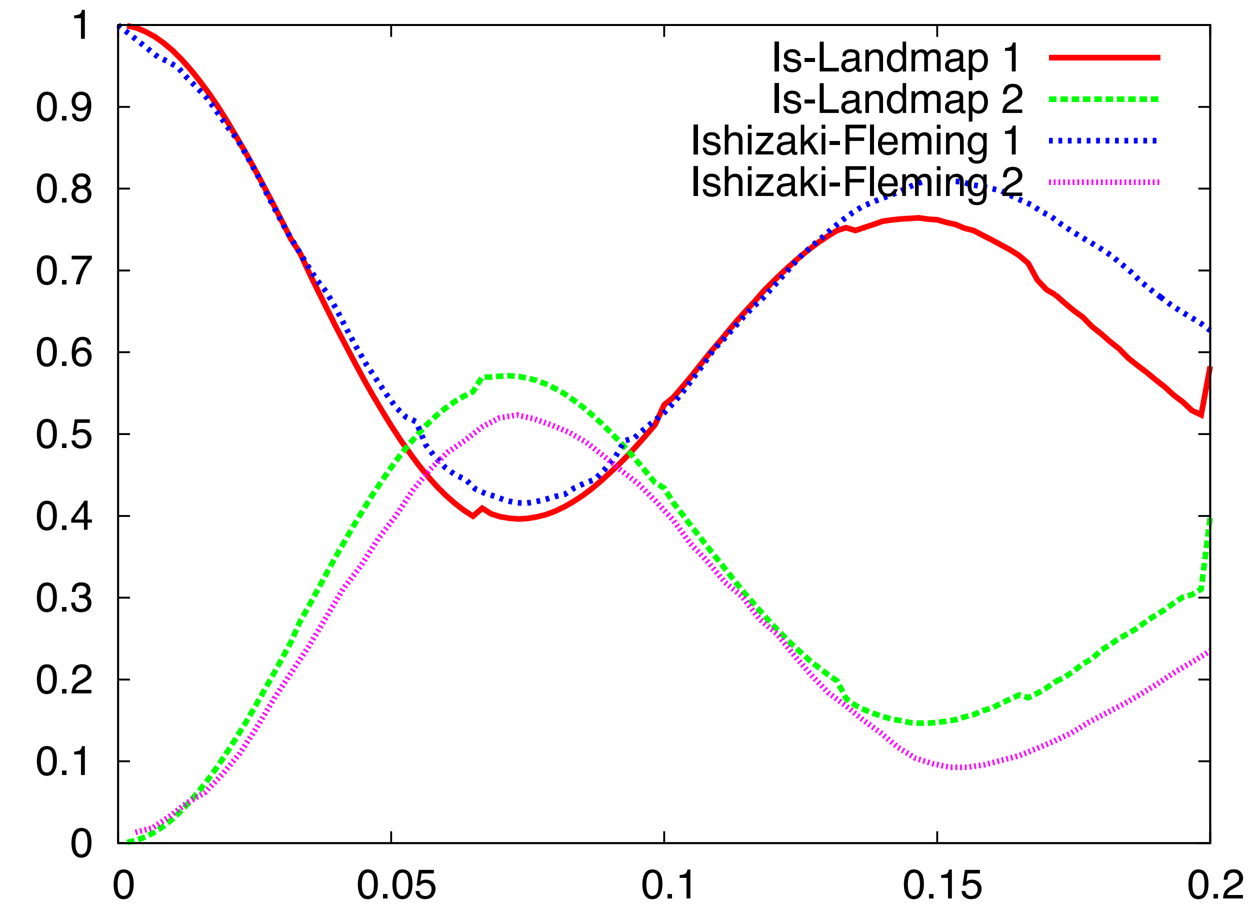

"Linearize everything": Tao-Miller, J. Phys. Chem 1: 891 (2010)

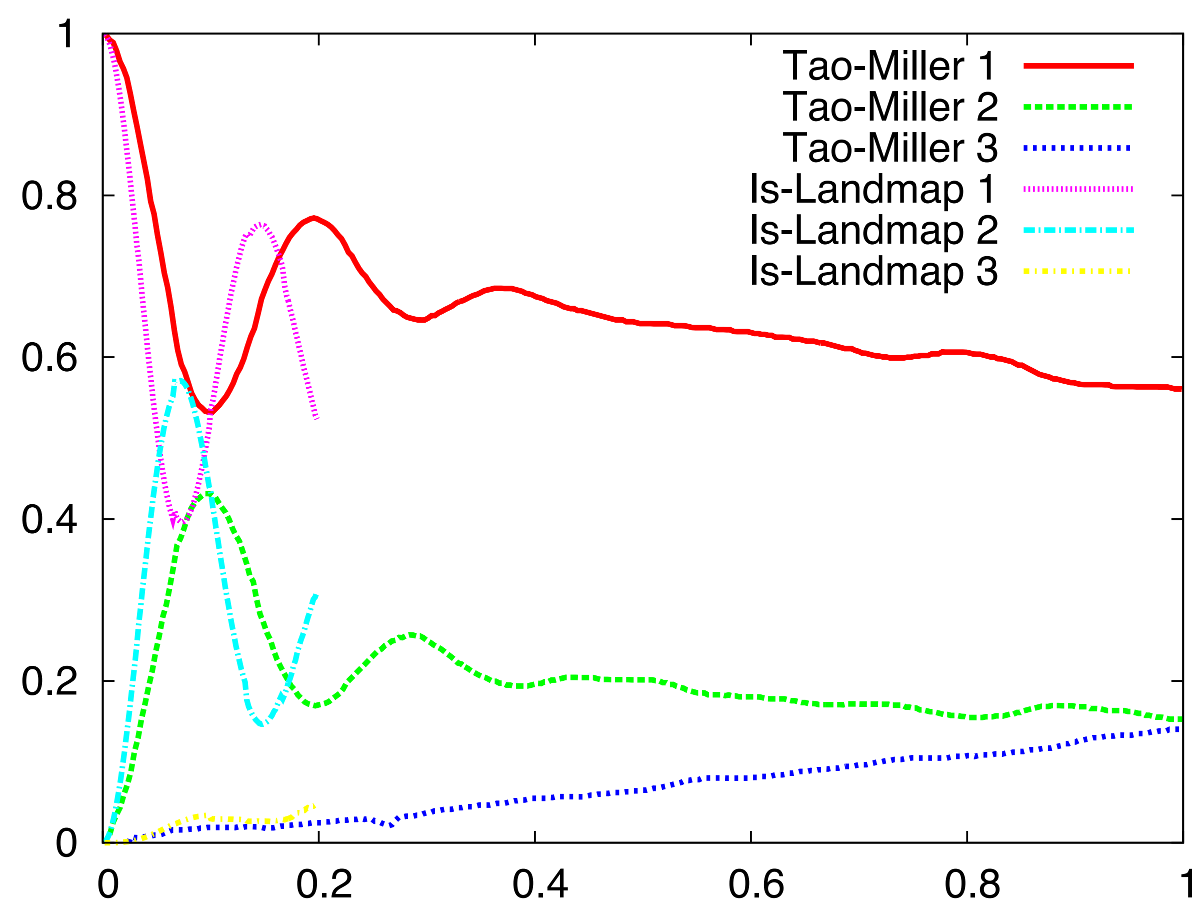

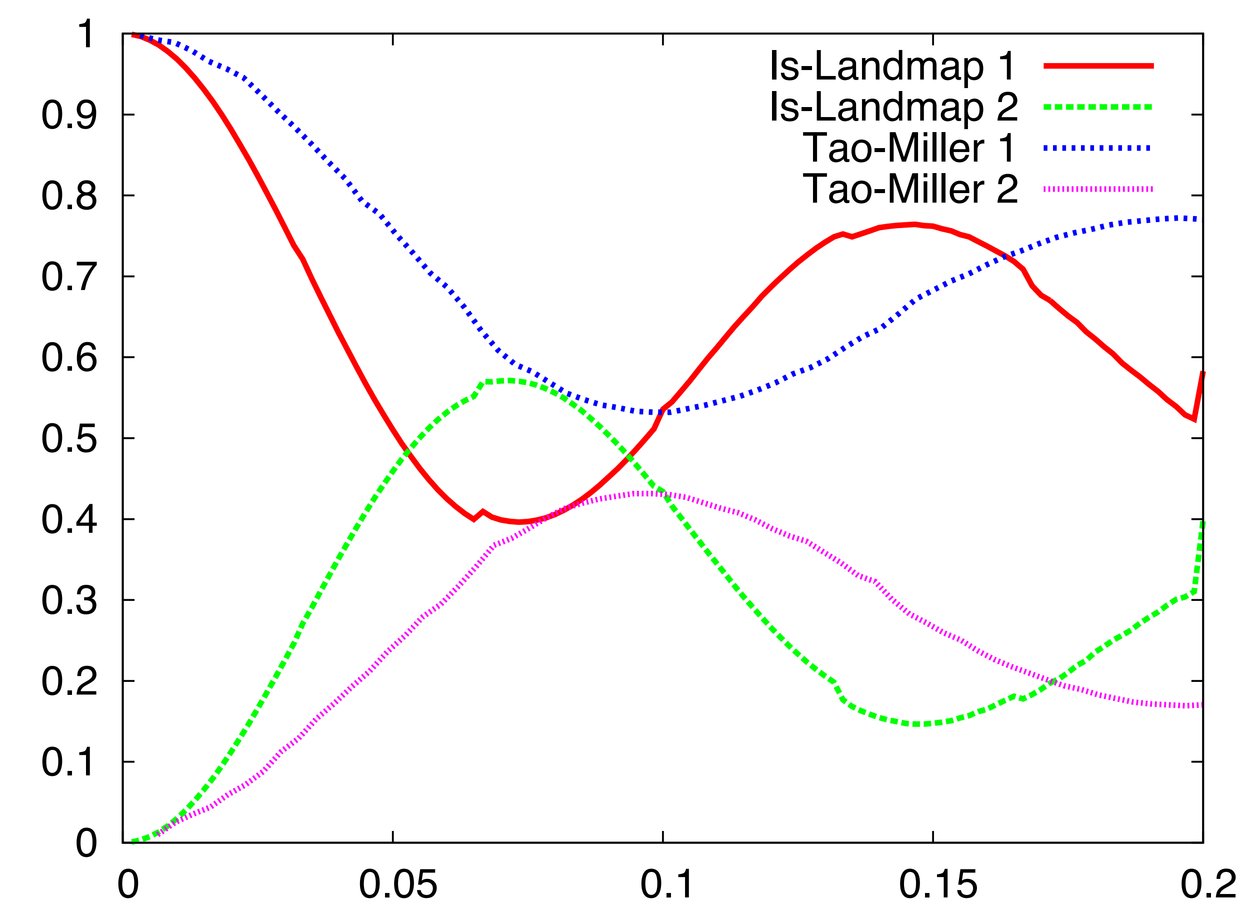

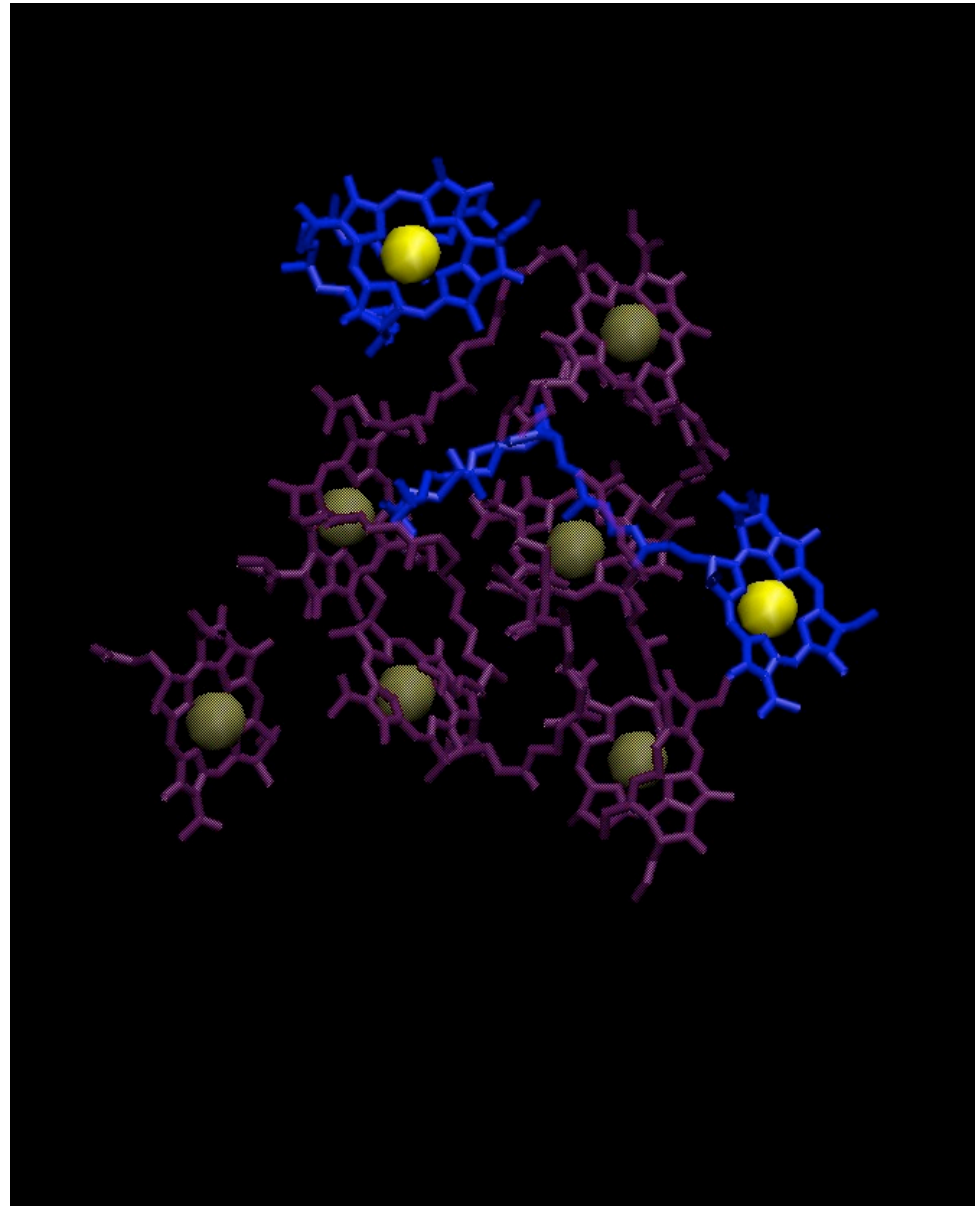

Tina Rivera

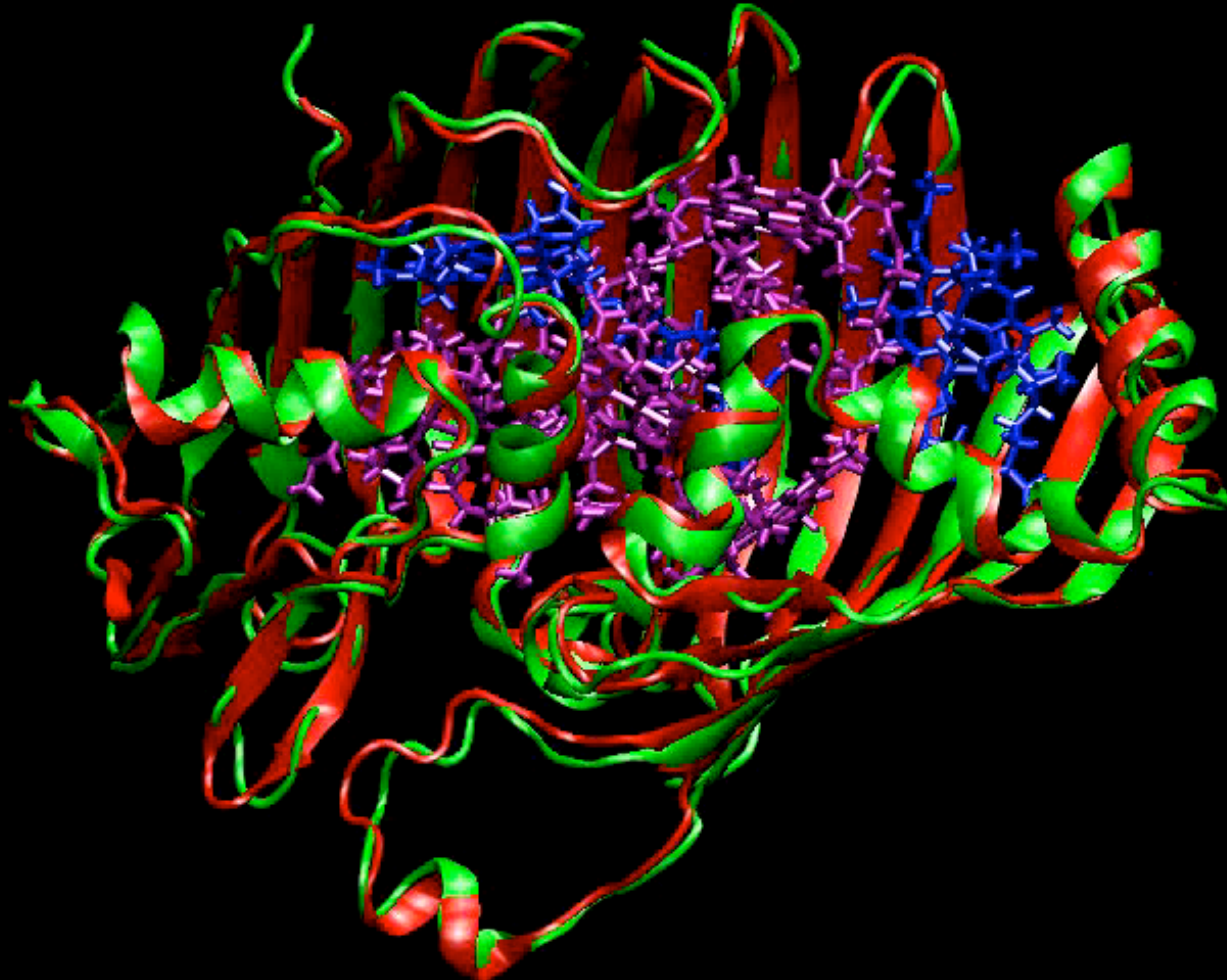

Synthetic: Dye Sensitized Semi-Conductor Solar Cell (DSSC)

Biological: Vesicle membrane covered in light harvesting chromophore complexes (efficient excitation energy transfer), & reaction centers (e-h charge separation)

Dye functions like Reaction Center

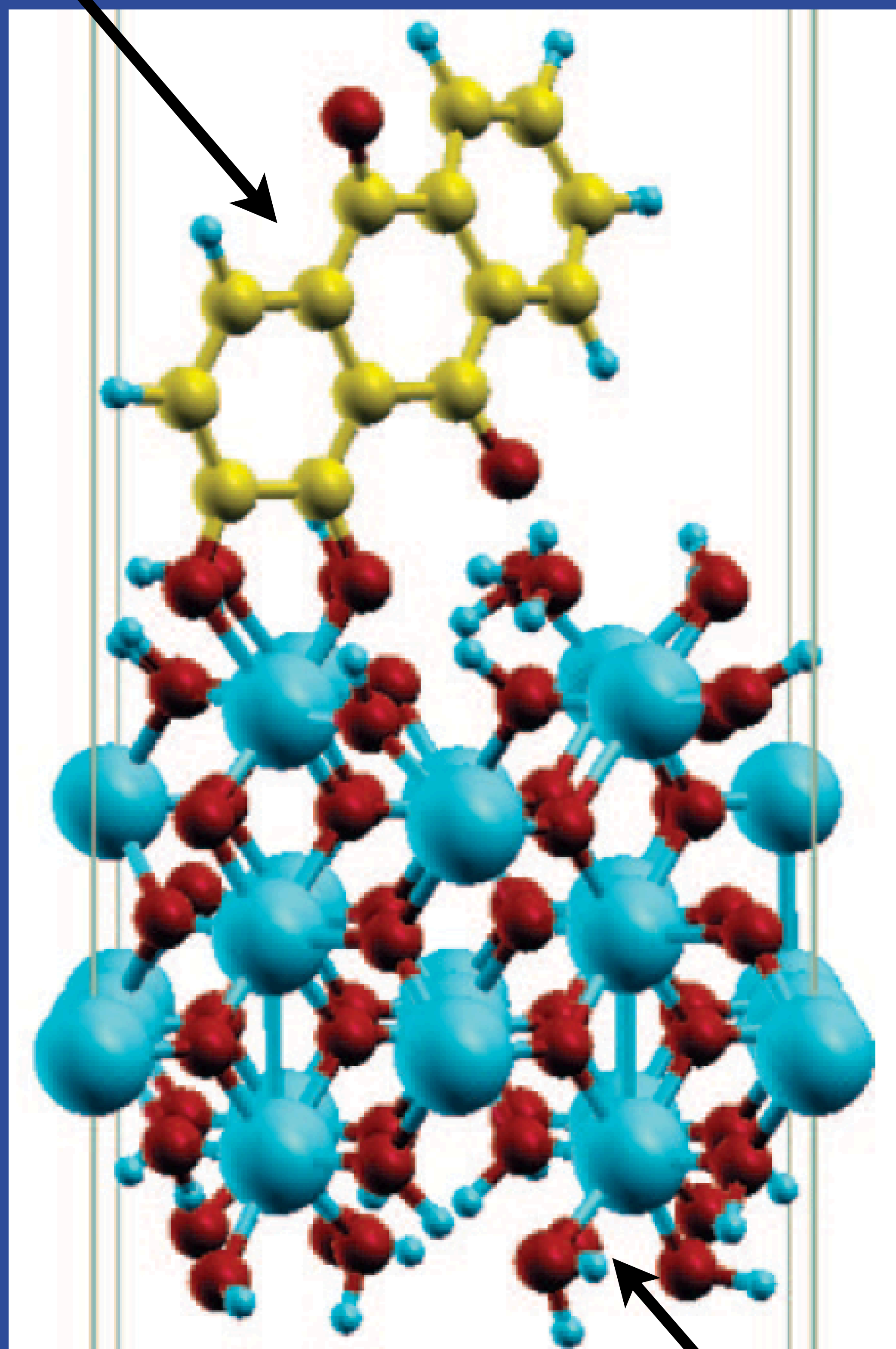

TiO_2 functions like membrane

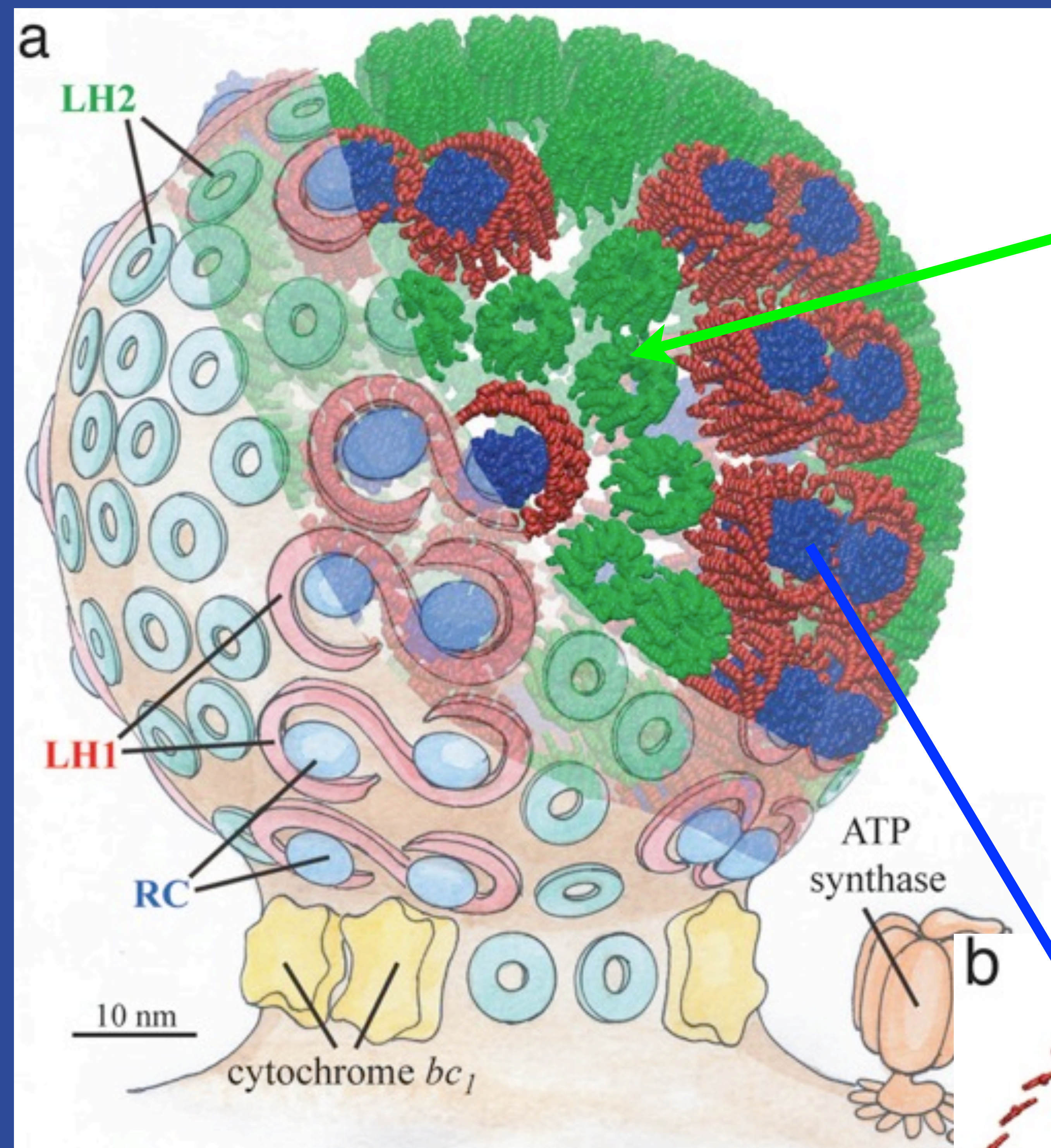

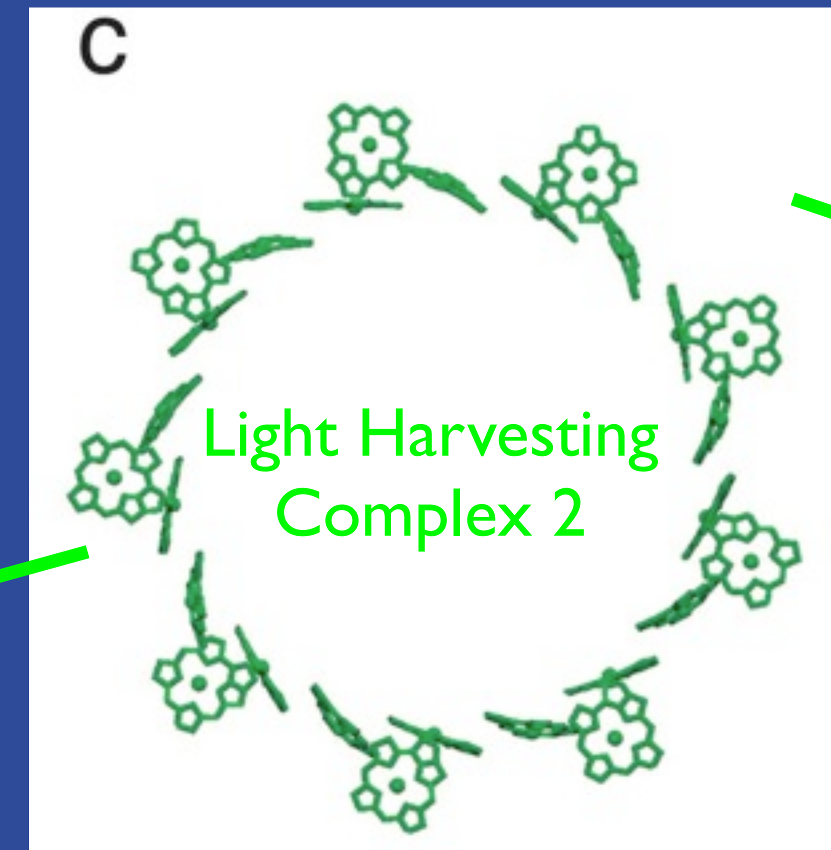

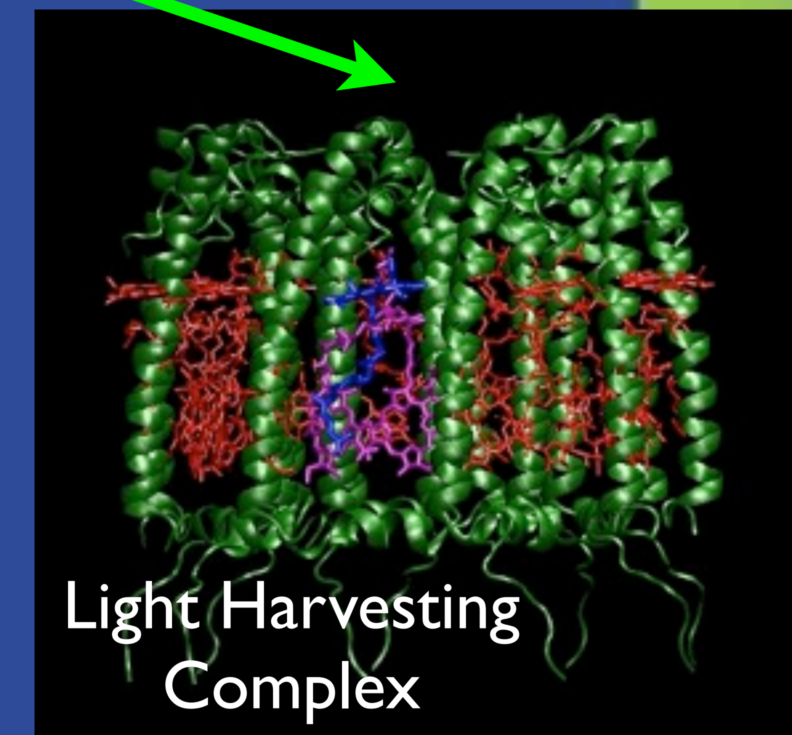

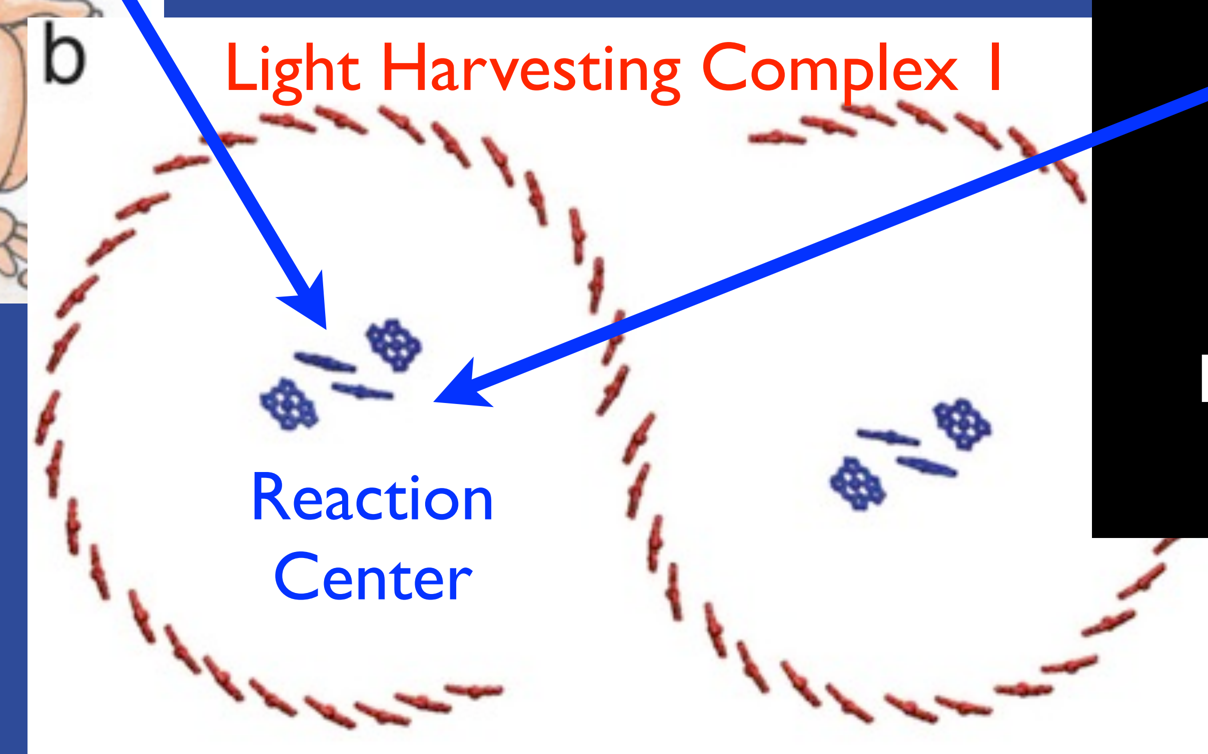

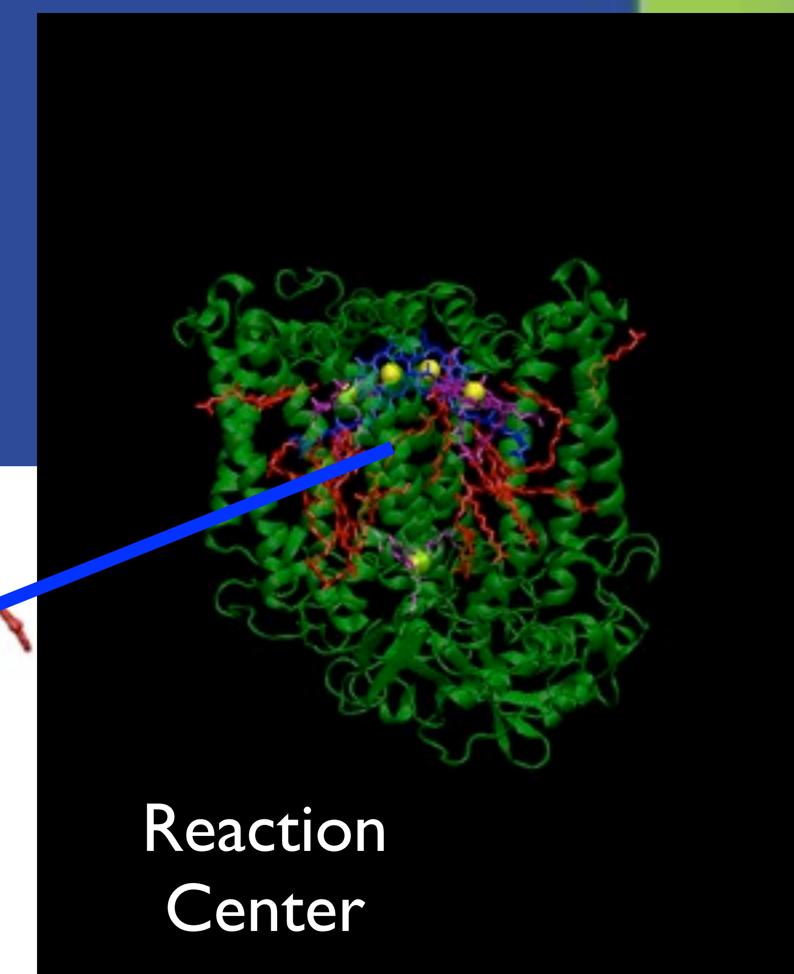

NOTE: Synthetic system lacks harvesting capability!

FMO complex from green sulfur bacteria

Membrane embedded trimer complex

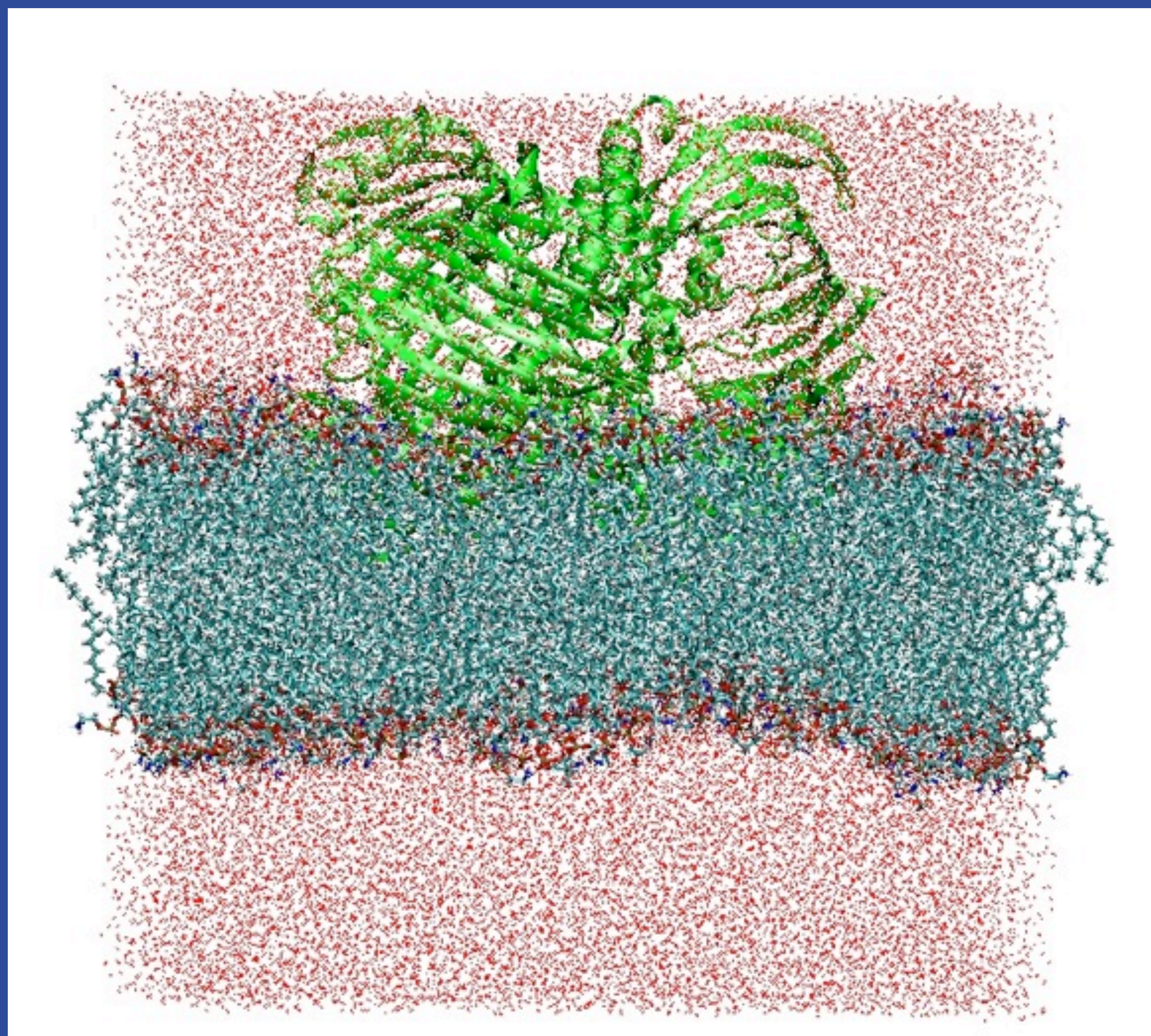

Monomer complex: 7 chlorophylls embedded in protein scaffolding

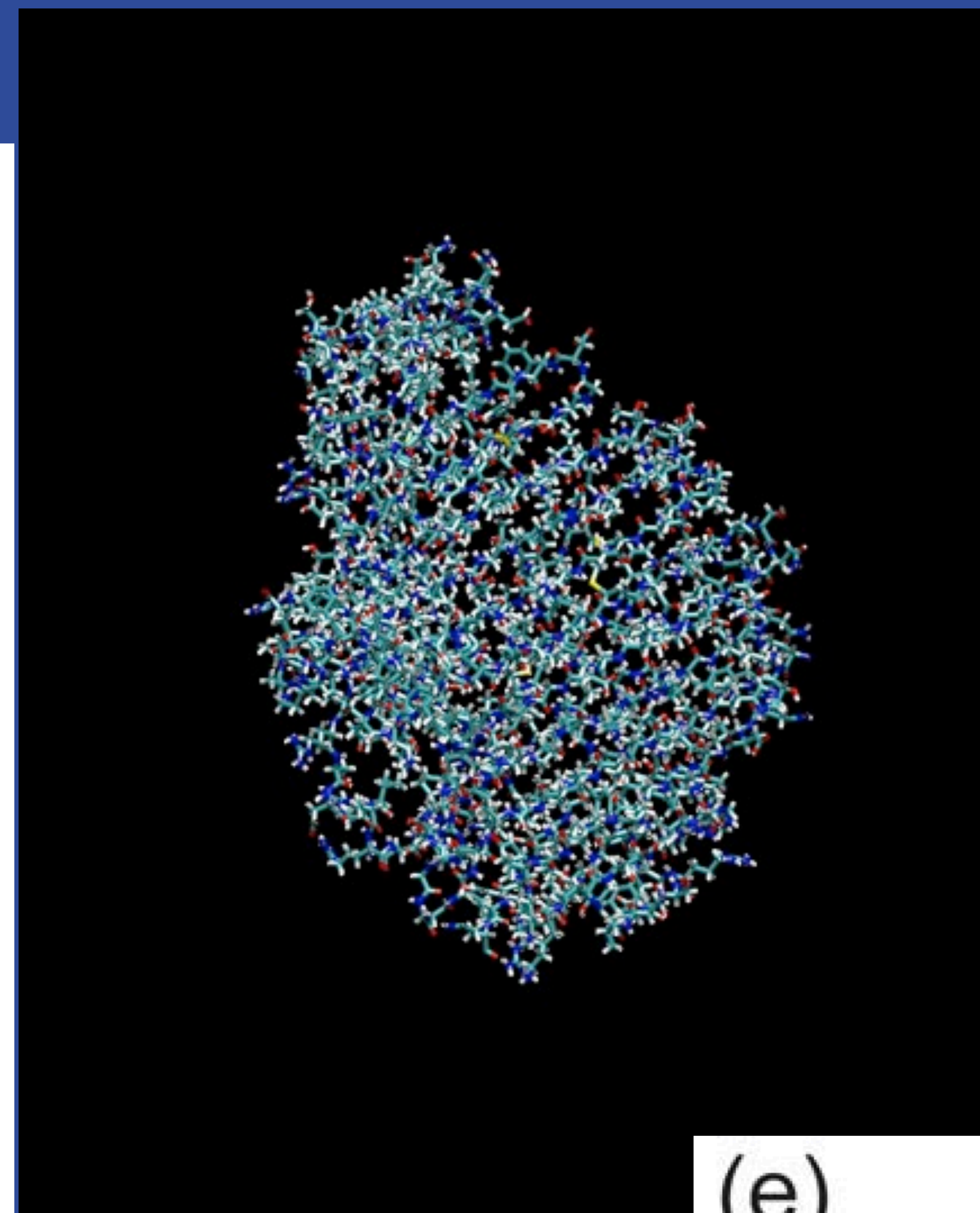

Hybrid
biological light harvesting complex and
synthetic DSSC material

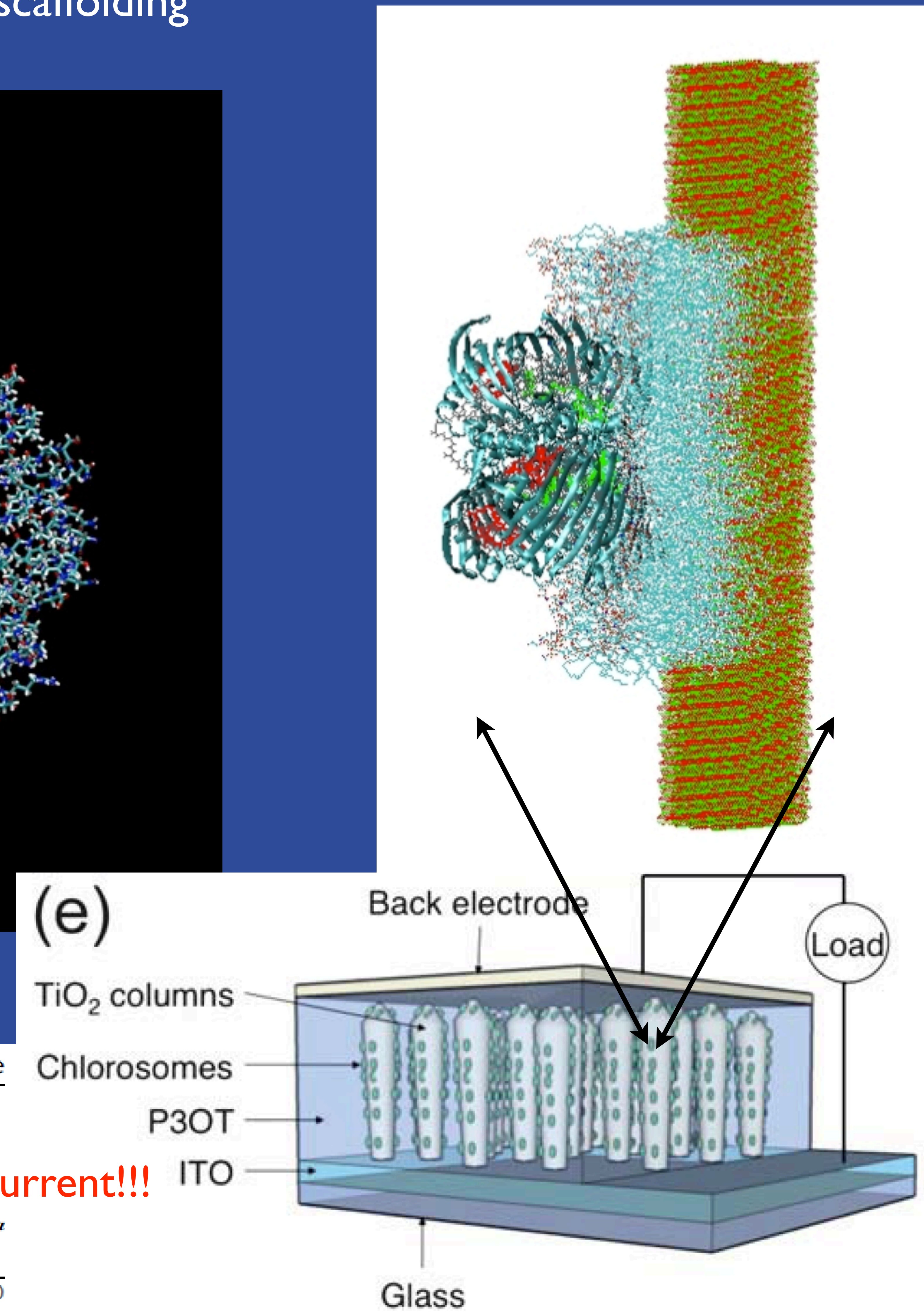

PAPER www.rsc.org/ees | Energy & Environmental Science

Electrospray-assisted characterization and deposition of chlorosomes to fabricate a biomimetic light-harvesting device

!!! 30x increase in Photocurrent!!!

Luis B. Modesto-Lopez,[a] Elijah J. Thimsen,[a] Aaron M. Collins,[b] Robert E. Blankenship[b] and Pratim Biswas*[a]

216 | *Energy Environ. Sci.*, 2010, 3, 216–222

FMO complex from green sulfur bacteria

Hybrid
biological light harvesting complex and
synthetic DSSC material

Monomer complex: 7 chlorophylls embedded in protein scaffolding

Membrane embedded trimer complex

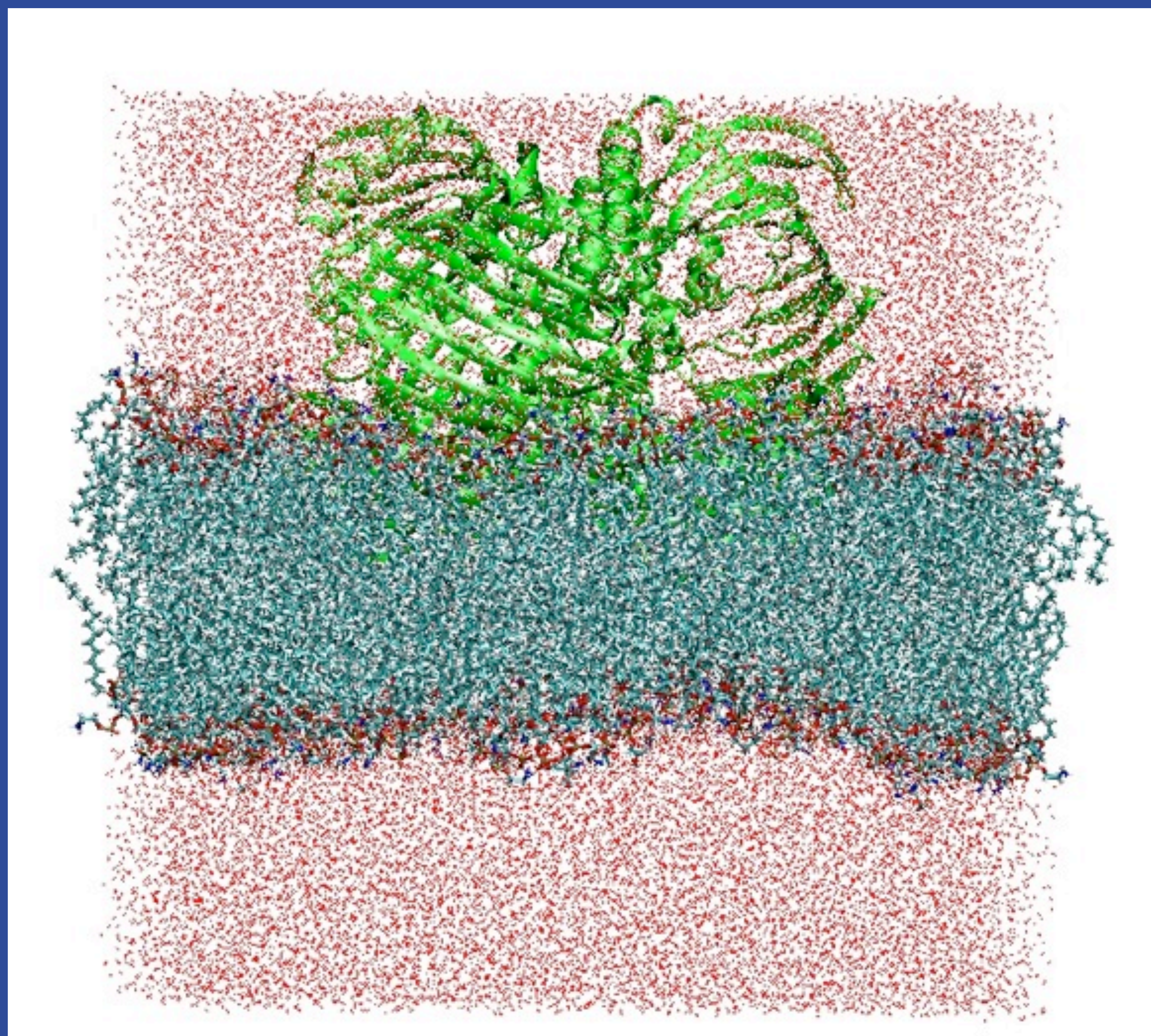

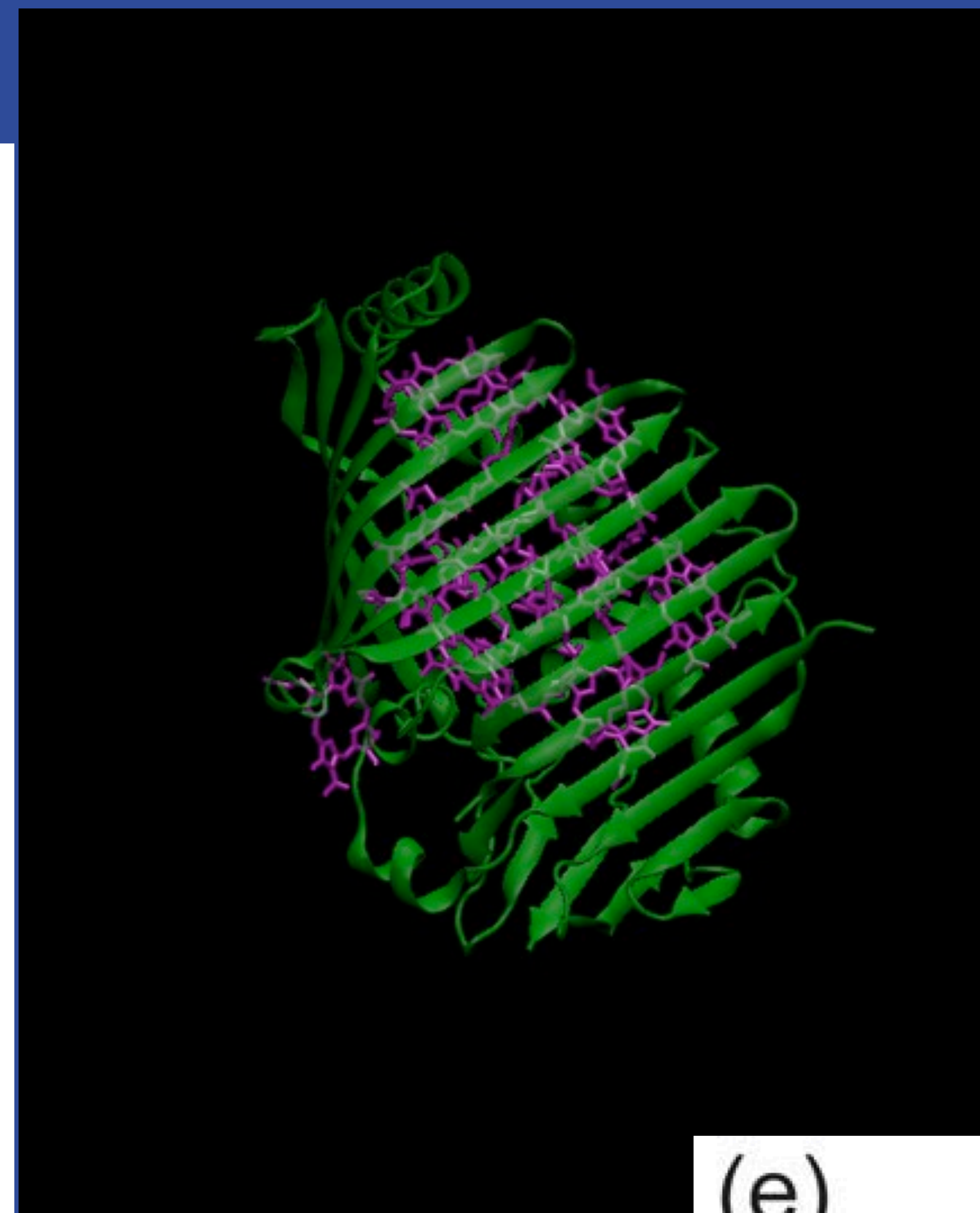

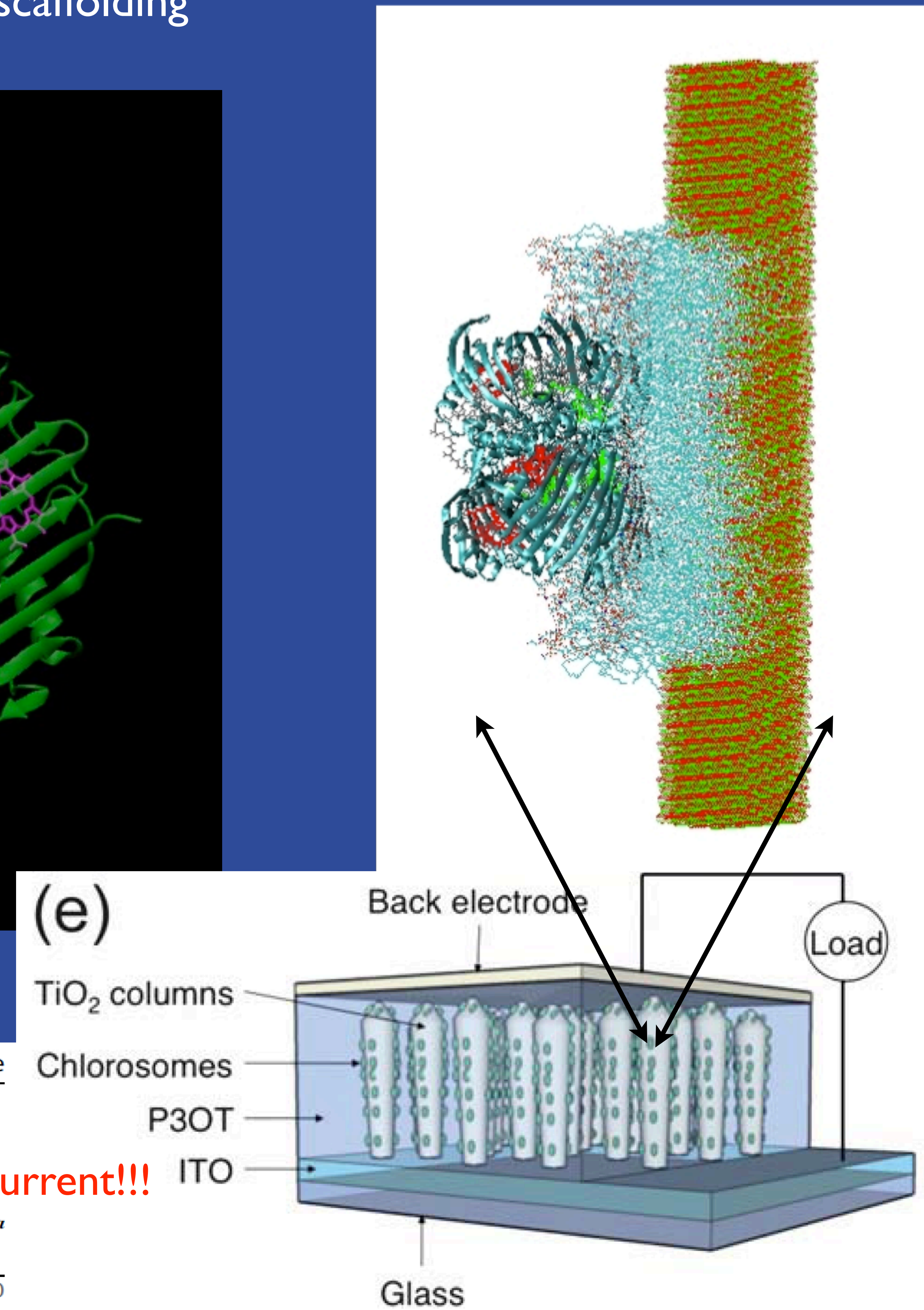

PAPER www.rsc.org/ees | Energy & Environmental Science

Electrospray-assisted characterization and deposition of chlorosomes to fabricate a biomimetic light-harvesting device

!!! 30x increase in Photocurrent!!!

Luis B. Modesto-Lopez,[a] Elijah J. Thimsen,[a] Aaron M. Collins,[b] Robert E. Blankenship[b] and Pratim Biswas*[a]

216 | *Energy Environ. Sci.*, 2010, 3, 216–222

FMO complex from green sulfur bacteria

Hybrid
biological light harvesting complex and
synthetic DSSC material

Monomer complex: 7 chlorophylls
embedded in protein scaffolding

Membrane embedded trimer complex

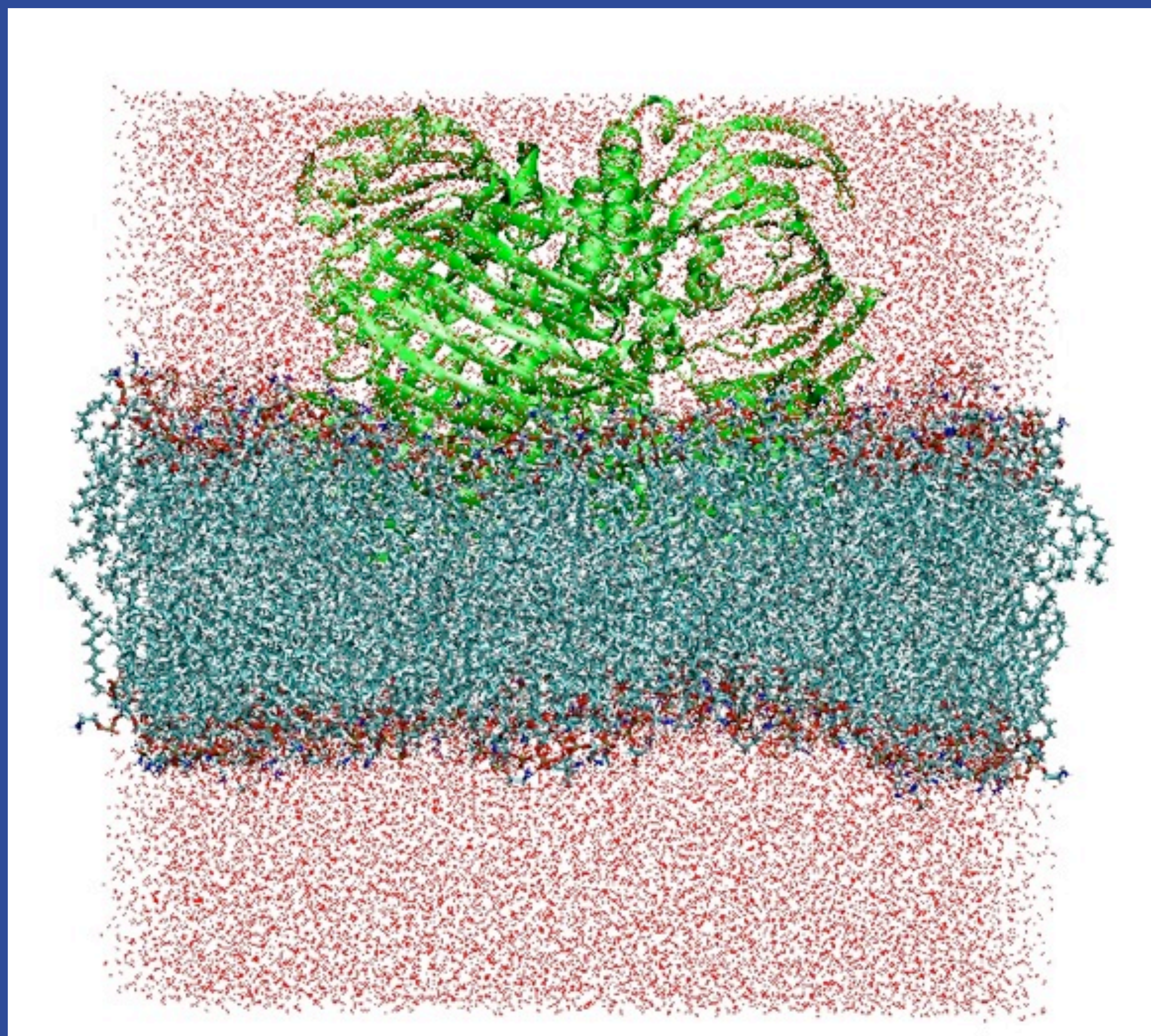

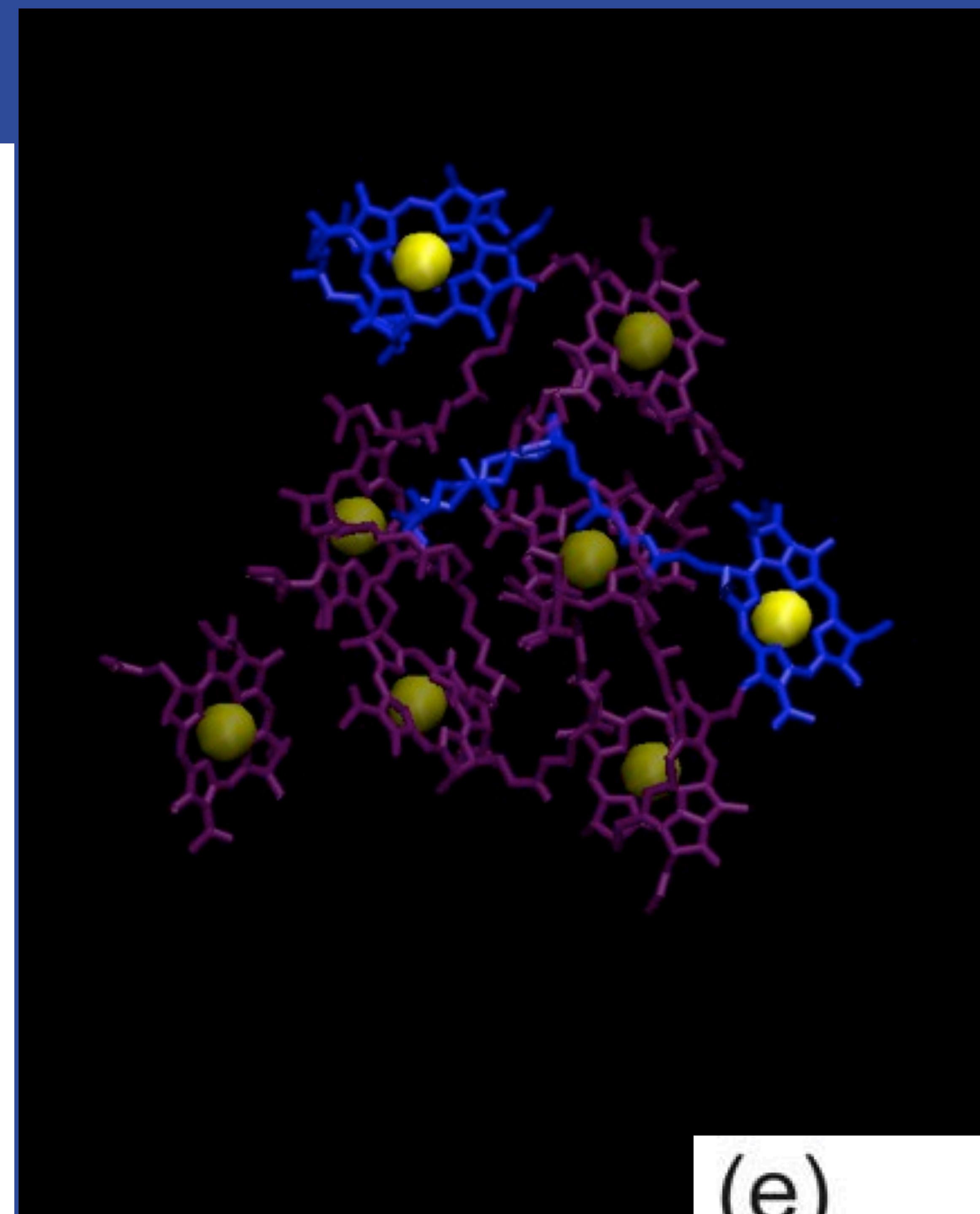

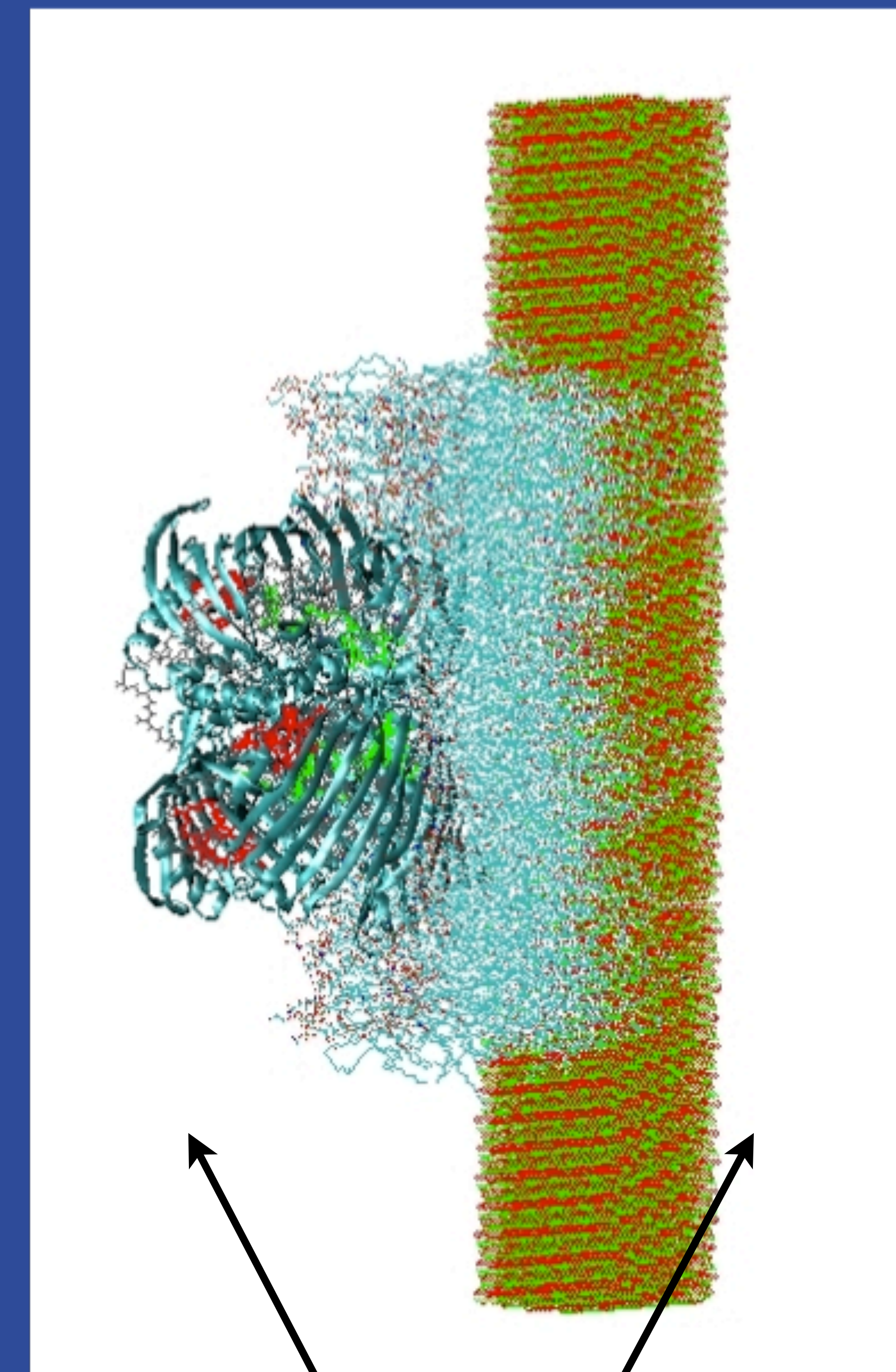

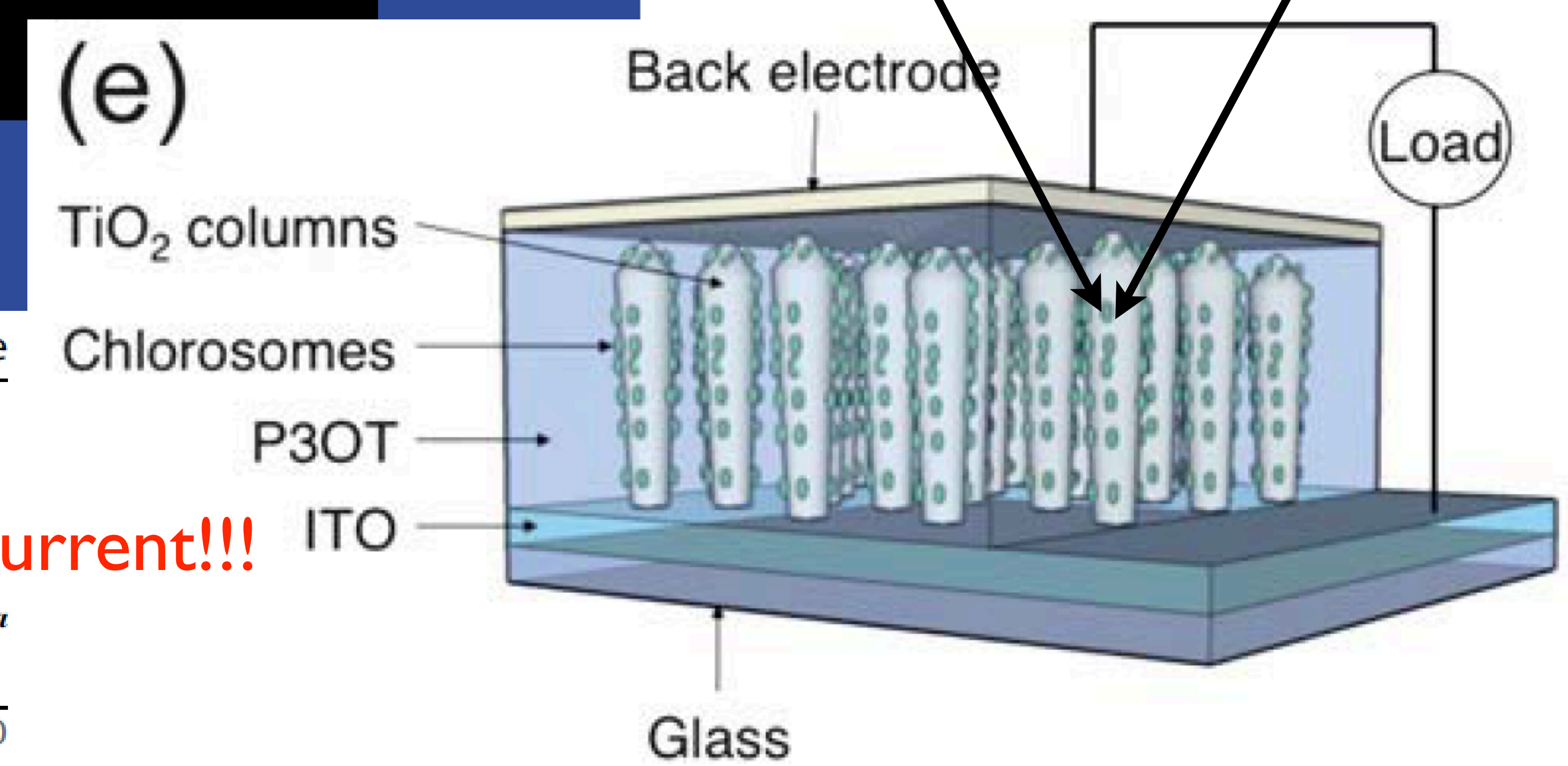

PAPER www.rsc.org/ees | Energy & Environmental Science

Electrospray-assisted characterization and deposition of chlorosomes to fabricate a biomimetic light-harvesting device

!!! 30x increase in Photocurrent!!!

Luis B. Modesto-Lopez,[a] Elijah J. Thimsen,[a] Aaron M. Collins,[b] Robert E. Blankenship[b] and Pratim Biswas*[a]

216 | *Energy Environ. Sci.*, 2010, 3, 216–222

Conclusions:

(1) Iterative linearized density matrix propagation provides a successively correctible trajectory based mixed quantum-classical dynamics method that can represent environmental decoherence and non-adiabatic effects.

(2) These methods can probe the mechanism underlying long-lived quantum coherent excited state dynamics e.g. photosynthetic antenna arrays, quantum computing applications.

(3) Iterating "short" time linearized propagators for long time density matrix dynamics, Monte Carlo density matrix element sampling & taming the exponential growth of trajectories.